

# **Energy Modeling of Deceleration Strategies for Electric Vehicles**

William Lee Hom

Thesis submitted to the faculty of the Virginia Polytechnic Institute and State University  
in partial fulfillment of the requirements for the degree of

Master of Science

In

Mechanical Engineering

Douglas J. Nelson, Chair

Scott T. Huxtable

Steve C. Southward

August 12<sup>th</sup>, 2022

Blacksburg, VA

Keywords: Electric Vehicle, Decel, Regenerative Braking,  
Coasting, Willans Line, Energy Consumption

© 2022 William L. Hom

# **Energy Modeling of Deceleration Strategies for Electric Vehicles**

William Lee Hom

## **ABSTRACT**

Rapid adoption of battery electric vehicles means improving energy consumption is a top priority. Regenerative braking converts kinetic energy to electrical energy stored in the battery pack while the vehicle is decelerating. Coasting is an alternative strategy that minimizes energy consumption by decelerating the vehicle using only road load. This work refines a battery electric vehicle model to assess regen, coasting, and other deceleration strategies. A road load model based on public test data calculates tractive effort based on speed and acceleration. Bidirectional Willans lines are the basis of the powertrain model simulating battery energy consumption. Regen braking tractive and powertrain power are modeled backward from prescribed linear velocity curves, and the coasting trajectory is forward modeled given zero tractive power. Decel modes based on zero battery and motor power are also forward modeled. Multi-Mode decel (using a low power mode with regen) is presented as an intermediate strategy. An example vehicle is modeled in fixed-route simulations using these strategies and is scored based on travel time, energy consumption, and bias towards minimizing one of those metrics. Regen braking has the lowest travel time, and coasting the lowest energy consumption, but such bias increases overall cost. Multi-mode strategies lower overall cost by balancing reductions in travel time and energy consumption. The model is sensitive to grade and accessory load fluctuation, making this work adaptable to different vehicles and environments. This work demonstrates the utility of regen braking alternatives that could enhance connected and automated vehicle systems in battery electric vehicles.

# **Energy Modeling of Deceleration Strategies for Electric Vehicles**

William Lee Hom

## **GENERAL AUDIENCE ABSTRACT**

As battery electric vehicle adoption accelerates, reducing energy consumption remains a priority. While regenerative braking saves energy by recharging the battery pack using kinetic energy, coasting (deceleration caused only by road load) has potential as well. This work focuses on refining a battery electric vehicle model and assessing various deceleration strategies. A road load model calculates wheel tractive effort, and Willans lines are used to model powertrain energy consumption. Coasting and other deceleration modes based on zero system power are modeled to produce speed trajectories, and regenerative braking power is modeled using prescribed linear velocity curves. Strategies that use multiple decel modes are also considered. An example battery electric vehicle is assessed using these strategies in fixed-route simulations. Vehicle performance is scored based on battery energy consumption and travel time. Regenerative braking has the lowest travel time, and coasting the lowest energy consumption, but those strategies also have the highest overall cost. Multi-mode strategies lower cost by balancing energy consumption and travel time. The strategies are sensitive to changes in road grade and accessory power, meaning the model can be used with different vehicles and environments. This work demonstrates the utility of alternatives to regenerative braking and how such strategies could enhance battery electric vehicles with autonomous capabilities.

## Acknowledgements

First, I would like to thank my family for motivating and supporting me throughout my time at Virginia Tech. Their love and encouragement empowers me to make the most of every single day. Thank you for all the wisdom and inspiration you've bestowed all these years.

Dr. Nelson: Thank you for giving me the opportunity to help lead HEVT, and for your continuous mentorship and support. I have been beyond blessed to have had you as an advisor both for HEVT and my research. Your patience, kindness, and wise counsel have helped shape me into a better engineer than I was before.

Thank you to my teammates on HEVT and BOLT for making the last three years of my college career so memorable. Through the highs and the lows, we accomplished a lot, learned a lot, and had a great time in the Ware Lab together. I'm honored to have been your teammate.

To the members of my committee, Dr. Huxtable and Dr. Southward: thank you for your instruction and guidance both in and out of the classroom.

Finally, to all my friends and classmates at Virginia Tech: it has been a pleasure learning and living alongside you for the past five years. I will always cherish the memories we've made together and the connections I've made with you all here in Blacksburg.

This work was partially supported by funding from the U.S. Department of Energy through the EcoCAR Mobility Challenge.

# Contents

<b>Contents .....</b>	<b>v</b>
<b>List of Figures .....</b>	<b>vi</b>
<b>List of Tables .....</b>	<b>viii</b>
<b>List of Symbols .....</b>	<b>ix</b>
<b>Chapter 1: Introduction .....</b>	<b>1</b>
<b>Chapter 2: Literature Review .....</b>	<b>4</b>
<b>Chapter 3: Vehicle Model Development .....</b>	<b>12</b>
<i>Tractive Effort Model.....</i>	<i>12</i>
<i>Powertrain Model.....</i>	<i>15</i>
<i>Vehicle Overview .....</i>	<i>21</i>
<b>Chapter 4: Decel Solution Simulation .....</b>	<b>25</b>
<i>Decel Velocity Curve Fundamentals.....</i>	<i>25</i>
<i>Tractive Power and Energy .....</i>	<i>28</i>
<i>Energy Capture with Regen Braking.....</i>	<i>32</i>
<i>Coasting as a Decel Mode.....</i>	<i>35</i>
<i>Pseudo-Coasting Decel Modes .....</i>	<i>40</i>
<i>Multi-Mode Decel.....</i>	<i>44</i>
<i>Fixed-Route Drive Cycle Simulation .....</i>	<i>45</i>
<b>Chapter 5: Results &amp; Discussion.....</b>	<b>47</b>
<i>Regen Mode .....</i>	<i>47</i>
<i>Coast Mode .....</i>	<i>48</i>
<i>Pseudo-Coasting Modes .....</i>	<i>50</i>
<i>Multi-Mode Decel.....</i>	<i>54</i>
<i>Fixed-Route Simulation .....</i>	<i>57</i>
<i>Discussion .....</i>	<i>61</i>
<i>Sensitivity Analysis .....</i>	<i>69</i>
<b>Chapter 6: Conclusions.....</b>	<b>75</b>
<b>References.....</b>	<b>77</b>
<b>Appendix A: Willans Line Overview .....</b>	<b>80</b>
<b>Appendix B: Cruise Power and Energy Consumption .....</b>	<b>83</b>
<b>Appendix C: 25 mph Simulation Results .....</b>	<b>85</b>
<b>Appendix D: 35 mph Simulation Results .....</b>	<b>89</b>
<b>Appendix E: 45 mph Simulation Results .....</b>	<b>95</b>

# List of Figures

Figure 1: Tractive Effort Model Free Body Diagram.....	12
Figure 2: Tractive Effort Model Calculations .....	15
Figure 3: Bidirectional BEV powertrain model.....	16
Figure 4: BEV Powertrain Modeling Step Given Required Tractive Power .....	17
Figure 5: Propel Mode Power Flow.....	17
Figure 6: Brake Mode Power Flow.....	19
Figure 7: BEV Model Energy Balance, Propel and Brake Modes .....	21
Figure 8: Basic Decel Solutions .....	28
Figure 9: Tractive Power vs. Time for Several Decel Curves.....	29
Figure 10: Decel Distance and Tractive Energy.....	30
Figure 11: Stopping distances from 25 mph for linear decel profiles.....	31
Figure 12: Distance- and Time-to-Stop from 25 mph .....	31
Figure 13: Powertrain energy and efficiency .....	33
Figure 14: Battery power and energy over regen braking event .....	33
Figure 15: Percent Tractive Power Lost Before Recharging Pack .....	34
Figure 16: Energy availability and capture, 25 mph-0mph .....	35
Figure 17: Power Flow, Coast Mode.....	37
Figure 18: Model Calculation Steps for Coasting .....	38
Figure 19: Coasting speed and distance to stop vs. time.....	39
Figure 20: Time and Distance to Stop, Coasting vs. Regen .....	39
Figure 21: Coast Distance and Travel Time, Percentage of Final.....	40
Figure 22: Power Flow, ZPM Mode.....	41
Figure 23: Model Calculations, ZPM Mode .....	41
Figure 24: Power Flow, ZPB Mode .....	42
Figure 25: Model Calculations, ZPB Mode.....	43
Figure 26: Example Multi-Mode Decel Strategy.....	45
Figure 27: Fixed-Route Drive Cycle Simulation .....	46
Figure 28: Vehicle Speed and Time to Brake, $-2.5 \text{ m/sec}^2$ Regen.....	47
Figure 29: HV Bus Energy, $-2.5 \text{ m/sec}^2$ Regen.....	48
Figure 30: Vehicle Speed and Time to Brake, Coast Mode .....	49
Figure 31: HV Bus Energy, Coast Mode .....	50
Figure 32: Vehicle Speed and Time to Brake, ZPM Mode .....	51
Figure 33: HV Bus Energy, ZPM Mode.....	51
Figure 34: Vehicle Speed and Time to Brake, ZPB Mode.....	52
Figure 35: HV Bus Energy, ZPB Mode .....	53
Figure 36: Vehicle Speed and Time to Brake, Coast-Regen Decel .....	54

Figure 37: HV Bus energy, Coast-Regen Decel.....	55
Figure 38: Vehicle Speed and Time to Stop, ZPB-Regen Decel.....	56
Figure 39: HV Bus Energy, ZPB-Regen Decel.....	57
Figure 40: Speed vs. Distance, Select Decel Strategies.....	58
Figure 41: $E_{batt}$ vs. Distance, Select Decel Strategies.....	59
Figure 42: Travel Time vs. Distance, Select Decel Strategies.....	60
Figure 43: Total $E_{batt}$ vs. Total Time, Selected Decel Strategies.....	61
Figure 44: Energy Relative to Max vs. Time Relative to Max, Select Decel Strategies.....	63
Figure 45: Cost-Bias Scores, Select Decel Strategies.....	65
Figure 46: Vehicle Trajectory with ZPB-Regen Strategy, Various Transition Speeds.....	68
Figure A.1: Component Efficiency vs. Output Power.....	81
Figure A.2: Bidirectional Willans Line Example.....	82
Figure B.1: Power Requirements vs. Cruise Speeds.....	83
Figure B.2: Cruise energy consumption vs. Cruise speed.....	84
Figure C.1: $-1.5 \text{ m/sec}^2$ Regen Braking Fixed-Route Simulation, 25 mph Case.....	87
Figure C.2: Coast Mode Fixed-Route Simulation, 25 mph Case.....	87
Figure C.3: ZPB Mode Fixed-Route Simulation, 25 mph Case.....	87
Figure C.4: Coast-Regen Fixed-Route Simulation, 25 mph Case.....	88
Figure C.5: ZPB-Regen Fixed-Route Simulation, 25 mph Case.....	88
Figure D.1: Stopping Distance, Linear Decel, 35 mph Case.....	91
Figure D.2: $-1.5 \text{ m/sec}^2$ Regen Braking Fixed-Route Simulation, 35 mph Case.....	91
Figure D.3: Coast Mode Fixed-Route Simulation, 35 mph Case.....	91
Figure D.4: ZPB Mode Fixed-Route Simulation, 35 mph Case.....	92
Figure D.5: Coast-Regen Fixed-Route Simulation, 35 mph Case.....	92
Figure D.6: ZPB-Regen Fixed-Route Simulation, 35 mph Case.....	92
Figure D.7: Speed vs. Distance, Fixed-Route Simulations, 35 mph Case.....	93
Figure D.8: Battery Energy vs. Distance, Fixed-Route Simulations, 35 mph Case.....	93
Figure D.9: Time vs. Distance, Fixed-Route Simulations, 35 mph Case.....	94
Figure E.1: Decel Distance, Linear Decel, 45 mph Case.....	97
Figure E.2: $-1.5 \text{ m/sec}^2$ Regen Braking Fixed-Route Simulation, 45 mph Case.....	97
Figure E.3: Coast Mode Fixed-Route Simulation, 45 mph Case.....	97
Figure E.4: ZPB Mode Fixed-Route Simulation, 45 mph Case.....	98
Figure E.5: Coast-Regen Fixed-Route Simulation, 45 mph Case.....	98
Figure E.6: ZPB-Regen Fixed-Route Simulation, 45 mph Case.....	98
Figure E.7: Speed vs. Distance, Fixed-Route Simulations, 45 mph Case.....	99
Figure E.8: Battery Energy vs. Distance, Fixed-Route Simulations, 45 mph Case.....	99
Figure E.9: Time vs. Distance, Fixed-Route Simulations, 45 mph Case.....	100

# List of Tables

Table 1: 2019 Nissan LEAF® SV/SL Road Load and Powertrain Parameters .....	22
Table 2: 2019 Nissan LEAF® SV/SL Overall Willans Line Parameters .....	22
Table 3: Complete 2019 Nissan LEAF® Vehicle Parameters .....	23
Table 4: Physical Constants for Vehicle Model .....	23
Table 5: Modeled vs. Reported Energy Consumption, 2019 Nissan LEAF® SV/SL .....	24
Table 6: Basic Decel Curves.....	27
Table 7: Length of Constant-distance simulations, various initial speeds .....	46
Table 8: Transition Speed vs. Cost-Bias Score, ZPB-Regen 25 mph case .....	67
Table 9: Downhill Grade Limits, Coast Mode .....	70
Table 10: Energy Consumption Sensitivity to Grade.....	71
Table 11: $t_{trip}$ Sensitivity to Grade.....	72
Table 12: Energy Consumption Sensitivity to $P_{accy}$ .....	73
Table 1C: Simulation Summary, 25 mph case.....	85
Table 2C: Simulation Summary, 25 mph case, cont'd .....	86
Table 1D: Simulation Summary, 35 mph case.....	89
Table 2D: Simulation Summary, 35 mph case, cont'd .....	90
Table 1E: Simulation Summary, 45 mph case .....	95
Table 2E: Simulation Summary, 45 mph case, cont'd.....	96



# List of Symbols

$F_{tr}$	Wheel tractive force	$P_{offset}$	Powertrain offset loss
$F_{rl}$	Road load force	$x_{f,cruise}$	Simulation cruise distance
$M$	Vehicle mass	$x_{f,decel}$	Decel distance
$f_i$	Inertial mass factor	$x_{f,brake}$	Friction brake distance
$a$	Vehicle acceleration	$x_{tot}$	Total simulation distance
$v$	Vehicle speed	$C_2 C_1 C_0$	Quadratic decel coefficients
$ABC$	EPA road load coefficients	$v^*$	Optimized velocity
$C_{rr0}$	Normalized constant road load coeff.	$v_f$	Decel final velocity
$C_{rr1}$	Normalized velocity-dependent road load coeff	$t_f$	Decel final time
$C_D A_f$	Veh. drag coeff. & frontal area	$E_k$	Energy, timestep $k$
$F_{rr}$	Rolling resistance force	$E_{tr}$	Tractive energy
$g$	Acceleration due to gravity	$E_{mech}$	Mechanical energy
$v_{avg}$	Average vehicle speed	$E_{elec}$	Electrical energy
$F_{grade}$	Grade force	$E_{accy}$	Accessory load energy
$\alpha$	Road grade	$E_{batt}$	Battery energy
$F_{aero}$	Aerodynamic drag force	$v_c$	Coast velocity
$\rho$	Air density	$\alpha\beta$	2-term coast ODE coefficients
$P_{tr}$	Wheel tractive power	$A_c B_c C_c$	3-term coast ODE coefficients
$v_0$	Decel initial speed	$k$	Discrete-time model time step
$P_{mech}$	Mechanical power	$v_{transition}$	Decel mode transition speed
$\eta_{gb}$	Gearbox marginal efficiency	$E_{cruise}$	Cruise energy
$P_{loss,gb}$	Gearbox offset loss	$t_{cruise}$	Cruise time
$\omega$	Motor speed	$t_{trip}$	Decel strategy travel time
$NPV$	Motor speed-vehicle speed ratio	$t_{trip,MAX}$	Travel time, solution set max.
$\tau$	Motor torque	$t_{trip,\%MAX}$	Travel time, rel. to solution set max.
$P_{elec}$	Electrical power	$E_{batt,MAX}$	Battery energy, solution set max.
$\eta_{mot}$	Motor/inverter marginal efficiency	$E_{batt,\%MAX}$	Battery energy, rel. to solution set max.
$P_{loss,mot}$	Motor/inverter offset loss	$r_{strat}^*$	Decel strategy overall cost
$P_{batt}$	Battery power	$\theta_{strat}^*$	Decel strategy bias
$P_{accy}$	Accessory load power		
$P_{brake}$	Friction brake power		
$P_{regen}$	Regen brake power		
$\varphi$	Regen brake fraction		
$P_{cutoff}$	Regen power limit		
$v_{cutoff}$	Regen brake cutoff velocity		
$M_t$	EPA road load test mass		
$\eta_{marg}$	Powertrain marginal efficiency		

# Chapter 1: Introduction

The exponential growth of the battery electric vehicle (BEV) market is generating significant interest in modeling vehicle energy consumption and effective range [1]. Since 2010, over 1.7 million BEVs and plug-in hybrid electric vehicles (PHEVs) have driven a collective 52 billion miles using only electricity [2]. While BEV and PHEV electricity consumption (4.4 TWh in 2020) replaces the consumption of hundreds of millions of gallons of gasoline [2], the properties of BEVs- primarily lower energy storage density and higher powertrain efficiency than internal combustion engine vehicles (ICEVs)- are motivating studies of various methods for extending vehicle range. The emergence of connected and automated vehicles (CAVs) is making optimization of energy efficiency and drive quality easier with a range of systems installed on those vehicles [3]. Processes that reduce energy consumption or even transfer it back into the vehicle in a usable form are of particular interest.

Regenerative braking (also referred to as regen braking or regen) is one of the most studied and implemented methods for reducing speed in a BEV. It takes advantage of the bidirectional energy transfer capabilities of an electric drivetrain by requesting negative torque from the powertrain and sending energy back into the high-voltage battery pack. The amount of braking energy that becomes stored electrical energy is dependent on both powertrain system efficiency (regen fraction, gearbox and motor losses, and accessory loads) and vehicle stability requirements. Converting some kinetic energy to electrical energy during braking reduces the amount of kinetic energy absorbed by friction brakes [4]. At the opposite end of the decel strategy spectrum, coasting is also a potential method for slowing BEVs from cruise speed to a stop. In an ideal scenario, coasting is a

deceleration due to only road load forces (aerodynamic drag, rolling resistance, and grade force) without any tractive effort or drag due to the powertrain. Traditionally, ICEVs can achieve a near-coasting condition by disconnecting the engine from the driveline via a clutch or neutral gear [5]. BEVs can emulate this state by controlling the powertrain in such a way that minimizes or eliminates all powertrain forces at the wheels. This operating state minimizes vehicle energy consumption over an extended distance, much longer than a typical regen braking event.

Although regenerative braking is often the default option for decelerating a BEV, prior work suggests that coasting, if properly implemented on a BEV, could also offer advantages with respect to energy consumption and range. Fair comparison of these strategies, which vary in both energy consumption and average acceleration, requires a constant-distance simulation whose scope extends beyond the deceleration phase itself. This work uses general BEV tractive effort and powertrain models to examine several modes for slowing an example BEV (in this case, a 2019 Nissan LEAF®) from cruising speed to a stop. These deceleration (decel) strategies are compared over a fixed distance, so a period of constant-speed cruise precedes the decel event. Studying decel strategies over a common route allows for a fair and complete understanding of energy consumption during a drive cycle using each decel mode. A 10 Hz discrete-time numerical simulation is conducted from the cruise speed down to a predetermined friction braking speed, and the distance that needs to be covered at cruising speed is also determined. The goals of this work are to first develop a two-part BEV power model (a tractive effort model based on road load and a powertrain model that utilizes bidirectional Willans lines) that is capable of modeling powertrain performance and energy consumption using

publicly available vehicle test data from the United States Environmental Protection Agency (EPA); second, numerically assess BEV performance during the cruise and braking phases of a drive cycle using a range of decel strategies such as coasting, regenerative braking, and intermediate methods; third, analyze the advantages and disadvantages of each decel strategy, especially with respect to battery energy consumption and travel time; and fourth, assess how to best utilize these strategies to improve BEV range and energy consumption in varying conditions.

The results demonstrate the value of using a Willans Line-based powertrain model to assess performance of any BEV for which the requisite, regulatory data is publicly available. They provide a framework for numerically calculating a vehicle decel profile with consideration for both energy consumption and travel time. Novel methods for controlling a BEV powertrain during decel and braking are identified, and possible applications to connected and automated vehicle systems are explored.

## Chapter 2: Literature Review

Regenerative braking is an important feature of electrified vehicles that enhances vehicle performance. While primarily an energy recovery system, proper implementation also improves braking performance and the dynamic stability of the vehicle [4]. Modern BEVs can transform kinetic energy into stored electrical energy during braking events through its electric powertrain, a useful alternative to the systems found in internal combustion engine-powered vehicles (ICEVs) that merely waste braking energy as heat in traditional friction braking systems. The opportunity for regen braking to reduce energy consumption is mostly in urban areas. Braking energy can be as much as 34% of tractive energy in a typical urban drive cycle and even as high as 80% in large cities with frequent stops and low average speeds like New York City [6]. The benefits are not exclusive to cities, as drivers with high annual mileage also stand to gain from using regen [7].

There are two different categories of regenerative braking. Category A regen braking is dependent on accelerator position, shifting, switch activation, or a combination of these driver inputs, and is most akin to engine braking in ICEVs. Category B regen occurs during normal “service braking”, which is normally triggered by the driver pressing the brake pedal. The share of energy available to absorb into the electric powertrain (versus through the friction brakes) depends on factors such as battery state of charge (SOC), vehicle speed, and drivetrain configuration [4]. Implementation of a control system to manage energy recovery during regen braking, as done by [8] and [9], can improve both regen efficiency and directional stability.

The potential impact of regenerative braking systems is quantified in [10], an examination of tractive and braking energy requirements at the wheel for several international

regulatory drive cycles. The work decomposes drive cycles into powered driving, braking, and idling phases based on tractive force requirements, calculating the energy of each phase. It also introduces “braking-wheel to traction-wheel effectiveness ( $\xi$ ),” the portion of braking energy that the vehicle transfers back to the wheel from energy storage during powered driving. Using a hybrid powertrain model, the study finds that regen braking can “significantly reduce” fuel consumption and is directly related to  $\xi$ , but the exact impact depends on the vehicle and drive cycle. However, high values of  $\xi$  are improbable due to the myriad of inefficiencies that reduce the amount of braking energy that can be converted into electrical energy, the complexity of energy management systems, and vehicle stability requirements [10]. Vehicle energy consumption is less sensitive to changes in mass than other factors (e.g., aerodynamic and rolling resistance forces) as  $\xi$  increases. This concept is explored further in [11], in which fuel consumption savings due to regen braking are correlated to an equivalent reduction in vehicle mass. Despite regenerative braking systems adding mass to a vehicle, powertrains with large values of  $\xi$  can have the same effect on energy consumption as reducing the overall mass of the vehicle [11].

Several metrics are developed in [12] for measuring regen braking efficiency in a hybrid electric vehicle. Overall efficiency is the ratio of battery energy to wheel energy, and powertrain efficiency is the ratio of battery energy to “driveshaft energy,” the mechanical energy transferred to the driveshaft via the transmission output. The latter efficiency measurement is important for measuring the efficiency of the electric powertrain because it excludes the energy absorbed by the friction brakes [12].

Both [13] and [7] quantify the potential energy savings of regenerative braking over various drive cycles for a range of electrified vehicles. In their analysis of HEV and BEV regen braking, Rask et al. identify three main limitations of regen brake systems that impact the amount of energy that can be recovered as electrical energy: low speed regen force limits, vehicle control system regen force limits, and power limitations inherent to electric powertrains [13]. Bjornsson and Karlsson find in their analysis of a micro-hybrid electric vehicle (mHEV) and BEV that a mHEV without engine braking can recover nearly as much energy as a BEV, even with a lower magnitude regen power limit [7]. Both studies acknowledge that reducing fuel consumption with deceleration fuel cutoff (DFCO, turning off fuel injection in an internal combustion engine and using engine drag to brake) or eliminating engine braking through decoupling (i.e., an approximate coasting condition) can help improve overall energy consumption.

A novel application of regenerative braking is “one pedal driving” vehicle control, where service braking levels of decel are commanded simply by lifting off the accelerator pedal. This control strategy maximizes the amount of energy being regenerated into the HV battery pack and minimizes wear on friction brakes. One pedal driving has been implemented in a range of electrified vehicles, including the Chevrolet Bolt, a mass-market BEV [14]. Some vehicles also enable drivers to use this strategy by using steering wheel-mounted controls like paddles [15]. One pedal driving is implemented in a hybridized 2019 Chevrolet Blazer RS by [16] as a part of an energy management strategy that reduces vehicle energy consumption over several standard drive cycles.

These studies of regenerative braking highlight some opportunities for future study. Most of these studies rely on the various government-issued drive cycles to analyze the

performance of electrified vehicles. While these drive cycles offer realistic driving profiles to fairly assess vehicles under braking, they do not allow for fair assessment of decel strategies that may deviate from these predetermined velocity profiles. Furthermore, given the positive effect of DFCO on regen efficiency in HEVs, it may be productive to explore how a similar state in BEVs impacts energy consumption, either separate from or in conjunction with regen braking. Finally, discussion of braking-wheel to tractive-wheel efficiency in [11] and the study in [12] both provide a good basis for assessing the true efficiency of regen braking. The fact that only a portion of the energy that is regenerated into the battery pack during braking makes it back to the wheel as tractive energy is notable. It begs the question whether other deceleration strategies result in lower energy consumption, especially with other stages of a drive cycle factored in.

Coasting has been previously studied as a method of minimizing energy consumption in both ICEVs and BEVs. Pure coasting, as defined by [5], is vehicle movement without either positive or negative traction force at the wheels. Without grade, the only forces slowing the vehicle down are road load forces like rolling resistance and aerodynamic drag. In a vehicle with a manual transmission, the vehicle can approximate coasting when the driver shifts into neutral, and the engine idles. Despite eliminating engine drag from the driveline, the vehicle still experiences some negative torque at the wheel caused by the final drive, wheel bearings, axles, and brake drag. [5] studied the benefits of coasting in a hybrid vehicle going downhill on a highway and found that fuel savings of up to 10% are possible. The study also notes that coasting is more efficient than recuperating energy through the electrified drivetrain in their conditions [5]. One caveat is that the velocity delta that develops during coasting may be unappealing to consumers who desire a certain



speed on the highway. For decel events, though, this departure from the cruising speed may be acceptable.

In [17], coasting is proposed as a means of improving fuel efficiency in an ICE vehicle. The study uses an algorithm to unlock the torque converter during coasting, separating the engine from the rest of the drivetrain and allowing the engine to idle. On flat roads, fuel consumption decreases by 7.9%, travel distance increases by 17%, and fuel consumption savings are even higher when coasting on an inclined road. This study demonstrates the value of limiting energy transfer through the powertrain and utilizing coasting to decelerate or maintain a desired vehicle speed when the road slope is favorable.

A decel strategy akin to coasting is implemented in [18] as a part of a hierarchical control (HC) strategy for an ICEV. The study divides a “driving task” into acceleration, constant speed, cruising (which most correlates to coasting in this study), and braking. The proposed cruising phase involves DFCO, engine torque set to zero, and the vehicle decelerating while remaining in-gear. The vehicle velocity trajectory during this phase is determined by a 3-term acceleration function, which accounts for aerodynamic, rolling, and grade forces. The HC strategy is used in a simulation to mimic a real urban drive cycle driven by a human, and the fuel consumption is compared. The drive cycle driven with the control strategy implemented consumes 30% less fuel than the human-driven cycle. The HC system plans drive cycle hills that tend to have longer coasting phases than ones driven by a human. Although this study could not factor in the impact of regen braking, it demonstrates the utility of implementing a decel mode with minimal energy consumption and a longer time horizon than regen braking [18].

The work done in [19] attempts to develop a coasting mode in BEVs that mimics engine braking in ICEVs. The study utilizes both a MATLAB/Simulink model and hardware-in-the-loop (HIL) setup to validate a control system that manages BEV coasting. The control algorithm matches the speed and acceleration profile of the baseline HEV for several initial speeds. In both initial speed cases, the controlled coast has minimal impact on battery state-of-charge (SOC), which means this decel strategy can be used in lieu of regenerative braking when the battery is near the upper SOC limit [19]. The initial, uncontrolled deceleration of the BEV is less drastic than that of the reference vehicle since there are less losses in the BEV drivetrain than the ICEV one. Another strategy for coasting in BEVs is zero-torque coasting as proposed by [20]. Rather than setting motor current to zero, which results in negative torque output due to motor electromagnetic properties, motor current is controlled in such a way that motor output torque is set to zero. This compensation results in the motor drawing some power, but torque remains at zero through the field-weakening region. As a result, the vehicle cruises longer in both simulated and HIL experiments [20]. The ability to control a BEV powertrain in this manner, and the work completed by [19] and [17], demonstrate that there are other methods for decelerating a BEV besides regen braking. These other methods should be compared to regen braking on an equal basis.

Assessing potential energy savings benefits of various decel strategies requires a low-cost vehicle model that is simplistic, yet robust enough to accurately portray the energy consumption of the various methods being considered. Willans Lines modeling is the subject of several studies seeking to establish it as a viable method of prediction power and energy consumption at all points within a BEV drivetrain. A Willans Line relates input

power to output power through a linear function with a given offset. The slope of the line is the marginal efficiency of the system, and the y-intercept is the offset loss, which symbolizes a constant loss present despite the level of power the system is outputting. Harvey and Nelson demonstrate the utility and accuracy of a Willans Line powertrain model in [21] and [22], where a method for developing a power-based model of the energy consumption of a BEV based on EPA test car list data is presented. The work addresses both the development of vehicle-specific tractive effort models, which is aided by the ABC road load coefficients published by the EPA for BEVs currently on the market, as well as a powertrain model that is derived from two US certification drive cycles. The proposed bidirectional Willans Line model, which models the entire powertrain with a single piecewise function, accounts for periods of braking within a drive cycle, and includes braking system factors such as regen fraction, low speed regen cutoff, and regen power limit. The process for characterizing a BEV powertrain described in [22] yields other important characteristics such as marginal efficiency, overall power offset loss, and accessory load. By modeling eight different BEVs, Harvey demonstrates the Willans Line method can accurately model energy consumption and range over standard drive cycles. Sensitivity to changes in accessory load could be beneficial for studying how varying accessory loads affect the feasibility of a given decel strategy. A summary of modeling powertrain components with Willans lines can be found in Appendix A.

The work in [23] extends power-based fuel consumption theory for ICEVs to BEVs and formally derives a model like the one proposed in [21]. Using a 200-kW electric traction motor, the ICEV model is adapted for the bidirectional power flow inherent to a BEV powertrain. Since BEV traction motors are much more efficient than traditional ICEV

engines, a linear relationship between output mechanical power and input battery power can be established with “good accuracy” just based on EPA Test Car List data [23].

## Chapter 3: Vehicle Model Development

### *Tractive Effort Model*

A generic BEV tractive effort model is developed using previously developed techniques.

Figure 1 is a basic free-body diagram of loads that are expected to act upon the vehicle during a normal drive cycle. At any given timestep  $k$ , they appear in the form of tractive forces  $F_{tr}$  and road load forces  $F_{rl}$  such that

$$F_{tr,k} + F_{rl,k} = f_i M a_k, \quad (1)$$

where vehicle mass  $M$  is multiplied by  $f_i$ , a coefficient to account for rotating mass. In a discrete-time velocity series, acceleration  $a_k$  is calculated as

$$a_k = \frac{v_k - v_{k-1}}{t_k - t_{k-1}}. \quad (2)$$

This study uses a  $f_i$  value of 1.04, which is also used by [21] and [22] due to the use of larger tires and wheels on contemporary passenger vehicles than in previous decades. It is slightly higher than the 1.03 value used in [24].

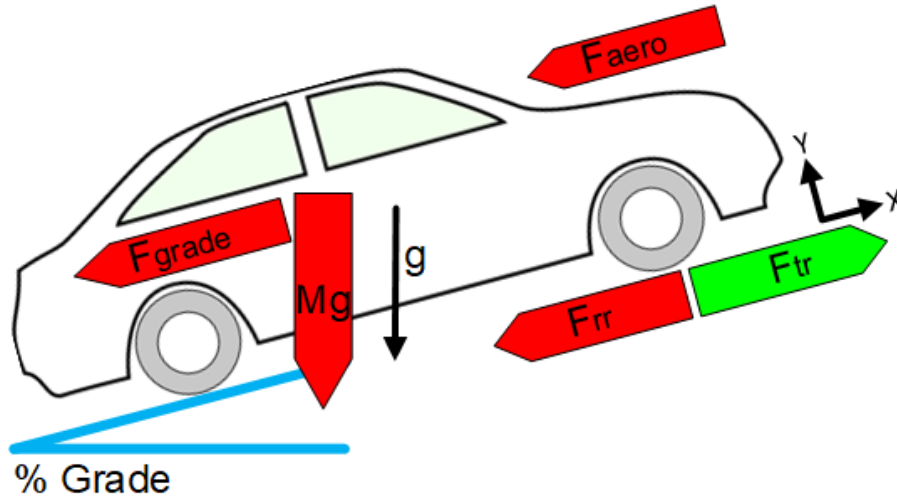


Figure 1: Tractive Effort Model Free Body Diagram

The force balance is representative of all the road load forces acting on the vehicle at the wheel and the overall inertial force induced when the vehicle accelerates and decelerates.

The EPA publishes road load coefficients for all vehicles in production as a part of mandatory fuel economy testing. They are determined via test procedures such as [24] and [25], and define road load in terms of velocity such that

$$F_{rl} = A + Bv + Cv^2. \quad (3)$$

They are specific to the vehicle and mass at which the vehicle completes the test,  $M_t$ .

Adapting the road load coefficients for this study yields

$$C_{rr0} = \frac{A}{M_t g}, \quad (4)$$

$$C_{rr1} = \frac{B}{M_t g}, \text{ and} \quad (5)$$

$$C_D A_f = \frac{C}{\frac{1}{2}\rho}. \quad (6)$$

$C_{rr0}$  is the constant coefficient of rolling resistance,  $C_{rr1}$  the speed-dependent coefficient of rolling resistance, and  $g$  is acceleration due to gravity.  $C$  is divided by  $\frac{1}{2}\rho$  so that the normalized coefficient correlates to the product of drag coefficient  $C_D$  and vehicle front cross-sectional area  $A_f$ . The new coefficients are not dependent on the mass of the vehicle, unlike those provided by the EPA. Independence from mass allows for more flexibility when analyzing vehicle performance under different passenger and cargo configurations beyond the EPA-reported test mass. The force due to rolling resistance is expressed as

$$F_{rr} = Mg(C_{rr0} + C_{rr1}v_{avg}), \quad (7)$$

where  $v_{avg,k}$  is the average of the current vehicle velocity and the velocity at the previous timestep such that

$$v_{avg,k} = \frac{v_k + v_{k-1}}{2}. \quad (8)$$

An additional term is needed to account for grade forces. Force due to grade is found to be

$$F_{grade} = Mg\alpha. \quad (9)$$

To simplify the calculation, the sine of the road grade angle is approximated as the road grade  $\alpha$  (expressed a decimal) via small angle approximation. Finally, aerodynamic drag is expressed as

$$F_{aero} = \frac{1}{2}\rho C_D A_f v_{avg}^2, \quad (10)$$

where  $\rho$  is air density. The road load forces are thus

$$F_{rl} = F_{rr} + F_{grade} + F_{aero}. \quad (11)$$

Knowing the road load forces and the desired acceleration allows for simple computation of the tractive effort required at the wheel. Positive or negative tractive power indicates whether the vehicle is in propel mode (where power flows from the high-voltage battery to wheels) or brake mode (power flows from the wheels to the battery). Tractive power is expressed as

$$P_{tr} = F_{tr} v_{avg}. \quad (12)$$

Figure 2 is a visualization of the calculation steps within the BEV tractive effort model for backward modeling of power at the wheel using a predetermined velocity curve as an input. A continuous velocity function is sampled at discrete steps to produce an input for a 10 Hz simulation of the tractive effort needed to maintain such a velocity profile. The model is compatible with any discretely sampled velocity profile of any drive cycle irrespective of sample rate. Given the velocities at the current and previous timestep, average velocity is used to model instantaneous tractive effort. For the initial timestep,

$v_{avg}$  is assumed to be equal to initial speed  $v_0$ , which is consistent with the decel phase starting after a period of constant-speed cruising.

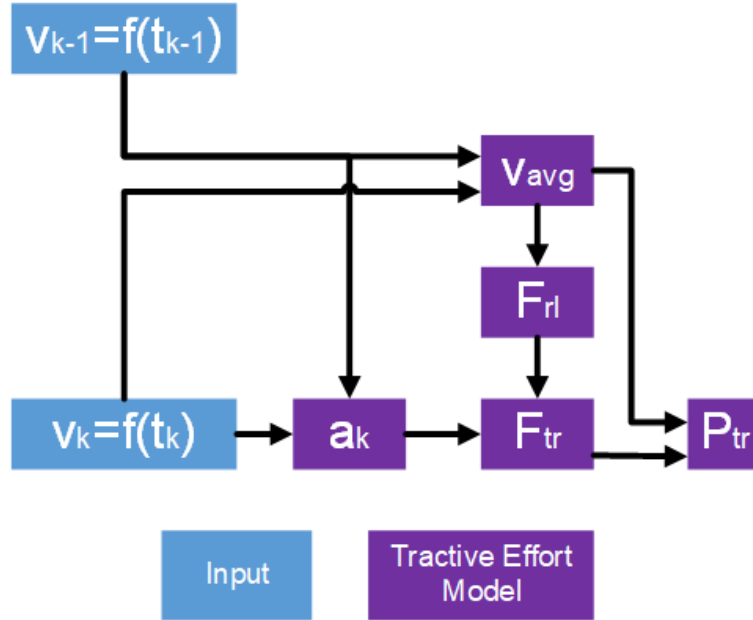


Figure 2: Tractive Effort Model Calculations

Conversely, prescribing a known or desired tractive effort enables calculation of the resulting acceleration and velocity profile. Such a forward model, which produces a velocity profile as an output, enables simulation of alternatives to regenerative braking. However, knowledge of powertrain performance and requisite battery energy is also necessary for such a study.

### Powertrain Model

A bidirectional powertrain model capable of both backward (wheel-to-powertrain) and forward (powertrain-to-wheel) modeling of power flow is created based on Willans Line models of key drivetrain components. Positive power is defined as flowing downstream from the high-voltage (HV) battery pack towards the wheels, and negative power as flowing upstream from the wheels towards the pack. Figure 3 illustrates the BEV powertrain model that forms the basis of this study.



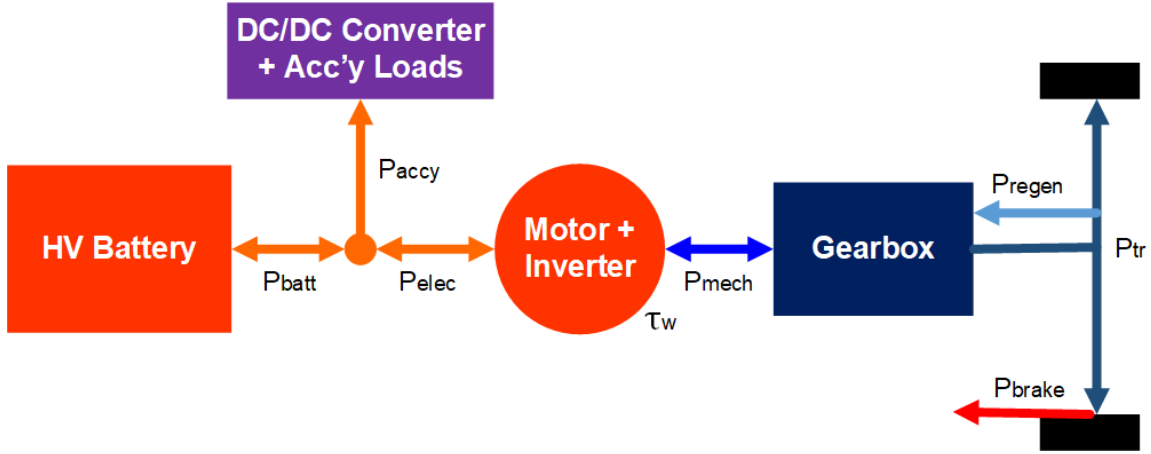


Figure 3: Bidirectional BEV powertrain model

Unlike the model presented in [22], the motor/inverter system and gearbox are modeled as separate entities. Each has its own bidirectional Willans Line model, but the series combination forms an overall Willans Line model like the one that is formed in [22]. The HV bus is represented by a node connecting the battery, motor-inverter system, and accessory loads. The DC/DC converter, a common component in BEVs, steps HV power down to the voltage required to feed vehicle accessory loads. The model also includes consideration for regen braking by dividing negative tractive power into two components. In a backward model of powertrain components, upstream power is a function of the power required downstream. Different Willans Lines, however, must be used depending on whether the vehicle is in propel or brake mode. Figure 4 illustrates the calculation steps needed to find the power being transferred through the BEV, including at the HV battery pack. The drive mode (propel or brake, denoted by the sign of  $P_{tr}$ ) dictates which set of equations is used to calculate power throughout the powertrain.

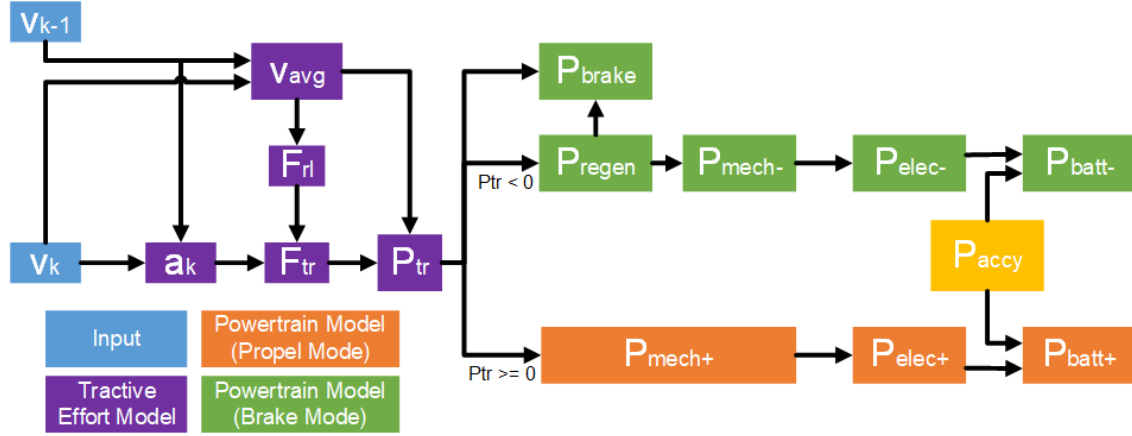


Figure 4: BEV Powertrain Modeling Step Given Required Tractive Power

Figure 5 shows the flow of power when the vehicle is in propel mode.  $P_{tr}^+$ , the desired tractive effort at the wheel when the vehicle is in propel mode, is assumed to be the power output by the gearbox.  $P_{mech}^+$  is found to be

$$P_{mech}^+ = \frac{1}{\eta_{gb}} P_{tr}^+ + P_{loss,gb}, \quad (13)$$

where  $\eta_{gb}$  and  $P_{loss,gb}$  are the marginal efficiency and offset loss of the gearbox, respectively. Since  $\eta_{gb}$  is less than unity and  $P_{loss,gb}$  is greater than zero,  $P_{mech}^+$  is greater than what is ultimately delivered to the wheels.

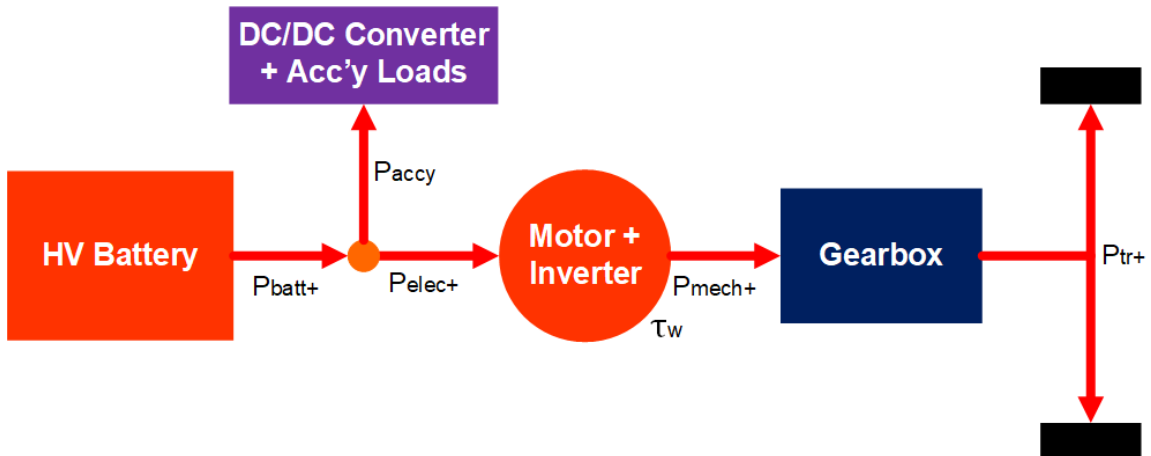


Figure 5: Propel Mode Power Flow

$P_{mech}^+$  is assumed to also be the output of the electric traction motor. Since the motor is modeled separately from the gearbox, motor speed and torque can be derived from  $P_{mech}^+$ .

$$\omega = v_{avg} * NPV, \text{ and} \quad (14)$$

$$\tau = \frac{P_{mech}}{\omega}. \quad (15)$$

Equation 14 yields motor speed in RPM when  $v_{avg}$  is expressed in mph.  $NPV$  is the ratio of motor speed to vehicle speed and has units  $\frac{RPM}{mph}$ . Equation 15 yields motor torque in Nm when  $P_{mech}$  is in watts and  $\omega$  is in terms of rad/s. Motor torque is calculated the same irrespective of vehicle drive mode. The motor is paired with an inverter that receives DC power from the high-voltage bus. The required HV power,  $P_{elec}^+$ , is expressed as

$$P_{elec}^+ = \frac{1}{\eta_{mot}} P_{mech}^+ + P_{loss,mot}, \quad (16)$$

where  $\eta_{mot}$  and  $P_{loss,mot}$  are the motor marginal efficiency and offset loss, respectively. For the purposes of this study,  $P_{accy}$ , the power required to feed the DC/DC converter and accessory loads is constant. Therefore, power draw from the battery pack for propel mode is

$$P_{batt}^+ = P_{elec}^+ + P_{accy}. \quad (17)$$

Figure 6 outlines the flow of power through the powertrain when the vehicle is in braking mode.

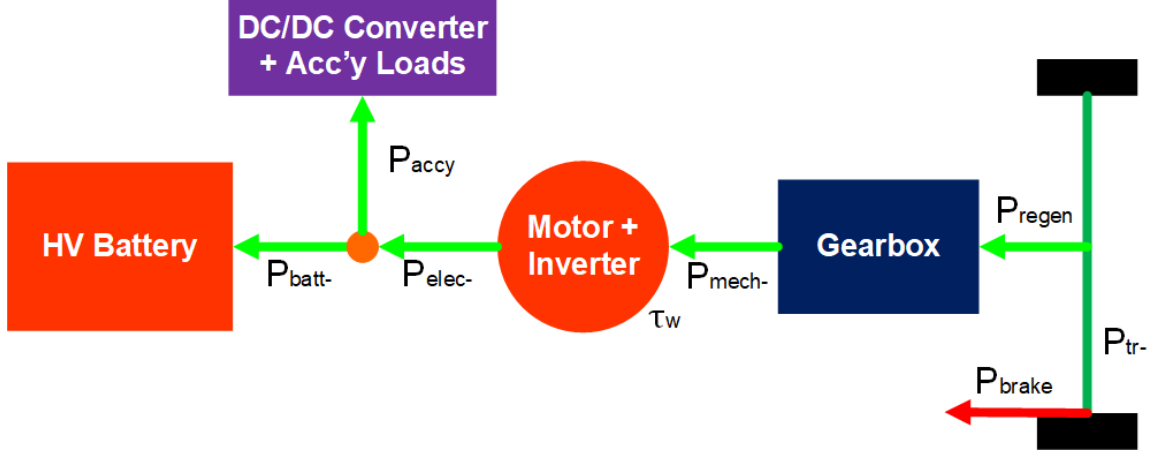


Figure 6: Brake Mode Power Flow

Negative tractive power  $P_{tr}^-$  is divided into two components-  $P_{brake}$ , the braking power absorbed by a traditional friction braking system, and  $P_{regen}$ , the power to be converted back into electrical power for charging the battery pack via the electric powertrain. The need for this split is documented in [26], and the method for doing so is outlined in [21].

$P_{regen}$  is calculated as

$$P_{regen} = \begin{cases} \varphi P_{tr}^-, \varphi P_{tr}^- \geq P_{cutoff} \\ P_{cutoff}, \varphi P_{tr}^- < P_{cutoff} \\ 0, v \leq v_{cutoff} \end{cases} \text{ IFF } v > v_{cutoff}, \quad (18)$$

where  $\varphi$  is the regen fraction and  $P_{cutoff}$  is the maximum amount of power allowed to regenerate through the powertrain.  $P_{regen}$  may also be limited based on the speed of the vehicle. A cutoff speed  $v_{cutoff}$  eliminates regenerative braking below a set speed for efficiency or performance regions. Thus, the equation for power absorbed by the friction brakes is

$$P_{brake} = P_{tr}^- - P_{regen}. \quad (19)$$

The method for calculating  $P_{mech}^-$  is like the propel case. However, the slope of the Willans Line is just the marginal efficiency of the gearbox.  $P_{mech}^-$  is calculated as

$$P_{mech}^- = \eta_{gb} P_{regen} + P_{loss,gb}. \quad (20)$$

As power flows back through the gearbox from the wheels, the magnitude decreases (i.e., less negative since  $P_{regen}$  is presumed to be negative) due to losses and the accessory load.  $P_{elec}^-$  and  $P_{batt}^-$  are calculated in a similar manner as  $P_{mech}^-$ :

$$P_{elec}^- = \eta_{mot} P_{mech}^- + P_{loss,mot}, \text{ and} \quad (21)$$

$$P_{batt}^- = P_{elec}^- + P_{accy}. \quad (22)$$

Since the magnitude of power regenerated into the powertrain decreases due to inefficiencies and accessory loads, some values of  $P_{regen}$  may result in  $P_{batt}^-$  being positive. In those cases, the negative tractive power at the wheel  $P_{tr}^-$  may be better dissipated through the friction brakes.

Energy in this model is calculated at each timestep  $k$  such that

$$E_k = E_{k-1} + P_k(t_k - t_{k-1}). \quad (23)$$

Figure 7 uses two Sankey diagrams to illustrate the energy balances for the propel and brake modes. Propel mode requires energy flow from the battery to the wheel for tractive effort, and brake mode allows for negative tractive effort at the wheel to be regenerated into electrical energy for storage in the HV battery pack. As stated in Appendix A, there may be some conditions where the magnitude of negative tractive energy is less than the magnitude of energy lost to friction braking, gearbox losses, motor losses, and accessory loads. In such an edge case, the battery is not recharged. Rather, battery discharge is required to meet accessory energy needs.

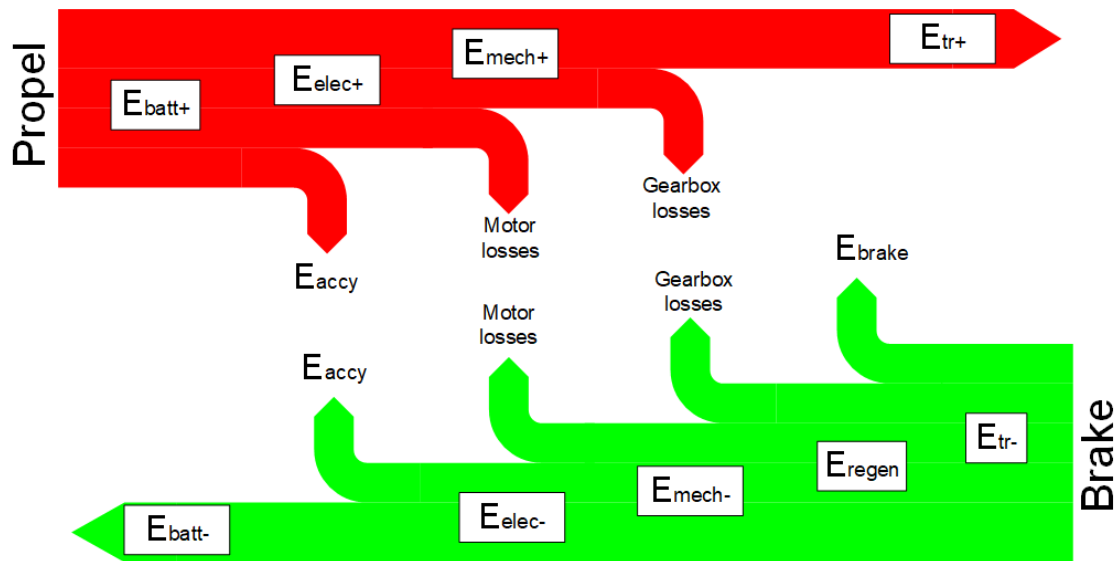


Figure 7: BEV Model Energy Balance, Propel and Brake Modes

### Vehicle Overview

The model can simulate the performance of any BEV with publicly available emissions and road load test results. In this study, the fuel economy and road load parameters of the 2019 Nissan LEAF® SV/SL are sourced from the EPA and applied to the BEV vehicle model. Table 1 displays the ABC coefficients and fuel economy data for configuration 0 of the LEAF® SV/SL trimlines [27]. The test mass and ABC coefficients are reported by the EPA in Imperial units, but they are displayed here in SI units for consistency. Vehicle fuel economy is tested over the EPA Urban Dynamometer Driving Schedule (UDDS) and Highway Fuel Economy Test (HWFET) drive cycles and reported in miles per gallon equivalent (MPGe), an alternative fuel economy measurement for electrified vehicles.

Table 1: 2019 Nissan LEAF® SV/SL Road Load and Powertrain Parameters

Parameter	Value [units]
$A$	135.0 [N]
$B$	3.185 [N/(m/s)]
$C$	0.4363 [N/(m/s <sup>2</sup> )]
$M_t$	1928 [kg]
UDDS Fuel Economy	162.6 [MPGe]
HWFET Fuel Economy	220.7 [MPGe]

Using the standard 33.7 kWh/gal conversion from MPGe to AC Wh/mi and the reported charge efficiency for each drive cycle from [28], battery energy consumption in terms of DC Wh/mi is found for the UDDS and HWFET tests. A Willans line is fit to the EPA city and highway fuel consumption by [29] using a method like the one proposed in [22]. Table 2 shows the combined Willans Line powertrain model parameters.

Table 2: 2019 Nissan LEAF® SV/SL Overall Willans Line Parameters

Parameter	Value [units]
$\eta_{marg}$	0.933
$P_{offset}$	116.9 [W]

Substituting Equations 13 for  $P_{mech}^+$  in Equation 14 yields the combined Willans Line function in terms of gearbox and motor parameters:

$$P_{elec}^+ = \frac{1}{\eta_{gb}\eta_{mot}} P_{tr}^+ + \left( \frac{P_{loss,gb}}{\eta_{mot}} + P_{loss,mot} \right) = \frac{1}{\eta_{marg}} P_{tr}^+ + P_{offset}. \quad (24)$$

Assuming gearbox parameters  $\eta_{gb} = 0.98$  and  $P_{loss,gb} = 0.1 \text{ kW}$ , the motor parameters  $\eta_{mot}$  and  $P_{loss,mot}$  are solved for. Applying Equations 4, 5, and 6 to the ABC coefficients yields the normalized road load coefficients. Table 3 lists the LEAF® parameters for the tractive effort and powertrain models. For this case, vehicle mass  $M$  is equal to  $M_t$ .  $v_{cutoff}$  is the speed at which regen braking is turned off; all braking below that speed is

done with friction brakes. The implementation of this is addressed in a later chapter. Table 4 lists the physical constants also govern the tractive effort model.

Table 3: Complete 2019 Nissan LEAF® Vehicle Parameters

Parameter	Value [units]
$C_{rr0}$	7.14e-3
$C_{rr1}$	1.684e-4 [1/(m/s)]
$C_D A_f$	0.727 [m <sup>2</sup> ]
$M_t$	1928 [kg]
$\eta_{gb}$	0.98
$P_{loss,gb}$	100 [W]
$\eta_{mot}$	0.952
$P_{loss,mot}$	12 [W]
$\varphi$	0.94
$P_{accy}$	302 [W]
$P_{cutoff}$	-60 [kW]
$NPV$	112.5 [rpm/mph]
$f_i$	1.04
$v_{cutoff}$	5 [mph]

Table 4: Physical Constants for Vehicle Model

Parameter	Value [units]
$\rho$	1.2 [kg/m <sup>3</sup> ]
$g$	9.81 [m/s <sup>2</sup> ]

The parameter values in Tables 3 and 4 are applied to the combined tractive effort-powertrain model, UDDS and HWFET drive cycle velocity profiles are used as inputs, and tractive energy requirements are modeled using a 1 Hz simulation. Energy consumption at the battery is calculated to verify the accuracy of the powertrain model. The net tractive energy required is found for each drive cycle by adding  $E_{tr}^+$  and  $E_{tr}^-$ , and net battery energy consumption is found for each drive cycle by adding  $E_{batt}^+$  and  $E_{batt}^-$ . Averaging net tractive energy and net battery energy over the length of the drive cycles yields energy



consumption in terms of Wh/mi. Table 5 compares the EPA-reported energy consumption to the energy consumption results obtained for the same drive cycles from the tractive effort and powertrain models.

Table 5: Modeled vs. Reported Energy Consumption, 2019 Nissan LEAF® SV/SL

	UDDS	HWFET
Distance [mi]	7.45	10.3
$E_{tr}^+$ [kWh]	1.79	2.24
$E_{tr}^-$ [kWh]	-0.873	-0.261
$E_{tr,net}$ [kWh]	0.913	1.98
Net Tractive Energy Consumption [Wh/mi]	122.6	193.3
$E_{batt}^+$ [kWh]	2.02	2.48
$E_{batt}^-$ [kWh]	-0.702	-0.217
$E_{batt,net}$ [kWh]	1.32	2.27
Net Battery Energy Consumption [DC Wh/mi]	177.4	220.9
Reported Net Battery Energy Consumption [DC Wh/mi]	181.2	220.8
% Error	-2.1%	<0.1%

The model underestimates energy consumption during the UDDS drive cycle, and it almost exactly predicts energy consumption over the HWFET cycle. These results are close to the results reported in [22] with respect to percent difference between modeled and EPA-reported battery energy consumption. This margin is acceptable for energy consumption estimation of other velocity profiles.

## Chapter 4: Decel Solution Simulation

Studying vehicle performance during both cruise and decel phases of a drive cycle is vital for comparing decel strategies with different average accelerations and stopping distances. A basic drive cycle hill is formed by appending a distance covered at given cruise speed to the distance covered as the vehicle slows down such that

$$x_{tot} = x_{f,cruise} + x_{f,decel}. \quad (25)$$

where  $x_{tot}$  is constant for all decel strategy simulations at the same cruise speed. The distance over which the vehicle decelerates depends on the average deceleration rate of the decel strategy, so each strategy requires different cruising distances.

### *Decel Velocity Curve Fundamentals*

Average acceleration (or deceleration in this case) directly affects both the distance needed to come to a complete stop and the travel time required. A basic velocity profile is expressed in terms of the quadratic

$$v(t) = C_2 t^2 + C_1 t + C_0. \quad (26)$$

Assuming decel begins at time  $t = 0$  and ends at  $t = t_f$ , the distance covered during the decel is expressed as

$$x_{f,decel} = \int_0^{t_f} v(t) dt = \left[ \frac{C_2}{3} t_f^3 + \frac{C_1}{2} t_f^2 + C_0 t_f + D \right] - D = \frac{C_2}{3} t_f^3 + \frac{C_1}{2} t_f^2 + C_0 t_f, \quad (27)$$

where D is the initial condition  $x_0$ . Average velocity is similarly found:

$$v_{avg} = \frac{1}{t_f} \int_0^{t_f} v(t) dt = \frac{\frac{C_2}{3} t_f^3 + \frac{C_1}{2} t_f^2 + C_0 t_f}{t_f} = \frac{C_2}{3} t_f^2 + \frac{C_1}{2} t_f + C_0 = \frac{x_{f,decel}}{t_f}. \quad (28)$$

Acceleration is the derivative of velocity with respect to time such that

$$a(t) = 2C_2 t + C_1 \quad (29)$$

and average acceleration is

$$a_{avg} = \frac{1}{t_f} \int_0^{t_f} a(t) dt = \frac{[C_2 t_f^2 + C_1 t_f + C_0] - C_0}{t_f} = \frac{[C_2 t_f^2 + C_1 t_f]}{t_f} = C_2 t_f + C_1. \quad (30)$$

If the decel curve is linear, and thus  $C_2 = 0$ , acceleration is constant throughout the decel period. Dib et al. derived a particular velocity trajectory solution in [30] as a baseline for an analytical solution and numerical implementation for an eco-driving optimal control problem. The second order solution is a function of  $v_0$ ,  $v_f$ ,  $x_f$ , and  $t_f$  such that

$$v^*(t) = v_0 - \frac{4v_0 t}{t_f} - \frac{2v_f t}{t_f} - \frac{6x_f t^2}{t_f^3} + \frac{6x_f t}{t_f^2} + \frac{3v_0 t^2}{t_f^2} + \frac{3v_f t^2}{t_f^2}. \quad (31)$$

Expressing Equation 31 in terms of the standard quadratic coefficients in Equation 26 yields

$$C_2 = -\frac{6x_f}{t_f^3} + \frac{3v_0}{t_f^2} + \frac{3v_f}{t_f^2}, \quad (32)$$

$$C_1 = -\frac{4v_0}{t_f} - \frac{2v_f}{t_f} + \frac{6x_f}{t_f^2}, \text{ and} \quad (33)$$

$$C_0 = v_0. \quad (34)$$

The impact of decel curve order is evaluated by comparing a simple linear decel trajectory from 25 mph (11.2 m/sec) to zero with two quadratic solutions. For fair comparison, average acceleration is held constant across all velocity curves, and a moderate decel rate of  $-1.5 \text{ m/sec}^2$  is used. Substituting Equations 32 and 33 into Equation 30 and simplifying yields

$$\frac{-11.2 \text{ m/sec}}{t_f} = -1.5 \text{ m/sec}^2, \quad (35)$$

so  $t_f = 7.45 \text{ sec}$ . Since  $C_0$  is constrained to be the initial speed of the vehicle, a range of decel solutions with this average acceleration can be derived by varying the values of  $C_2$  and  $C_1$ , which directly relate to decel distance  $x_f$ . This set of possible solutions is limited by two constraints: first, that the vehicle should not exceed the initial speed at any time;

and second, that the initial acceleration at  $t_0$  should not exceed  $-2.5 \text{ m/sec}^2$ . This latter constraint is based on consumer appeal research in [31]. The first constraint means  $C_1$  cannot be positive, so the first decel curve is found by making that term equal to zero. The second quadratic is found by letting  $C_1 = -2.5$ , the maximum initial acceleration. The final distance  $x_f$  for each case can be calculate using Equation 32 or Equation 33. Table 6 lists the parameters and acceleration statistics for the solutions.

Table 6: Basic Decel Curves

	$t_f = 7.45 \text{ sec}, a_{avg} = -1.5 \text{ m/sec}^2$					
	$C_2 \left[ \frac{m}{sec^3} \right]$	$C_1 \left[ \frac{m}{sec^2} \right]$	$C_0 \left[ \frac{m}{sec} \right]$	$x_f [m]$	$a_{max} \left[ \frac{m}{sec^2} \right]$	$a_{min} \left[ \frac{m}{sec^2} \right]$
Linear	0	-1.50	11.2	41.6	-1.50	-1.50
Quadratic 1	-0.201	0	11.2	55.5	0	-2.99
Quadratic 2	0.134	-2.50	11.2	32.4	-0.503	-2.50

Figure 8 is a plot of the three decel solutions. The linear case requires a moderate length stopping distance, but the vehicle would be constantly decelerating at  $-1.5 \text{ m/sec}^2$  for the whole decel period. Quadratic 1 is advantageous because it minimizes jerk between the decel period and a hypothetical constant speed case. However, the shape of the curve suggests the deceleration occurs over a longer distance than the other two solutions. The maximum acceleration of this solution is  $-2.99 \text{ m/sec}^2$ , and although it occurs at low speeds, it is outside of the bounds for low-speed accelerations observed in [31]. Quadratic 2 enables the vehicle to stop in a shorter distance than the linear curve, but requires a larger initial deceleration,  $-2.5 \text{ m/sec}^2$ .

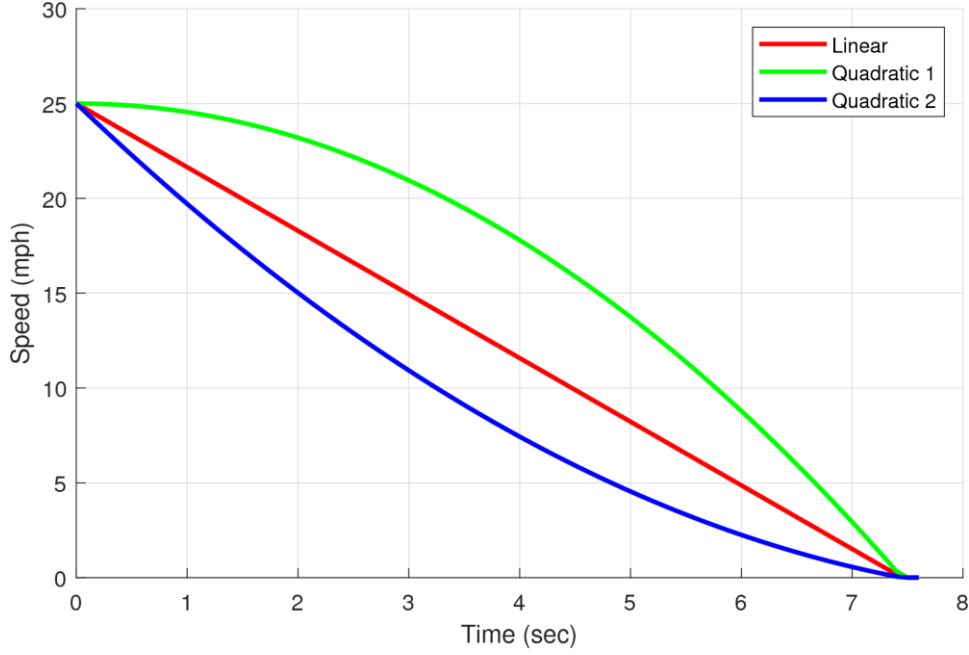


Figure 8: Basic Decel Solutions

### Tractive Power and Energy

An important consideration for designing a BEV decel strategy is the brake energy available for regenerative braking. More brake energy during a decel event ostensibly means there is more energy available to regenerate into stored battery energy. Rearranging Equation 1 and substituting for  $F_{tr}$  in Equation 12 gives the tractive power required at the wheel during the decel stage as

$$P_{tr} = (f_i Ma - F_{rl})v_{avg}. \quad (36)$$

Figure 9 documents the change in  $P_{tr}$  over the course of the decel event for each trajectory with the 2019 Nissan LEAF® road load parameters applied. Since the vehicle is braking, tractive power is negative. Inertial power, the product of  $f_i Ma$  and  $v_{avg}$ , is negative since the vehicle is decelerating. Road load, which always opposes vehicle motion, reduces the amount of tractive effort required at the wheel to slow down with acceleration  $a$ . A BEV following the Linear or Quadratic 2 decel experiences maximum braking power at  $t_0$  due to inertial power of also being the greatest magnitude at that

point. However, braking power for the Quadratic 1 curve reaches its greatest magnitude in the middle of the decel event. Despite road load power decreasing with speed, inertial power grows in magnitude as acceleration becomes more negative, then reaches a minimum and approaches zero as velocity decreases.

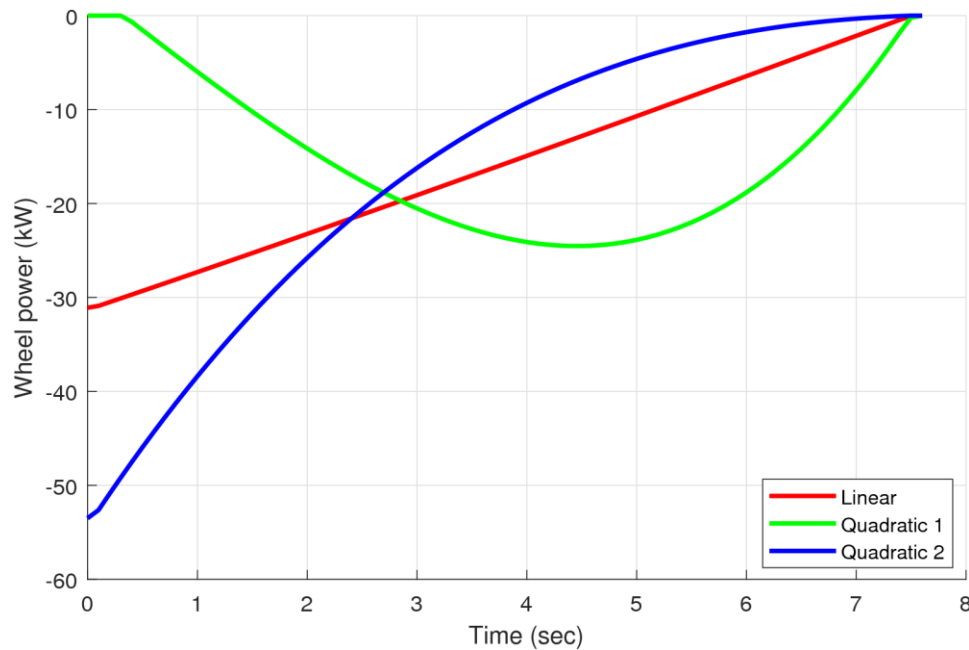


*Figure 9: Tractive Power vs. Time for Several Decel Curves*

Just as the area under the curves in Figure 8 represent the distance each decel trajectory requires, the space between these curves and the x-axis show how braking energy accumulates over the course of each decel event. Figure 10 summarizes the distance and brake energy requirements for a Nissan LEAF® following each of these decel curves. There is only a 20-meter difference between the shortest and longest decel, and all three only required about 30 Wh of braking energy. The Quadratic 1 decel curve accumulates the least amount of braking energy, which could be due to higher road load over the longer distance traveled with respect to the other two solutions. Since the two quadratic curves define the bounds of possible solutions for this travel time, initial speed, and average acceleration given other constraints, other quadratic solutions likely fall within

those two with respect to distance. They also probably require about 30 Wh of braking energy.

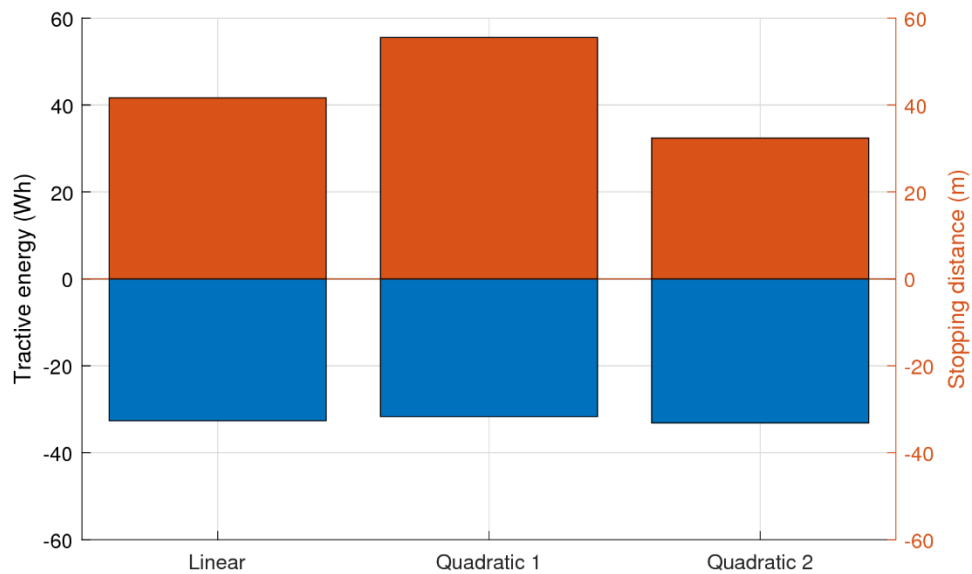


*Figure 10: Decel Distance and Tractive Energy*

The linear decel solution requires a moderate stopping distance and minimizes jerk (the rate of change of acceleration), which is advantageous from a consumer appeal perspective. It is also much simpler to calculate decel time and distance for a linear function than quadratic ones. Therefore, since there is also no advantage with respect to brake energy for considering quadratic decel solutions, this study only assesses regenerative braking along linear velocity curves.

A decel case for a potential urban drive cycle, slowing down from 25 mph to a stop at an intersection with regenerative braking, is considered. Figure 11 identifies the different distances needed to stop at other constant decel rates. As explained in [31], harsh braking may not be appealing to consumers in most situations except when minimal stopping distance is necessary.

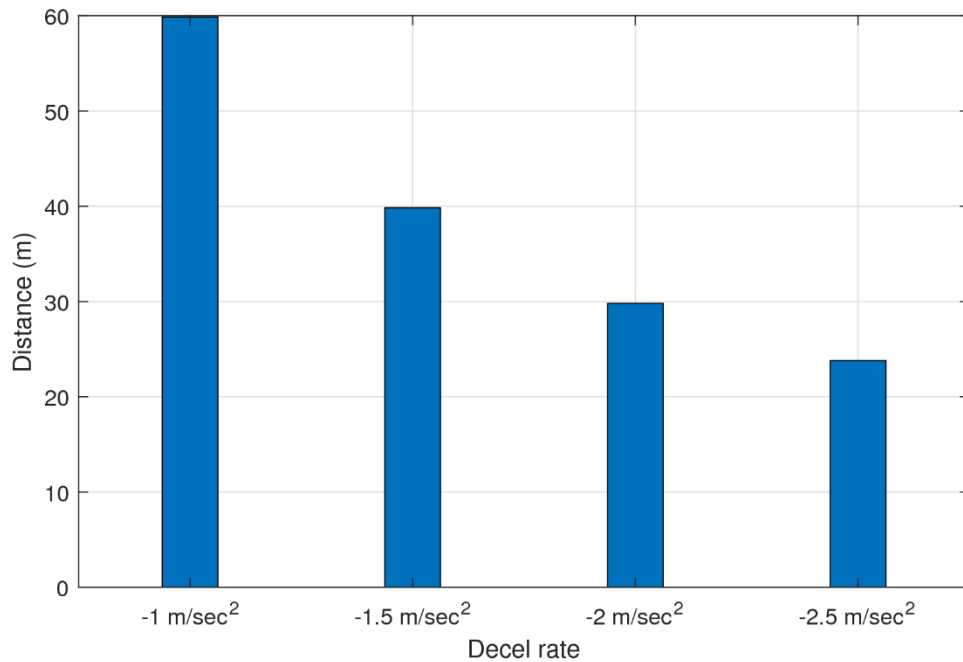


*Figure 11: Stopping distances from 25 mph for linear decel profiles*

Figure 12 illustrates the distance and time to stop for two of the linear velocity profiles with constant accelerations. The -1.5 m/sec<sup>2</sup> case represents moderate braking, and -2.5 m/sec<sup>2</sup> is a harsher braking event. In this case, increasing the braking decel rate from 1.5 to 2.5 m/sec<sup>2</sup> reduces both travel time and braking distance by 40%.

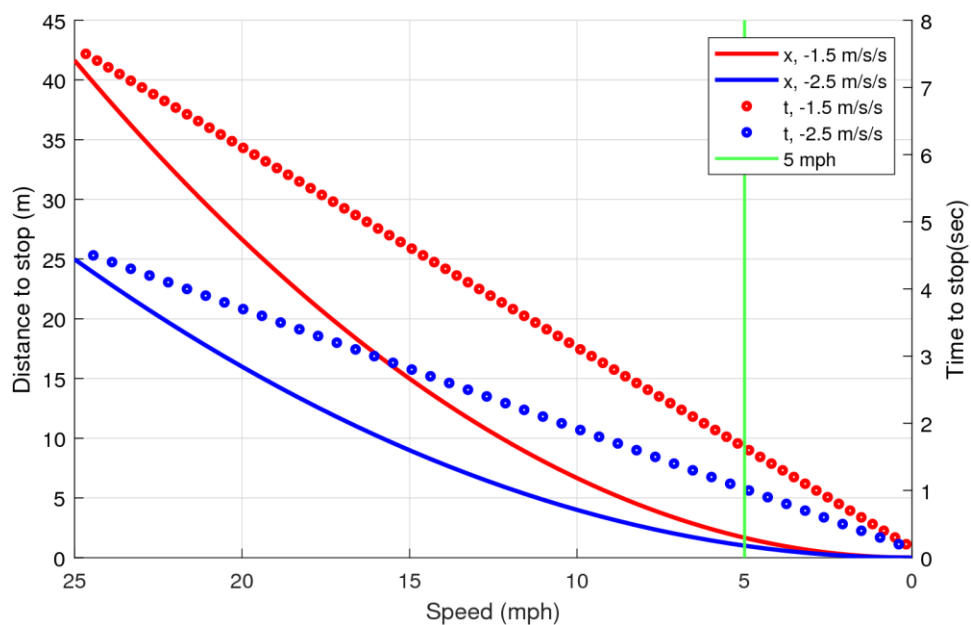


*Figure 12: Distance- and Time-to-Stop from 25 mph*



### *Energy Capture with Regen Braking*

Understanding powertrain performance over a range of decel rates is important to determine whether harsher braking events have any significant benefit with respect to energy regeneration. For a set of linear deceleration profiles from 25 mph to zero speed using the decel rates in Figure 12,  $P_{tr}$  is calculated and used as an input for the BEV tractive effort-powertrain model configured with parameters for the 2019 Nissan LEAF® SV/SL. Electrical energy that returns to the high-voltage bus via the inverter ( $E_{elec}^-$ ) is compared to braking energy  $E_{tr}^-$ . For this ideal case, the regen brake fraction  $\phi$  is 1 and no regen cutoff speed is used so that regen braking is assessed under ideal conditions. Figure 13 shows the electrical energy regenerated compared to the tractive energy at the wheel for the decel cases shown in Figure 12. Powertrain efficiency, the ratio of instantaneous electrical power to available tractive power, remains above 92% until low speeds in both cases. Despite the difference in decel rate, each decel event results in about 30 Wh of energy being regenerated to the HV bus, which is 93% of the available tractive energy available for both scenarios.

Factoring in the accessory load  $P_{accy}$ , the energy that recharges the battery pack is shown in Figure 14. Accessory loads reduce the magnitude of battery recharge power, which results in less energy available to charge the battery pack than what enter the HV bus. Notably, by the time the vehicle reaches 5 MPH, 96% of  $E_{batt}$  is already back in the pack.

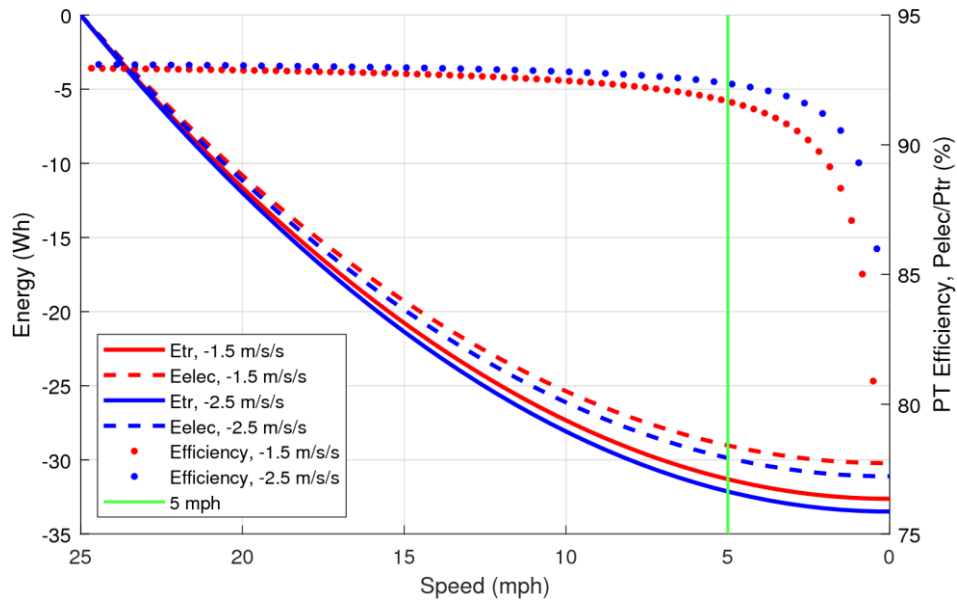


Figure 13: Powertrain energy and efficiency

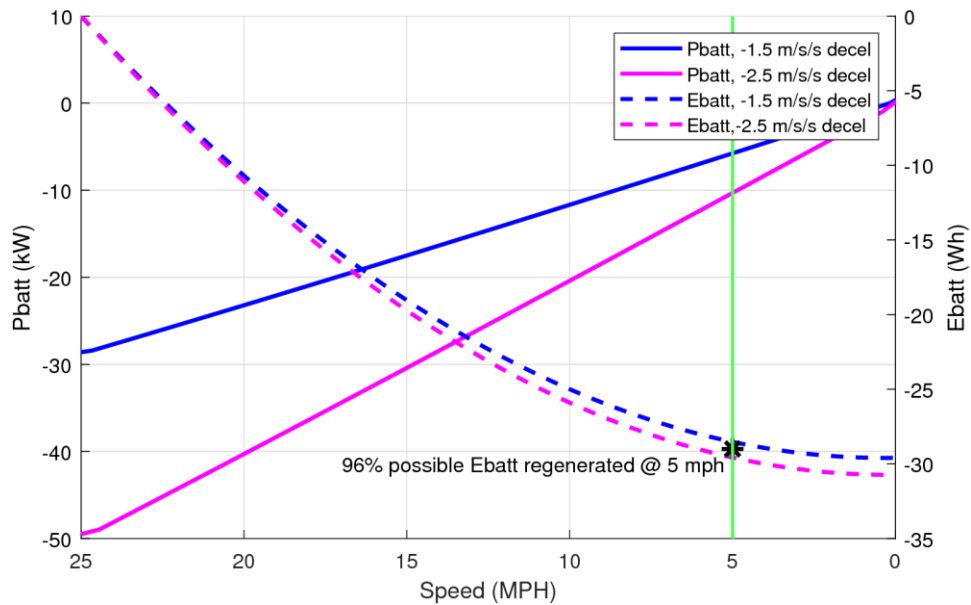
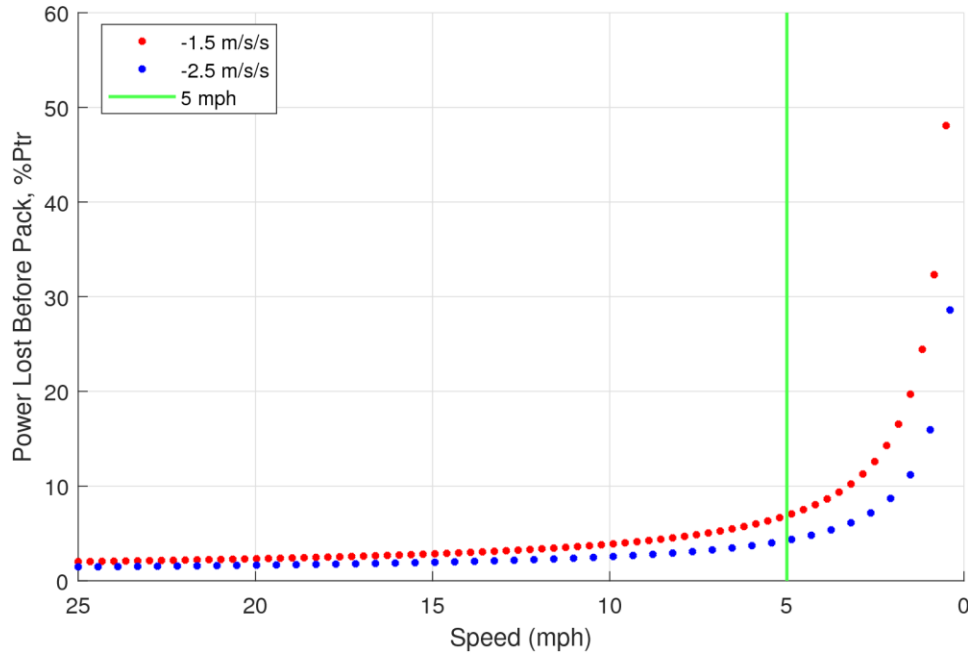


Figure 14: Battery power and energy over regen braking event

The constant reduction in power due to required accessory loads increases the amount of power lost before it can reenter the battery pack. Figure 15 highlights the increase in losses before the pack with respect to  $P_{tr}$ . These losses are due to the regen brake fraction, accessory loads, and inefficiency in the motor, inverter, and gearbox. As the magnitude of tractive power required to adhere to the prescribed velocity profile

approaches zero, the amount of power lost before it reaches the battery pack increases exponentially. This trend is consistent with prior studies that note limited regenerative braking use at lower speeds due to efficiency reasons [13].



*Figure 15: Percent Tractive Power Lost Before Recharging Pack*

Accounting for realistic constraints on regen braking, Figure 16 displays the energy available for regen and what is ultimately stored in the battery pack using the four linear decel trajectories in Figure 11. Here, regen braking is modeled with the regen brake fraction and regen cutoff speed parameters from Table 3 applied. Overall, 10% of the total brake energy is lost within the gearbox, motor, and inverter; accessory loads also reduce the amount of energy that returns to the battery. Despite stopping distance varying by over 35 meters, the tractive energy required for each decel rate does not increase significantly as decel rate increases. The amount of energy regenerated into the pack varies similarly. Increasing the decel rate by a factor of 2.5 does not produce a similar increase in battery energy regeneration. The slight difference is most likely due to the higher decel rates reducing road load losses by lowering stop distance. Decel rate is most

correlated to tractive and battery power, the rate at which energy is regenerated into the battery pack. Increasing decel rate also does not significantly affect powertrain efficiency. Factoring in regen fraction and low-speed cutoff, around 85% of brake energy ends up as stored electrical energy in the HV battery.

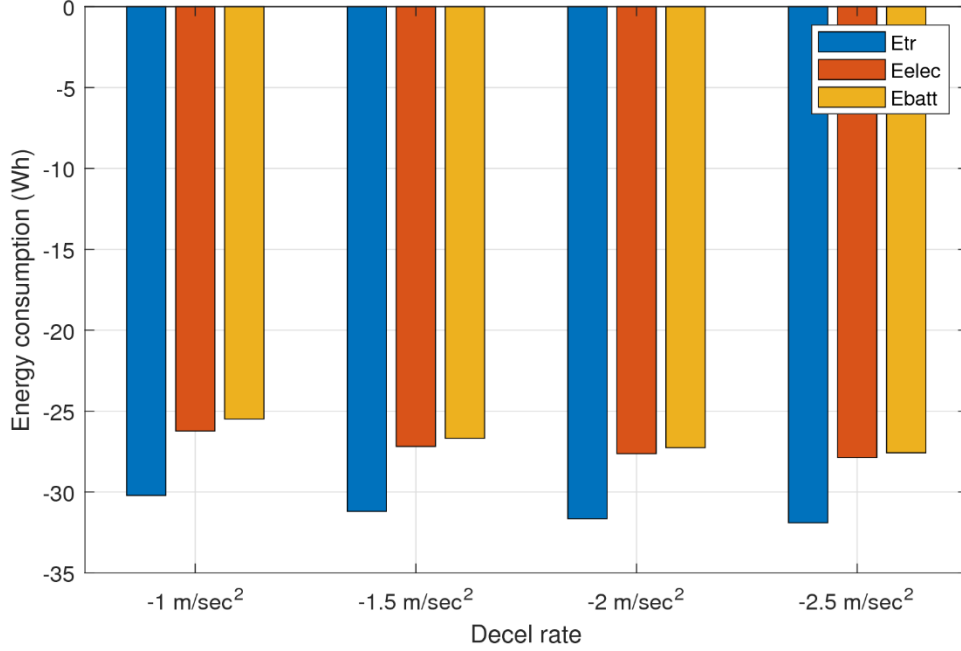


Figure 16: Energy availability and capture, 25 mph-0mph

### Coasting as a Decel Mode

Coasting, the state in which a vehicle is only decelerating due to road load forces, can be used by BEVs to come to a stop as an alternative to regenerative braking. Since there is zero tractive effort at the wheel, vehicle deceleration is exclusively caused by road load forces. A differential equation that governs coasting velocity is given in [32] as

$$\frac{dv_c}{dt} = \frac{-1}{2M} \rho C_D A_f v_c^2(t) - g c_r = -\alpha^2 v_c^2(t) - \beta^2. \quad (37)$$

In addition to aerodynamic losses, rolling resistance is assumed to be constant. Solving the ordinary differential equation yields the result

$$v_c(t) = \frac{\beta}{\alpha} \tan \left\{ \arctan \left( \frac{\alpha}{\beta} v_c(0) \right) - \alpha \beta t \right\}, \quad (38)$$

where  $v_c(0)$  is the initial speed. Since this study uses a three-term road load model, an analytical coasting solution based on a three-term road load function is required for validating the accuracy of a numerical coasting model and comparing coasting to other decel methods. An ordinary differential equation defining coasting speed in terms of a three-term road load function is given in [33] as

$$\frac{dv_c}{dt} = -(A_c + B_c v_c + C_c v_c^2). \quad (39)$$

The road load coefficients

$$A_c = \frac{g}{f_i} (C_{rr0} + \alpha), \quad (40)$$

$$B_c = \frac{g}{f_i} C_{rr1}, \quad (41)$$

$$C_c = \frac{\frac{1}{2}\rho C_D A_f}{f_i M}, \text{ and} \quad (42)$$

$$D_c = B_c^2 - 4A_c C_c \quad (43)$$

are based on the normalized ABC road load coefficients that are a part of the tractive effort model. Solving Equation 39 using the dsolve function in MATLAB® yields the coasting function

$$v_c(t) = v_c(0) - \frac{2(C_c v_c(0)^2 + B_c v_c(0) + A_c)}{B_c + 2C_c v_c(0) + \cot\left(\frac{t\sqrt{-D_c}}{2}\right)\sqrt{-D_c}}. \quad (44)$$

Figure 17 illustrates power flow through the powertrain when the BEV is using coast mode. To produce zero tractive effort at the wheel, the motor needs to output enough mechanical power to overcome gearbox losses. Thus, the battery pack supplies some electrical power to the motor and inverter via the HV bus in addition to accessory loads.

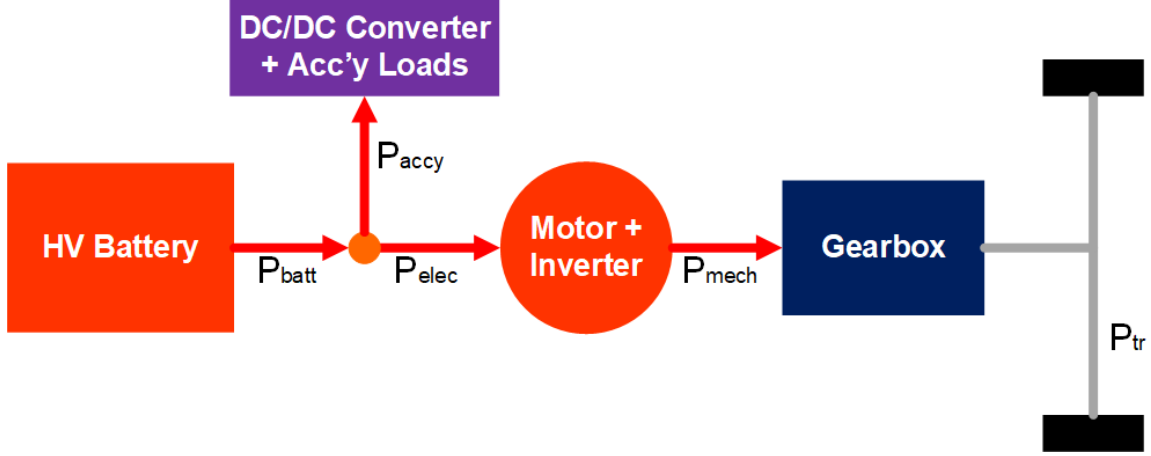


Figure 17: Power Flow, Coast Mode

The tractive effort model is used to produce a discrete-time numerical coasting solution.

Given  $F_{tr} = 0$ , Equation 1 is rearranged to find acceleration for every timestep  $k$ :

$$a_k = \left( \frac{F_{rL,k}}{f_i M} \right). \quad (45)$$

The velocity at the next timestep,  $v_{k+1}$ , is thus found to be

$$v_{k+1} = v_k + a_k(t_{k+1} - t_k). \quad (46)$$

Figure 18 outlines the calculation steps for finding vehicle trajectory and powertrain performance for coast mode. The red arrows indicate places where the tractive effort model is adapted to conduct forward modeling of vehicle speed. Instances where  $P_{tr} = 0$  are considered  $P_{tr}^+$  since positive electrical power is required to overcome inefficiencies and losses, so the powertrain is modeled as such. Even though the velocity profile is a forward model, powertrain performance is still based on the input  $P_{tr}^+$ . Motor torque, which is omitted from Figure 18, is based on average speed as seen in Equations 14-15 for all decel modes.

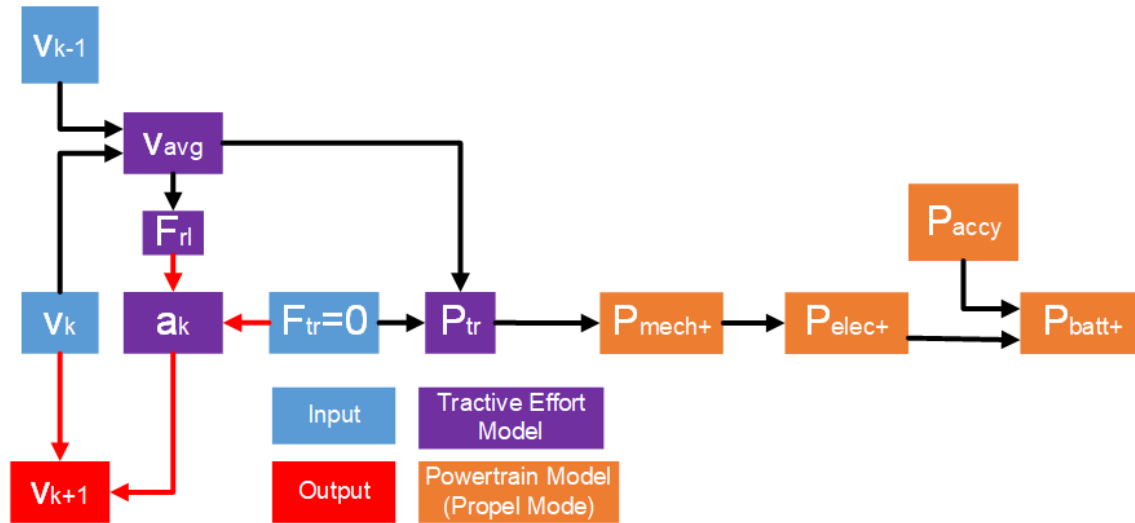


*Figure 18: Model Calculation Steps for Coasting*

Figure 19 displays the numerically calculated coasting profile from 60 mph to zero speed. During the first 100 seconds of coasting, the vehicle coasts down to 25 mph, and the curvature of the plot reflects the impact of aerodynamic drag at high speeds. Below 25 mph, decel is more linear. The numerically calculated coasting velocity profile has a close correlation with the analytical solution. The maximum residual observed is only 0.01 m/sec, demonstrating that the 10 Hz simulation can model vehicle speed while in coast mode within an acceptable margin of error.

The distance-to-stop calculation is based on integration of the discrete-time coasting velocity profile. Compared to the decel curves for regen braking in Figure 11, coasting results in a higher stopping distance and longer travel time. This behavior especially evident at low speeds, as shown in Figure 20. While it takes the vehicle less than 5 seconds to go from 5 mph to a stop when braking at  $-1.5 \text{ m/sec}^2$ , it takes a coasting vehicle over 30 seconds to slow down that same amount due to the miniscule road loads at low speeds.

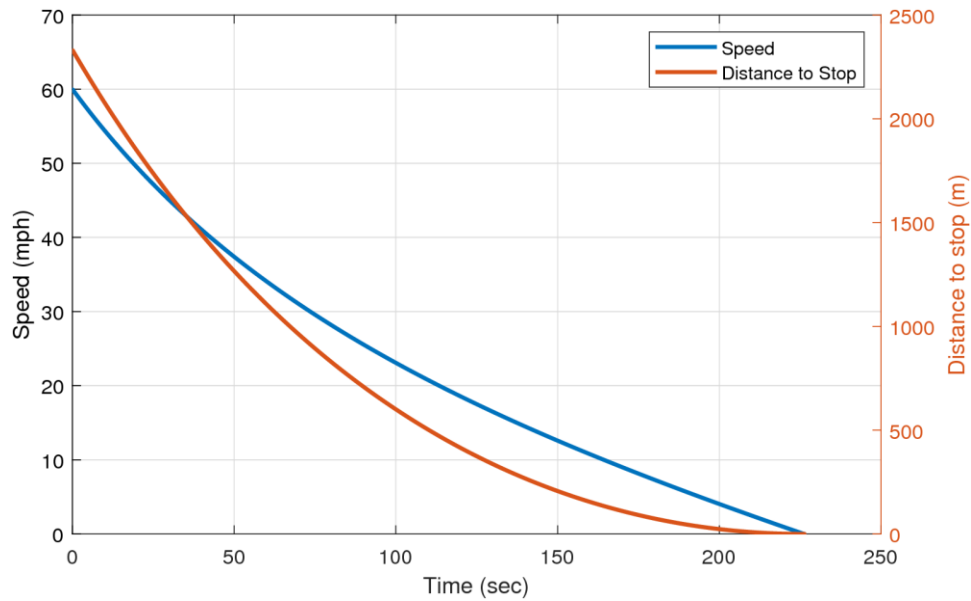


Figure 19: Coasting speed and distance to stop vs. time

In that time, the vehicle crawls a mere 35 meters. Just as powertrain performance makes regen braking unfeasible at slow speeds, slow decel rates caused by low road load make coasting an unattractive option when the vehicle is very close to zero speed.

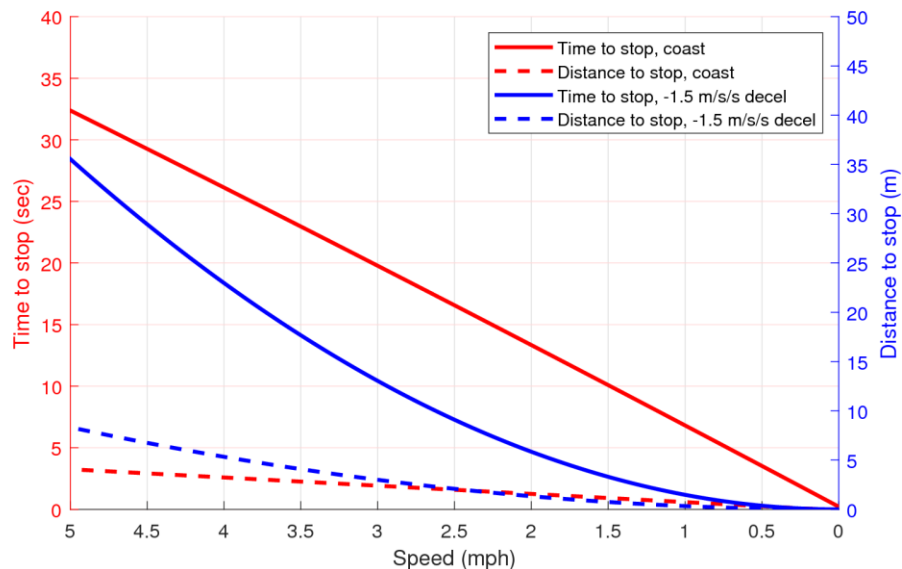


Figure 20: Time and Distance to Stop, Coasting vs. Regen

If the vehicle switches off coast mode in favor of friction braking at a low-speed threshold like 5 mph, travel time is reduced, but total distance is not significantly affected. Figure 21 documents the accumulation of distance and travel time starting at an initial speed of 60



mph. The lag between coast distance accumulation and travel time demonstrates the advantage of not coasting at low speeds. Switching off coast mode at 5 mph saves 15% of travel time while only reducing distance traveled by 5%. Even if coasting ends at 10 mph, total distance traveled only decreases by 10% while travel time is reduced by 30%.

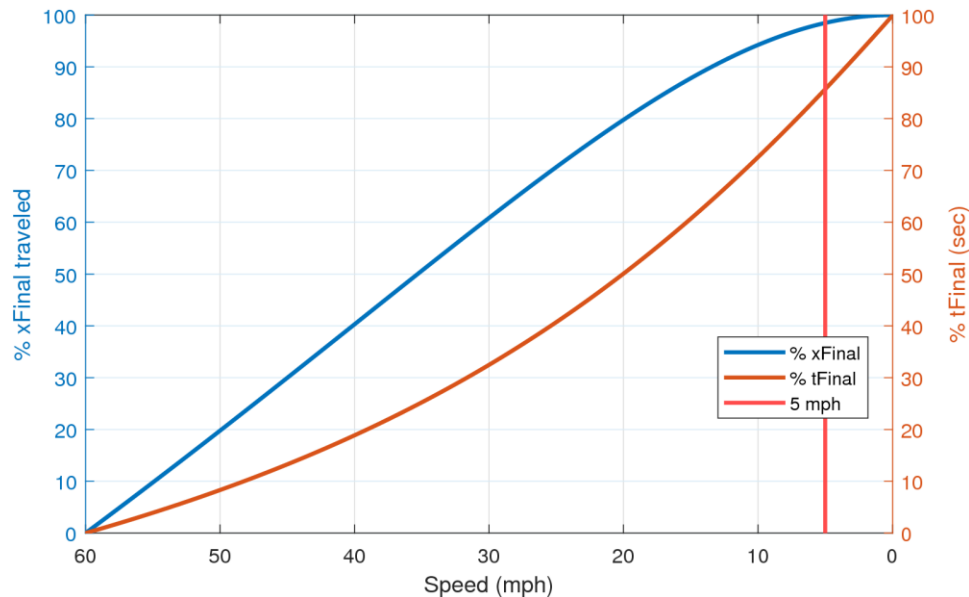


Figure 21: Coast Distance and Travel Time, Percentage of Final

### Pseudo-Coasting Decel Modes

Other methods of controlling the powertrain to decelerate the vehicle like coasting are presented. The term “pseudo-coasting” is used to refer to any drive mode that results in a similar velocity profile as coasting, but negative tractive effort at the wheel from powertrain inefficiency contributes to deceleration.

Figure 22 shows power flow through the powertrain when the vehicle uses a pseudo-coasting powertrain mode based on zero motor torque output to the gearbox. Using this zero mechanical power (ZPM) mode, the motor and inverter draw only enough power to compensate for the offset loss associated with those components.

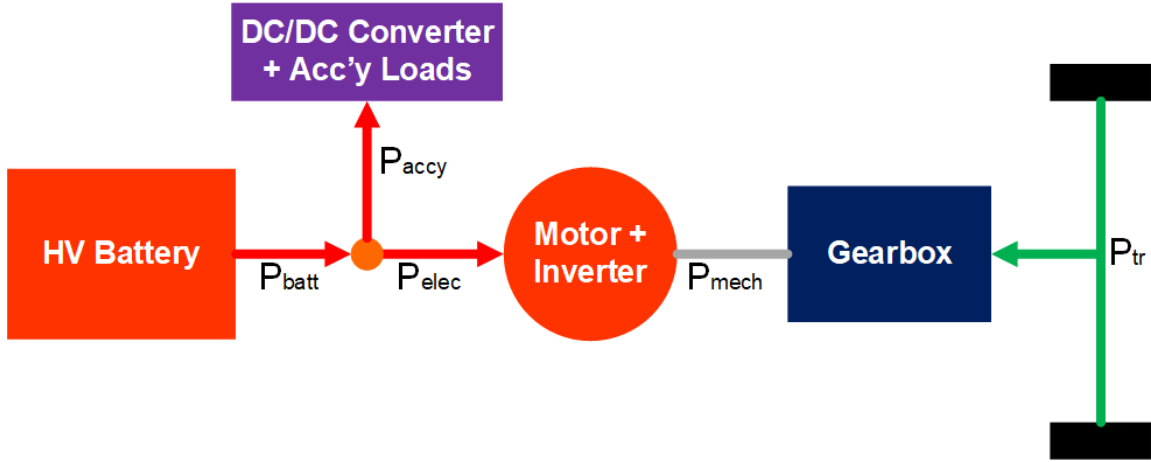


Figure 22: Power Flow, ZPM Mode

Since there is no power being passed through the gearbox, a slight negative tractive effort is produced at the wheel due to the gearbox offset loss. Figure 23 outlines the calculation steps for determining resultant tractive effort, vehicle trajectory, and power consumption using the ZPM mode. The powertrain model for positive tractive power is used due to the motor consuming some power to overcome the motor-inverter offset loss.

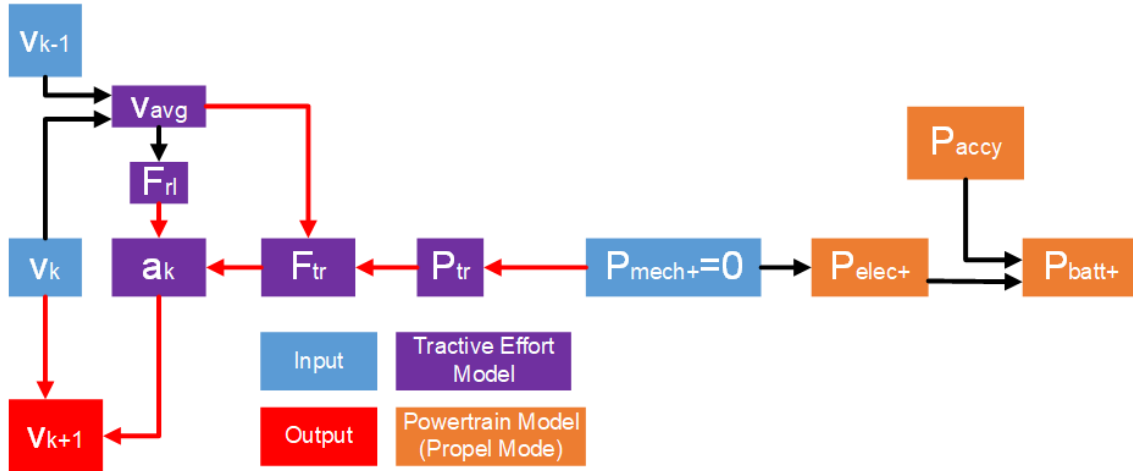


Figure 23: Model Calculations, ZPM Mode

Rearranging Equation 16 and substituting for zero motor output describes this power flow:

$$P_{elec}^+ = \frac{0}{\eta_{mot}} + P_{loss,mot} = P_{loss,mot}. \quad (47)$$

Like the coasting model, some values are found via forward modeling. Given  $P_{mech}^+$  is zero, Equation 13 is rearranged for forward modeling to find tractive power at the wheel:

$$P_{tr} = \frac{-P_{loss,gb}}{\eta_{gb}}. \quad (48)$$

This value is negative, so tractive effort is also negative and found to be

$$F_{tr,k} = \frac{P_{tr}}{v_{avg,k}}. \quad (49)$$

Equation 49 applies for any forward calculation where tractive power derived from the powertrain model is applicable. Using Equation 1, the acceleration value used to determine velocity at the next time step is found to be

$$a_k = \frac{F_{tr,k} + F_{rl,k}}{f_{iM}}. \quad (50)$$

Both  $F_{rl}$  and  $F_{tr}$  are negative, so  $a_k$  is more negative than coast mode deceleration. Higher deceleration is consistent with tractive power being negative (less than in with coasting). As a result, the ZPM mode stops the vehicle in a shorter distance and time than coast mode.

Zero Battery Power (ZPB) is another powertrain mode that could be used to manage vehicle deceleration. Figure 24 is a diagram of power flow through the vehicle powertrain when the vehicle is using the ZPB mode.

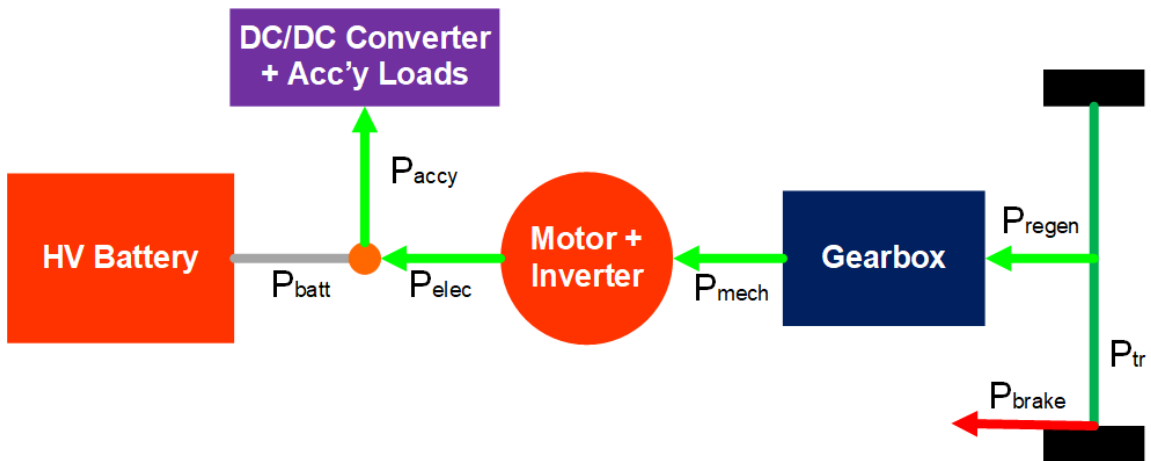


Figure 24: Power Flow, ZPB Mode

This mode meets accessory power needs using the regen braking capabilities of the electric drivetrain.  $P_{accy}$  is used to determine other power requirements between the HV bus and wheel. Figure 25 visualizes this forward modeling process.

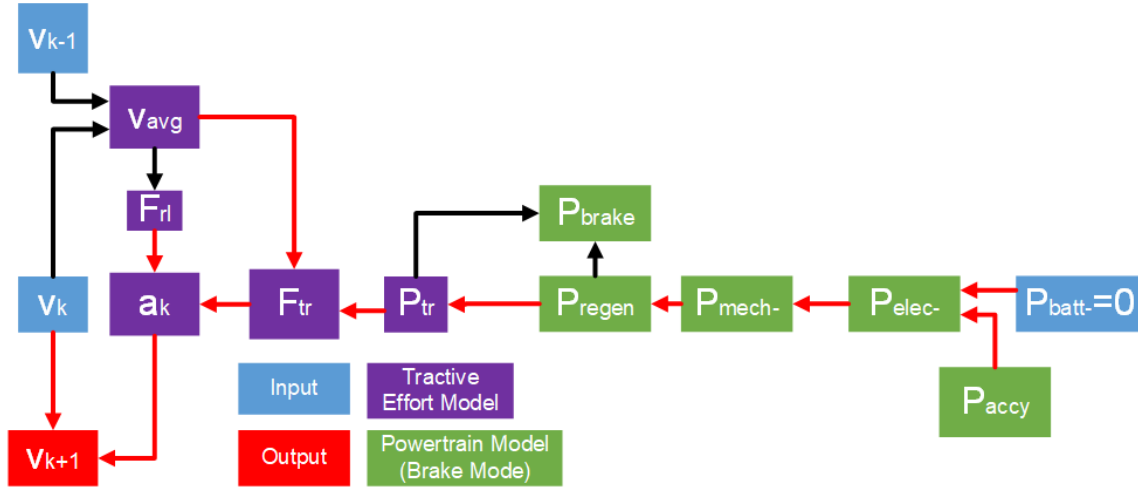


Figure 25: Model Calculations, ZPB Mode

$P_{elec}^-$  is calculated by rearranging Equation 22 and setting  $P_{batt}^-$  equal to zero such that

$$P_{elec}^- = -P_{accy}, \quad (51)$$

where  $P_{elec}^-$  is negative to indicate power regenerated back into the HV bus.  $P_{mech}^-$  is found by rearranging Equation 21 such that

$$P_{mech}^- = \frac{P_{elec}^- - P_{loss,mot}}{\eta_{mot}}. \quad (52)$$

Subtracting  $P_{loss,mot}$  from  $P_{elec}^-$  and dividing by motor/inverter marginal efficiency  $\eta_{mot}$ , which is less than unity, results in a required  $P_{mech}^-$  that is more negative and greater in magnitude than the  $P_{elec}^-$  power transferred to the HV bus. Negative power flowing from the wheels is reduced in magnitude due to losses and inefficiency within the powertrain. Determining  $P_{regen}$ , the power input into the gearbox when the vehicle is using regenerative braking, requires a rearrangement of Equation 20:

$$P_{regen} = \frac{P_{mech}^- - P_{loss,gb}}{\eta_{gb}}. \quad (53)$$

$P_{regen}$  required to feed the accessory loads is assumed to be close to  $P_{accy}$ , which is far less than  $P_{cutoff}$ . Therefore, via Equation 18, the tractive effort required at the wheel for ZPB mode is found to be

$$P_{tr}^- = \frac{P_{regen}}{\varphi}. \quad (54)$$

Tractive force and acceleration are found using Equations 49 and 50. The vehicle experiences greater deceleration than in with the ZPM or coast modes because of the negative tractive power required to feed the accessory loads. As required (or requested, as is the case with regen braking) tractive power increase, so does deceleration.

The decel trajectory created by the ZPB mode is affected by the regen brake fraction. The value of  $\varphi$  used in this study results in accelerations that are only slightly harsher than those observed in the coasting and ZPM mode. However, Equation 54 shows that as  $\varphi$  approaches zero, the negative tractive power required to meet accessory load demand increases along with friction braking power. Using the ZPB mode with reduced values of  $\varphi$ , therefore, results in harsher deceleration over a shorter decel distance. Though out of scope of this work, reducing regen fraction dynamically seems advantageous for improving vehicle stability and performance at lower speeds.

### ***Multi-Mode Decel***

A combination of decel modes can be utilized to balance the advantages and disadvantages of each. Implementing a multi-mode decel strategy with additional logic in the BEV model aids in determining whether changing decel modes in the middle of a deceleration phase improves vehicle performance during decel. Figure 26 illustrates a hypothetical decel strategy with multiple decel modes. Coasting and the zero power modes can be used at higher speeds to cover large distances with relatively gentle

deceleration, and regen at lower speeds could prevent the inefficient coasting seen in Figures 20 and 21. The model determines where the decel mode changes using transition speeds such that for timestep  $k$ , if  $v_k$  is less than  $v_{transition}$ , then the next decel mode is used for the current timestep and until another transition speed is reached.

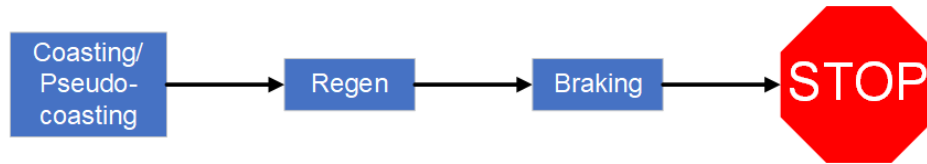


Figure 26: Example Multi-Mode Decel Strategy

Transitioning to friction braking when the vehicle is very close to zero speed is related to this strategy. Though the logic for switching off regenerative braking is based on the parameter  $v_{cutoff}$ , such a transition only affects the regen brake fraction and the calculations of  $P_{regen}$  and  $P_{brake}$ . It does not represent a shift in decel mode, nor does it affect the way all other powertrain and velocity values are modeled. Applying the logic for both velocity parameters allows for study of more complex decel strategies that more accurately reflect real driving.

### *Fixed-Route Drive Cycle Simulation*

Coasting, regen, and the pseudo-coasting modes all require different distances to accomplish the same net change in speed, and all take different amounts of time due to varying accelerations and velocity profiles. A fixed-route simulation with common start and stop positions is used to fairly compare the strategies. Vehicle performance from cruise speed to zero speed is assessed primarily with respect to travel time and energy consumption. Figure 27 shows how each decel strategy is tested. Based on analysis of coasting and regenerative braking at low speeds, each strategy ends with friction braking at a moderate deceleration rate ( $-1.5 \text{ m/sec}^2$ ) from 5 mph to zero speed. Cutting off regen

braking at low speeds eliminates the issue of extensive accessory energy consumption due to extended time spent coasting down at low speeds. It also eliminates the impact of motor efficiency and vehicle stability issues that, in practice and as observed in prior studies, preclude the use of regen braking at speeds very close to zero. The decel strategies, therefore, are assessed from the initial speed to 5 mph.

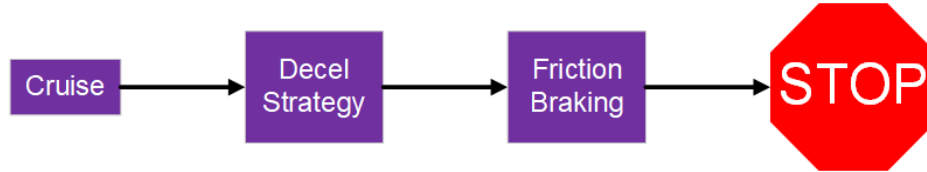


*Figure 27: Fixed-Route Drive Cycle Simulation*

The distance of the drive cycle  $x_{tot}$  for each initial speed  $v_0$  is longer than any of the decel strategies being investigated. The distance not covered by the decel strategy itself or the common low-speed friction braking event is modeled as a constant speed cruise period at the initial speed of the decel event. This study simulates decel strategies from several cruise speeds that are common in urban drive cycles. The distances used for each simulation are shown in Table 7. They are based on the coasting trajectory data displayed in Figure 19.

Table 7: Length of Constant-distance simulations, various initial speeds

$v_0$	$x_{tot}$
25 mph	700 m
35 mph	1200 m
45 mph	1650 m

Maintaining a constant speed requires the powertrain provide enough tractive power to compensate for the road load forces acting on the vehicle at that speed. Appendix B details the power and energy required to maintain speeds that are common in urban and highway drive cycles.

## Chapter 5: Results & Discussion

Ten different decel strategies are simulated for each of the cruise speeds given in Table 7. The data for six of the strategies tested at 25 MPH (and select data collected at 35 and 45 mph) are addressed in the body of this work. Three of the strategies omitted from this chapter use regen braking and decel rates from Figure 11, and a multi-mode decel strategy that uses the ZPM mode is also omitted from this chapter. The complete dataset, as well as results for the 35 mph and 45 mph simulations, can be found in Appendices C, D, and E.

### Regen Mode

The baseline results for decelerating with regenerative braking are presented here. Figure 28 shows the decel curve for the vehicle using regen braking and following a linear velocity profile with a constant  $-2.5 \text{ m/sec}^2$  deceleration. This decel rate is used in the multi-mode strategies discussed later in this section. Regen is used from the initial speed (25 mph) to the cutoff speed  $v_{cutoff}$  (5 mph). Below 5 mph, only friction braking is used.

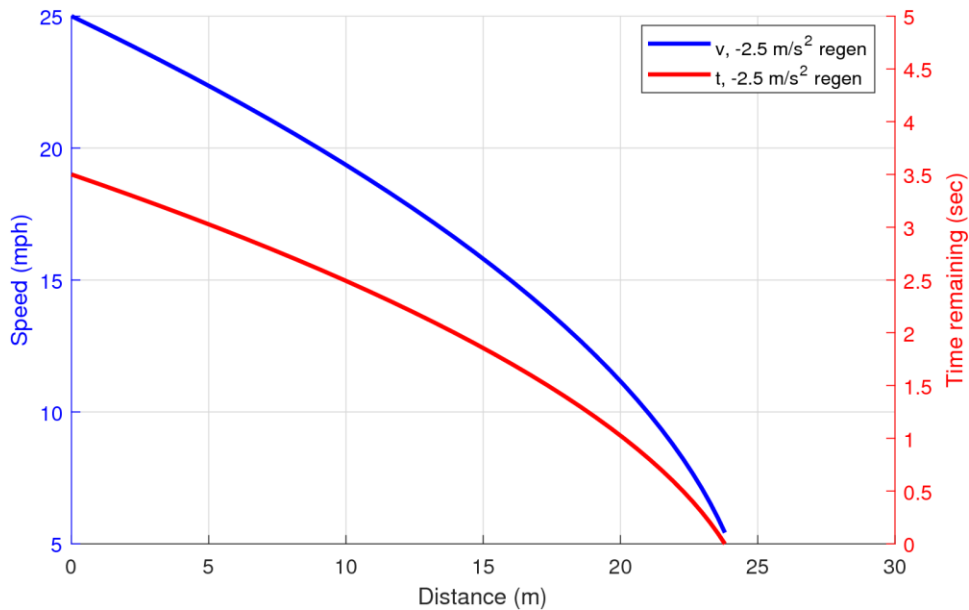


Figure 28: Vehicle Speed and Time to Brake,  $-2.5 \text{ m/sec}^2$  Regen



In this section, energy is plotted with speed on the x-axis to increase the ease of comparing decel events. All modes require different decel distances, but they share a common speed interval. Various quantities of HV bus energy for the decel event are plotted in Figure 29.  $E_{elec}$ , calculated using  $P_{elec}$  data and Equation 23, totals over 28 Wh. Of the 28 Wh returned to the HV bus, less than 1 Wh is consumed by accessory loads. The energy consumed by accessory loads is why net battery energy  $E_{batt}$  is less negative than what enters the HV bus. Notably, despite decelerating in 62% less time and distance using the  $-2.5 \text{ m/sec}^2$  linear decel than with the trajectory with the slowest regen braking rate modeled in this study ( $-1 \text{ m/sec}^2$ ), the vehicle only regenerates 8% more energy back into the pack than that mildest regen case. The reduction in losses to road load does not significantly affect energy regeneration.

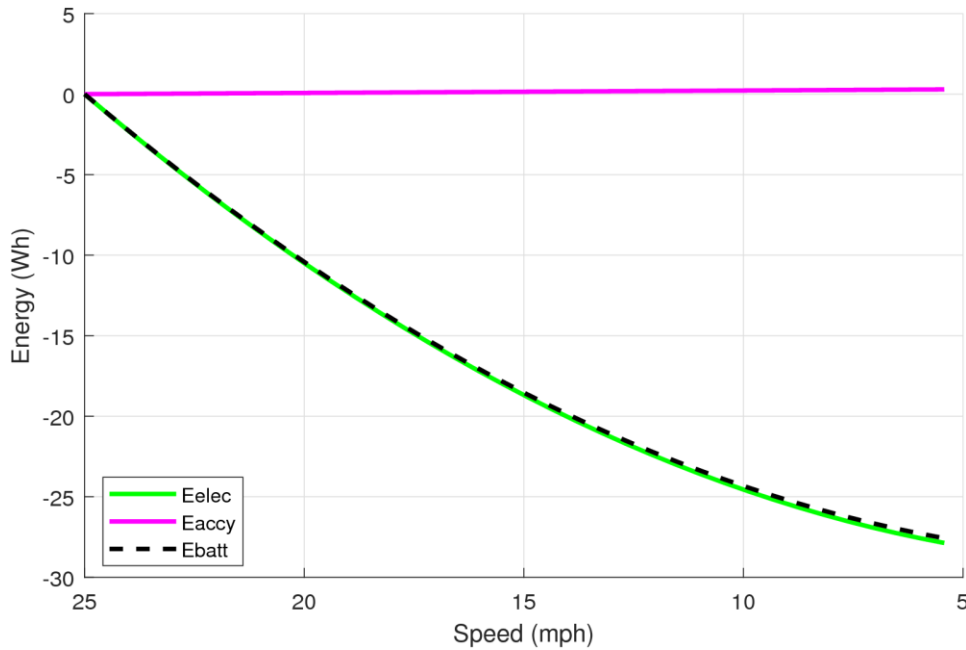
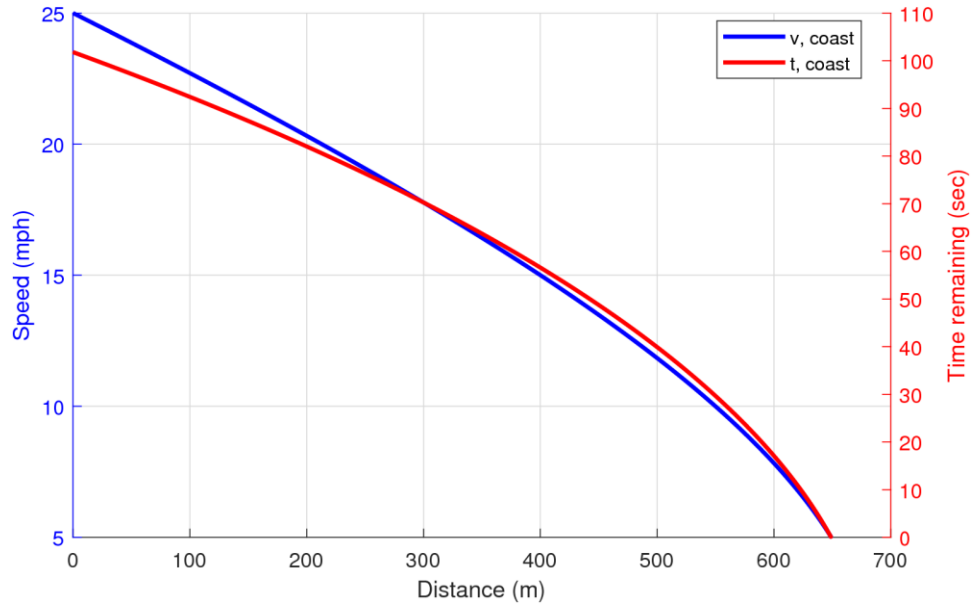


Figure 29: HV Bus Energy,  $-2.5 \text{ m/sec}^2$  Regen

### Coast Mode

Figure 30 displays the vehicle speed and time traces for the coast mode. The vehicle coasts 650 meters for 100 seconds until the low-speed threshold is reached. The average

acceleration experienced by the vehicle in this decel mode is a fraction of the decel rates explored for regen braking, varying only between  $-0.11$  and  $-0.07$  m/sec<sup>2</sup>. This is the range of decel rates caused by road load between 5 and 25 mph, as the powertrain is generating zero tractive effort at the wheel.



*Figure 30: Vehicle Speed and Time to Brake, Coast Mode*

HV bus energy for decel using coasting is plotted in Figure 31.  $E_{elec}$  increases linearly to 3.3 Wh as speed decreases. This is the amount of energy the motor consumes to negate powertrain losses and maintain zero tractive effort at the wheel. This power requirement is, in fact, less than what is needed to feed the accessory loads, which is why  $E_{accy}$  has a larger slope. Total battery energy consumption  $E_{batt}$  is dominated by the energy needed to feed accessory loads. The extended duration over which this decel event takes place makes accessory loads the primary energy consumer on the vehicle during coasting.

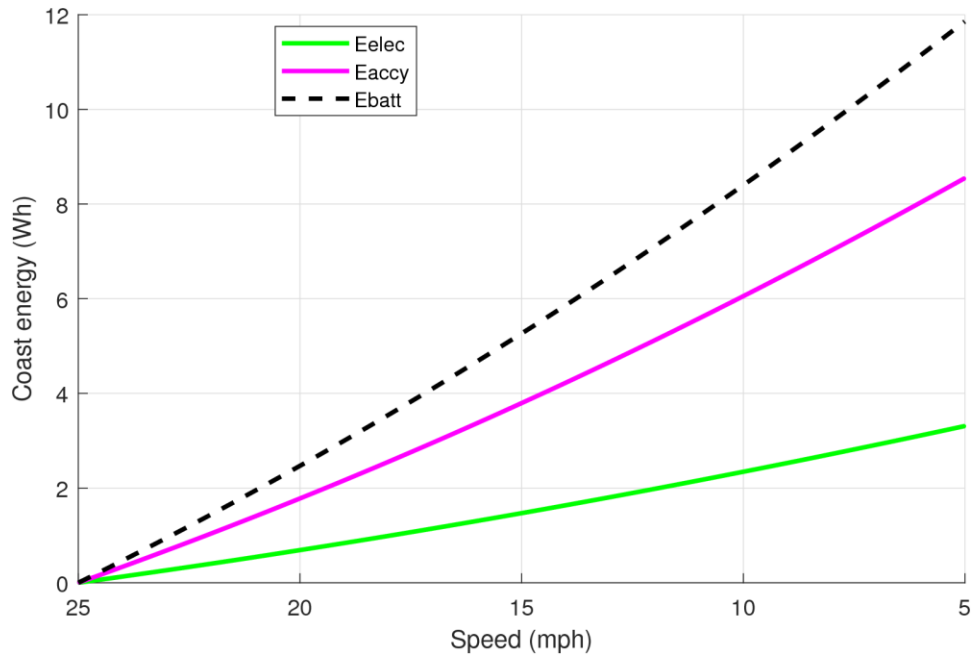
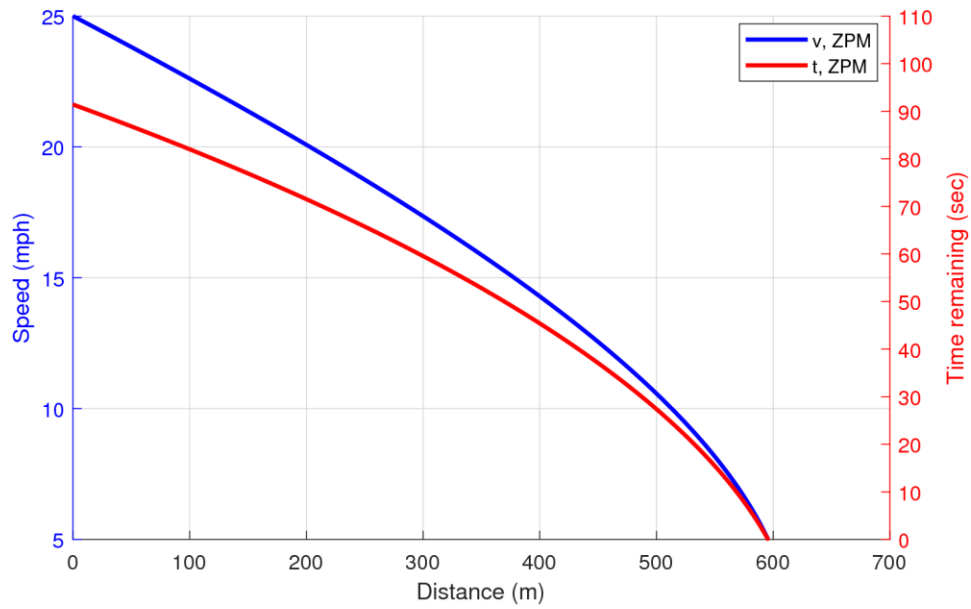


Figure 31: HV Bus Energy, Coast Mode

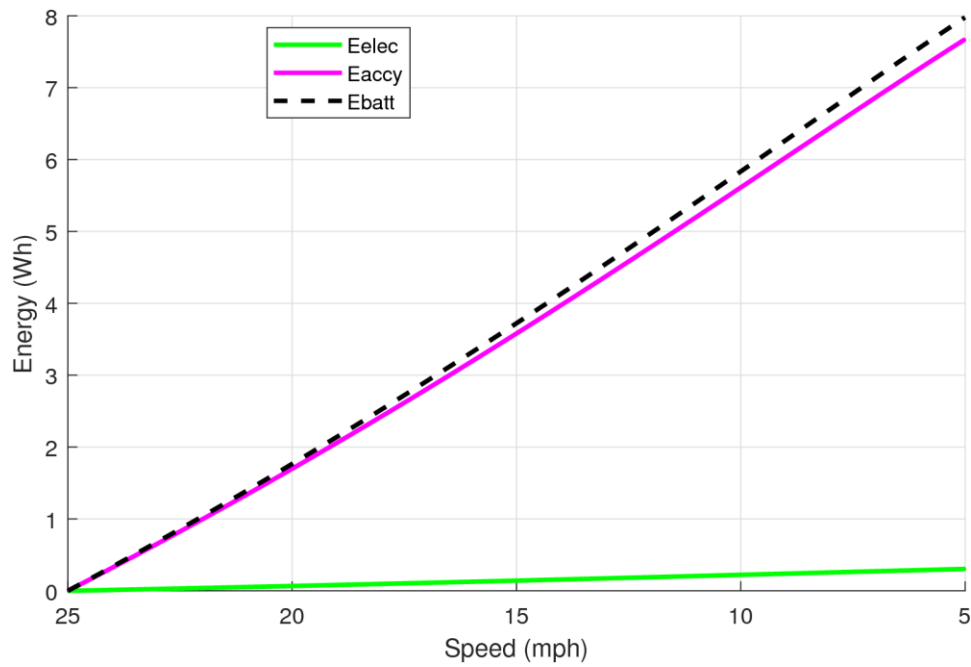
### Pseudo-Coasting Modes

Figure 32 shows the speed profile and decel time for the vehicle using the ZPM decel mode. Using this strategy requires 10% less distance and time to decelerate the vehicle from cruising speed to the cutoff speed. The difference between ZPM mode and coast mode is the addition of negative tractive power due to drivetrain losses between the wheel and input of the gearbox. As a result, the ZPM mode slows the vehicle down 10% faster than coasting does.

Since the powertrain is not supplying energy to overcome losses in the driveline, overall battery energy consumption falls with this decel mode compared to coasting. The energy plot in Figure 33 demonstrates how energy for accessory loads dominates this strategy. Of the 8 Wh of battery energy consumed during this decel event, only 3.8% of it goes to the inverter and motor.



*Figure 32: Vehicle Speed and Time to Brake, ZPM Mode*



*Figure 33: HV Bus Energy, ZPM Mode*

Figure 34 displays the decel results for the vehicle using the ZPB mode. As explained in the previous chapter, this mode neutralizes battery power by regenerating enough power back into the HV bus to offset the accessory loads. The vehicle experiences higher

average deceleration and a higher max deceleration ( $-0.18 \text{ m/sec}^2$ ) using the ZPB mode than with either the coast or ZPM modes.

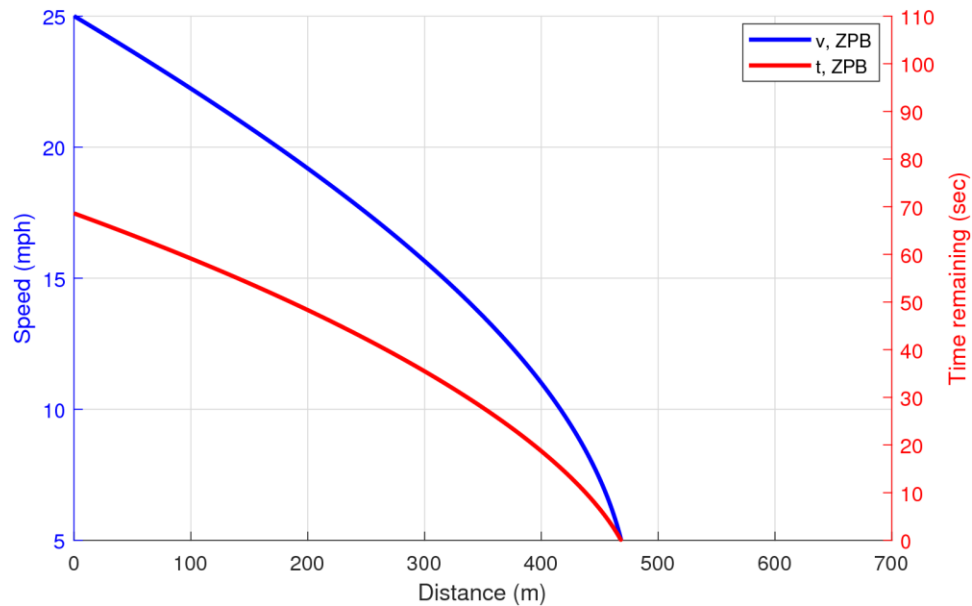


*Figure 34: Vehicle Speed and Time to Brake, ZPB Mode*

The distance required to slow the vehicle in ZPB mode to the low-speed cutoff region is 21% less than ZPM mode. However, as plotted in Figure 35, energy being regenerated back into the HV bus matches the power draw of the accessory loads, resulting in zero battery energy consumption during the decel event.

The coast, ZPM, and ZPB mode results demonstrate how BEV control systems can be configured to operate at low power once the driver lifts off the accelerator pedal. In a BEV with minimal autonomous capabilities, these powertrain modes allow the vehicle to cover extended distances while slowing down and minimizing the energy transfer through the electric powertrain. Coasting utilizes some power to produce zero tractive effort from the powertrain at the wheel, which creates the gentlest decel trajectory of any decel mode in this study. The ZPM mode slows the vehicle down faster than coasting by only providing enough power to create zero motor torque. The closest mode to DFCO in an ICEV is the

ZPB mode. While DFCO turns off fuel injection and uses engine friction to brake, ZPB mode reduces battery power output to zero by commanding mild levels of regen braking. Like DFCO, ZPB mode minimizes system energy consumption and results in negative tractive effort at the wheel.

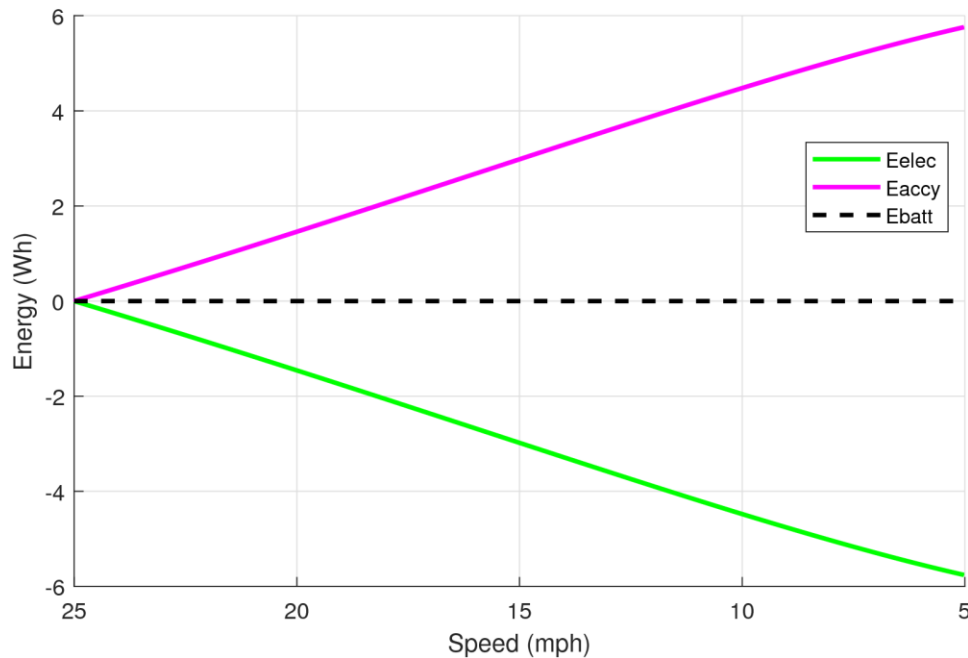


*Figure 35: HV Bus Energy, ZPB Mode*

The characteristics of the novel decel modes contrast with those of regenerative braking, which uses high negative tractive power to rapid decelerate a BEV. Regen braking immediately after cruising is like the one pedal driving mode implemented in some BEVs currently, which defaults to service braking using regen right after the driver ends accelerator input. This harsh decel with no intermediate, gentler decel phase requires more driving at cruising speed than decel modes with lower average deceleration rates. Since driving at cruise speeds requires much more electrical power than any decel mode, using regen immediately after cruising has negative implications for energy consumption.

## Multi-Mode Decel

Results for the Coast-Regen and ZPB-Regen decel strategies are reviewed here. Figure 36 graphs the speed and time-to-cutoff for the Coast-Regen strategy.

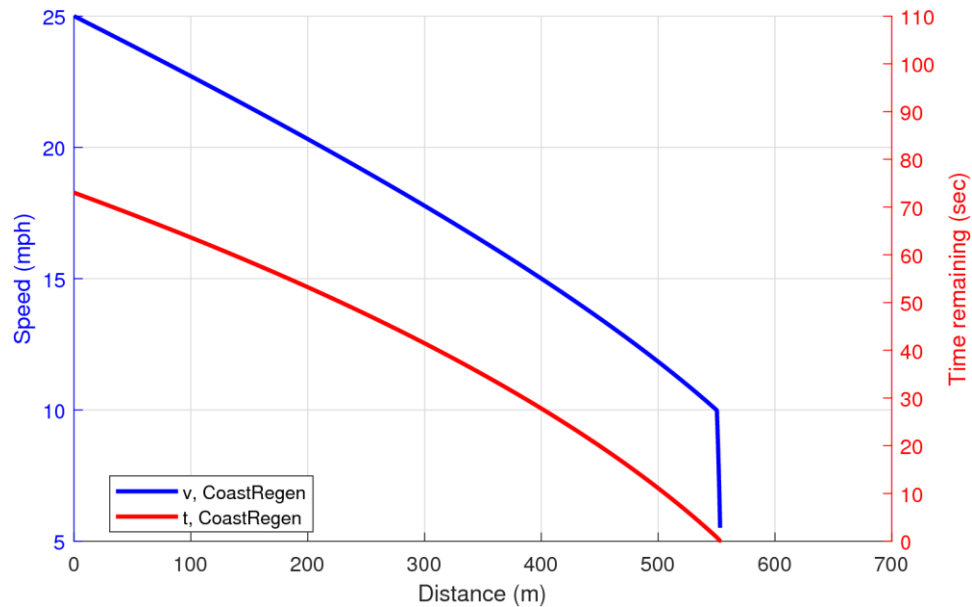
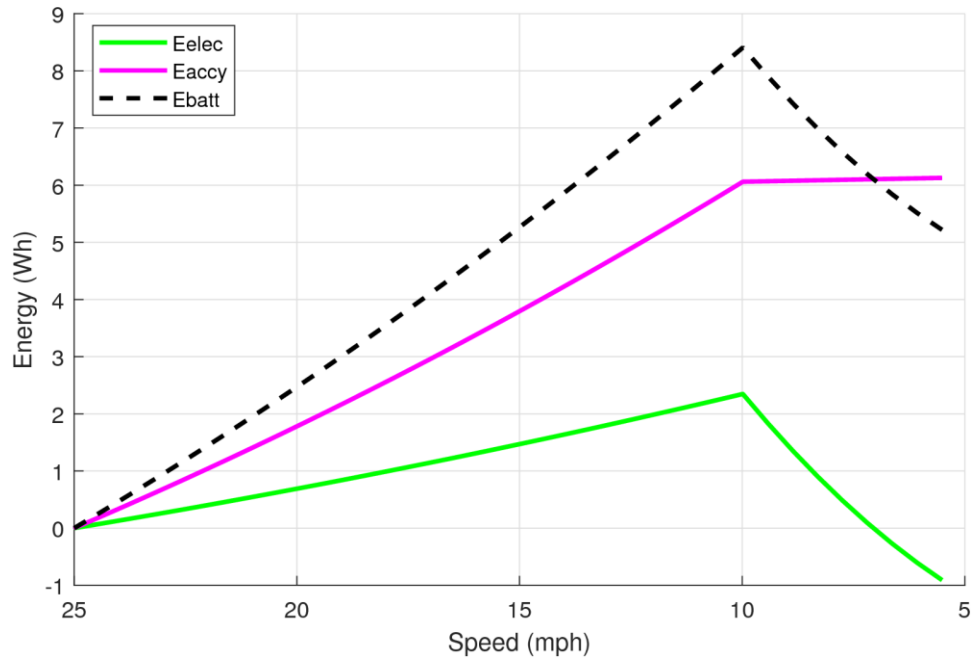


Figure 36: Vehicle Speed and Time to Brake, Coast-Regen Decel

The transition speed is set to 10 MPH based on an inspection of energy consumption and distance traveled in the context of the fixed-route study. Compared to a pure coasting decel, this strategy reduces travel time by 28%. However, it also shortens decel distance by 15%, resulting in an equivalent increase in cruising distance and longer periods of high battery power outflow.

The HV bus energy observed during a Coast-Regen decel is plotted in Figure 37. As in the coast-only case, accessory loads dominate energy consumption when the vehicle is coasting.



*Figure 37: HV Bus energy, Coast-Regen Decel*

During the brief regen braking phase between 10 and 5 mph, the vehicle can recover all the energy used to power the motor and inverter during coasting plus an additional 1 Wh that replaces some of the energy consumed by accessory loads. Consequently, this strategy consumes 50% less energy than the coast-only strategy. When comparing the coast-regen strategy to the regen-only strategy, the coast-regen strategy consumes 5 Wh of battery energy rather than recharging the pack with nearly 30 Wh of energy as the regen-only strategy does. The coast-regen strategy also decelerates the vehicle over a distance that is longer by a factor of 20, which reduces the distance which the vehicle needs to cover at cruise speed. In sum, the energy spent in coast mode more than compensates for the energy saved by not driving at cruising speed.

The ZPB-Regen decel results are plotted in Figure 38. 10 mph remains the transition speed for consistency and to fairly compare multi-mode solutions.



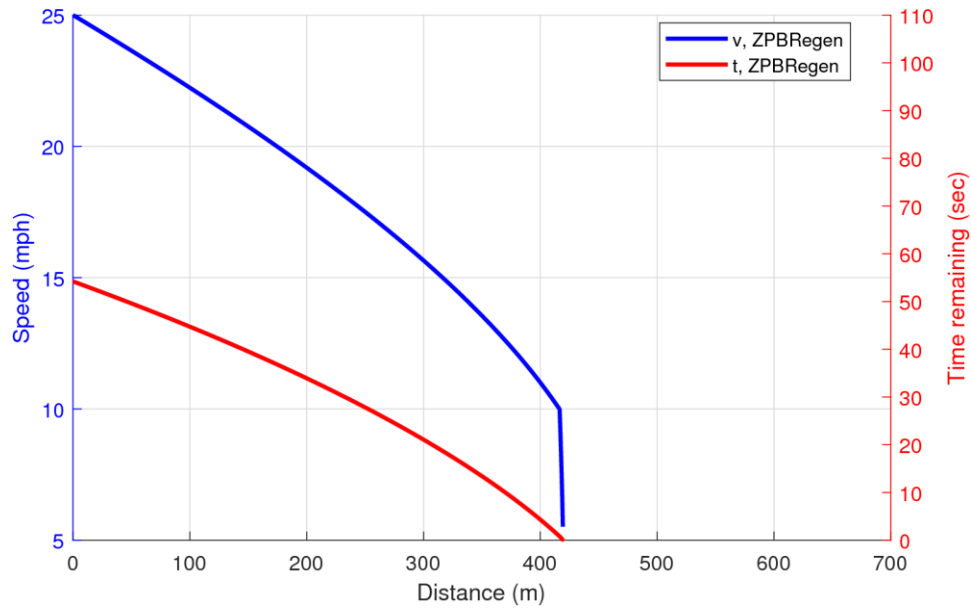


*Figure 38: Vehicle Speed and Time to Stop, ZPB-Regen Decel*

The distance covered using this strategy is 24% shorter than that of the Coast-Regen strategy, and decel time is reduced by 26%. These differences are attributable the ZPB mode, which induces greater deceleration than coasting while regenerating power to feed the accessory loads.

The HV bus energy plot for the ZPB-Regen strategy is shown in Figure 39. It is overall a net-regen event: after using the ZPB mode to feed accessory loads, tractive energy is used during regen below the transition speed to charge the pack. Despite recharging the battery, the tradeoff between decel distance and cruise distance remains. Accounting for cruise power and energy consumption needs for each decel strategy is vital for making any conclusions about their utility in real BEV applications.

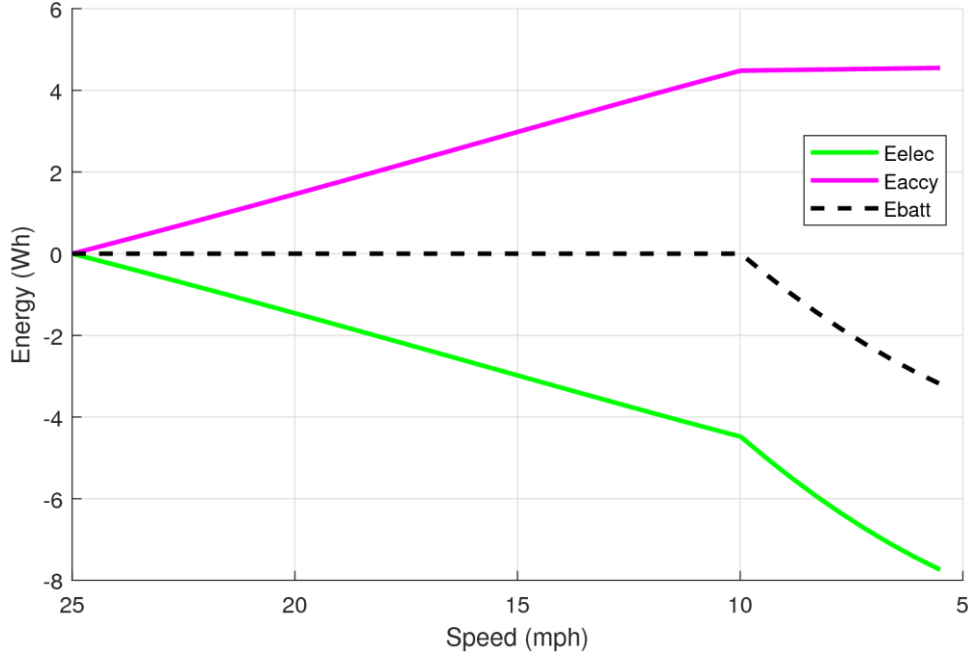


Figure 39: HV Bus Energy, ZPB-Regen Decel

### Fixed-Route Simulation

The constant-distance simulations are completed with the addition of a cruising phase to each, the length of which depends on the distance covered while slowing down. For this study, Equation 25 is adapted to reflect the two parts of the decel phase:

$$x_{tot} = x_{f,cruise} + x_{f,decel} + x_{f,brake} , \quad (55)$$

where  $x_{f,decel}$  is the distance covered by a given decel strategy, and  $x_{f,brake}$  is the distance covered during the friction braking below 5 mph. For all cases,  $x_{f,brake}$  is 1.7 meters, less than 1% of the total simulation distance. Cruise times and distances are documented in the summary table in Appendix C. To gain a better understanding of the effect of moderate regen braking immediately following cruising (as would be the case if the vehicle has one pedal driving control enabled), the  $-1.5 \text{ m/sec}^2$  linear regen case is analyzed here.

Figure 40 documents the velocity curves of five decel strategies over the full 700-meter simulated travel distance for the 25 mph case. The solutions that use coast mode only

(green) and regen only (blue) form the bounds of the solution set. The portion of the curve that remains constant at 25 mph denotes the distance the vehicle must cruise to complete the fixed-route study with the chosen decel strategy. Since coasting uses the most distance to slow the vehicle down from cruise speed to friction brake speed, the distance the vehicle needs to cruise before entering cruise mode is minimized. Conversely, regenerative braking via a linear decel at  $-1.5 \text{ m/sec}^2$  only accounts for only 6% of the total fixed-route distance, so the vehicle needs to cruise at 25 mph for nearly the whole study.

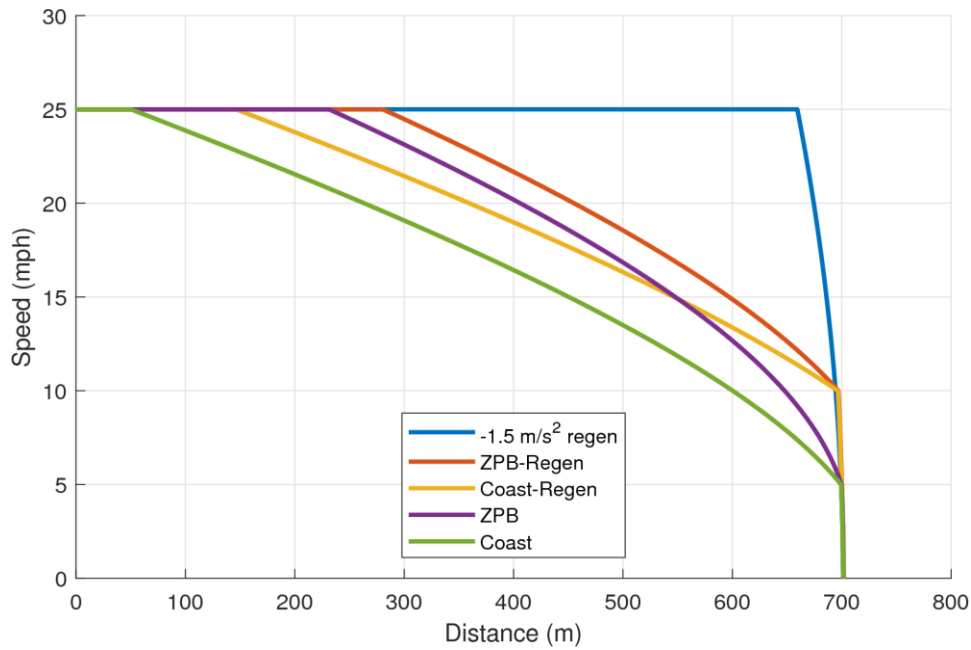


*Figure 40: Speed vs. Distance, Select Decel Strategies*

The effect of these different cruise speeds is evident in Figure 41, the plot of  $E_{batt}$  with respect to distance. The length of each cruise phase is reflected in the portion of the plot increasing at the power level needed to maintain the cruise speed. As demonstrated in Figure 40, using regenerative braking requires the longest cruise phase, so it also has to the greatest battery energy consumption. Although 52% of the battery energy consumed during cruising is recovered in the decel phase, the regen-only strategy still uses the most

energy (24 Wh). Across the whole set of regen braking solutions simulated in this work, none vary from the  $-1.5 \text{ m/sec}^2$  case by more than 2% with respect to total  $E_{batt}$ , which suggests that decel rate does not significantly impact energy consumption of a regen-only strategy, even when the cruise phase is factored in.

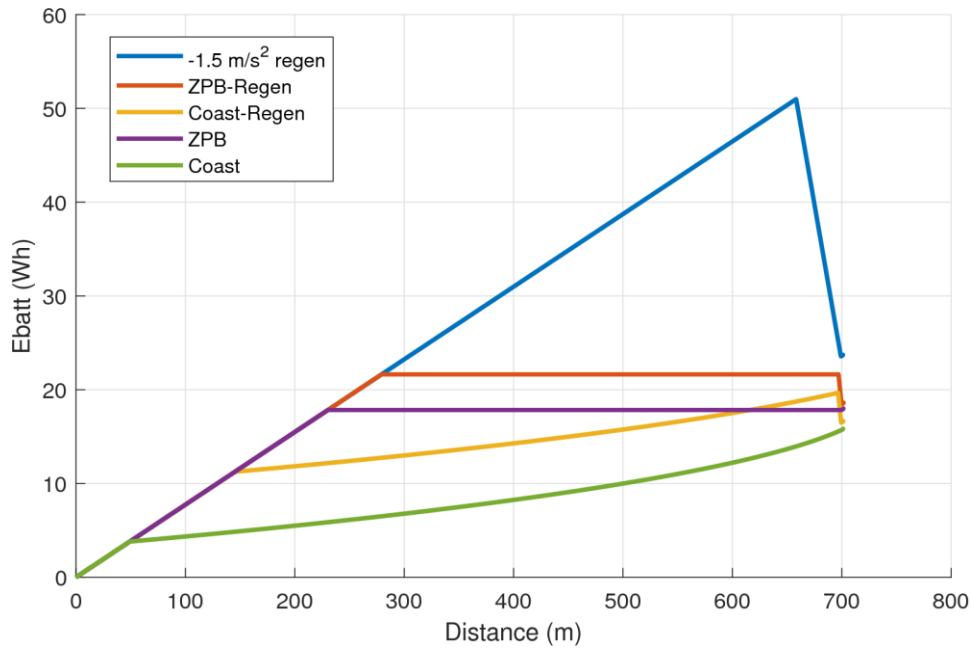


*Figure 41:  $E_{batt}$  vs. Distance, Select Decel Strategies*

As expected, the coast-only solution is the most energy efficient, consuming 31% less energy than the regen braking solution. The energy consumption delta can be attributed to the coast-only strategy having the shortest cruise phase and the inverter-motor system needing less than 200 W of electrical power for 93% of the trip. The remaining solutions use between 16 and 19 Wh. They require less than half the cruise distance of the regen solution, and all have the vehicle spending most of the trip operating a power level that is a fraction of what is required to support cruising at 25 mph.

Trip time is the other metric by which each strategy is assessed. Figure 42 tracks how travel time increases for each solution. For the portion of the trip completed at cruise speed, time increases linearly with distance. However, trip time is nonlinear for the non-

regen decel modes due to having much lower decel rates than the regen braking cases being considered. As a result, the longer the decel mode takes with respect to distance, the greater the divergence from the nominally linear curve of the regen-only strategy.

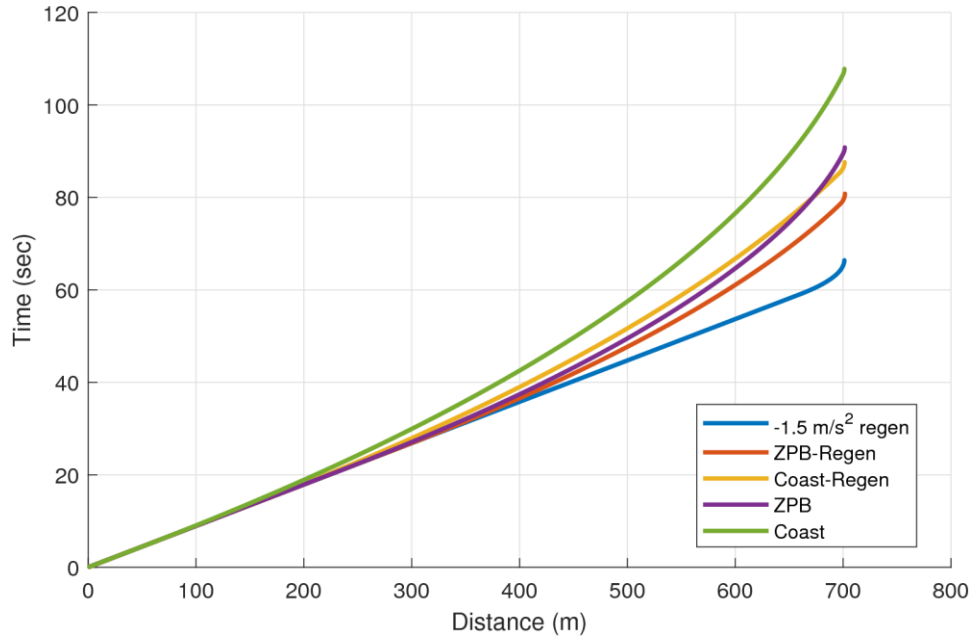


*Figure 42: Travel Time vs. Distance, Select Decel Strategies*

The coasting solution has the highest travel time (110 seconds, 62% higher than the regen solution), and the other pseudo-coasting and multi-mode cases have travel times between 14 and 24 seconds longer than the regen solution (66 seconds). The variance in trip times can be attributed to the same section of the trip that makes non-regen decel solutions advantageous with respect to energy consumption. Between 300 and 600 meters into the trip, where the alternate strategies are slowly decelerating the vehicle, the regen-only strategy keeps the vehicle at cruise speed. Though it consumes much more energy, using only regenerative braking ensures a vehicle finishes the fixed-route study at least 14 seconds before an identical vehicle using any other decel strategy.

These results are for the 2019 Nissan LEAF® SV/SL, but the model (including the methods by which the decel modes are calculated and possibly applied to CAV systems)

can be adapted for use with other BEVs. The model inputs (vehicle mass, road load, and the overall powertrain Willans line) can all be set *a priori*.

## Discussion

Energy consumption and travel time are the primary metrics by which decel strategies are assessed because they directly influence vehicle performance and consumer acceptability. Figure 43 plots the final energy consumption with respect to travel time for the selected decel strategies and all three cruise speeds. Each solution set falls along a curve of decreasing energy consumption and increasing time. For a given vehicle configuration and cruise speed, there are limits with respect to how much energy consumption and time can be reduced. Minimum travel time is dependent on the maximum acceptable decel rate, reductions in energy consumption are restricted by powertrain losses, and both are affected by the cruise speed.

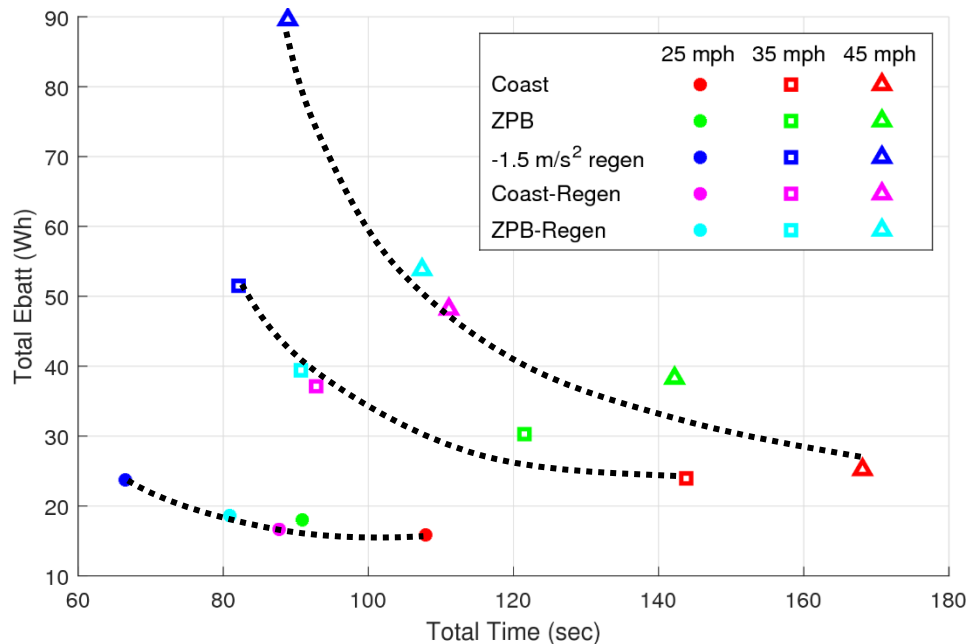


Figure 43: Total  $E_{batt}$  vs. Total Time, Selected Decel Strategies

The change between coast and coast-regen and between ZBP and ZPB-regen strategies demonstrates the effect of adding regen braking in series with coasting and pseudo-

coasting modes. Combining regen braking with gentler decel modes like coast or ZPB results in a reduction in travel time and a slight increase in energy consumption. This difference is dependent on the transition speed. As the transition speed approaches the cruise speed, the multi-mode strategy results in vehicle performance closer to the pure regen strategy. This pattern can be seen in all three solution sets, though the differences between regen and coasting with respect to energy and travel time increase with cruise speed. The position of the pseudo-coasting and multi-mode strategies for the 25 mph case relative to coasting and regen is slightly different than in the higher speed cases. While the 25 mph multi-mode strategies are close to the ZPB strategy, the multi-mode strategies in the 35 mph and 45 mph cases are more definitively halfway between the regen and ZPB strategies. This difference is most likely due to the transition speed being set at 20 mph for the 35 and 45 mph cases (rather than 10 mph like in the 25 mph solutions).

Because of this energy-time tradeoff, determining an ideal decel strategy requires a choice of how to balance (or favor one of) these two metrics. Very rarely are regen only and coast-only the best ways to slow the vehicle. Based on Figures 40-43, balance can be most readily achieved by pairing two decel modes in series. Reducing energy consumption or travel time can be done by altering  $v_{transition}$ , making the decel strategy more like one of the decel modes which comprise it.

For a set of decel strategies including coast-only and regen-only strategies, a method of scoring and assessing time-energy bias is proposed. Figure 44 shows the decel strategy times and energies relative to the maximum values observed in the solution sets for each

cruise speed. In this form, relative travel time and energy consumption are calculated such that

$$t_{trip,\%MAX} = \frac{t_{trip}}{t_{trip,MAX}} \text{ and} \quad (56)$$

$$E_{batt,\%MAX} = \frac{E_{batt}}{E_{batt,MAX}}, \quad (57)$$

where  $t_{trip,MAX}$  and  $E_{batt,MAX}$  denote the maximum values in each set.

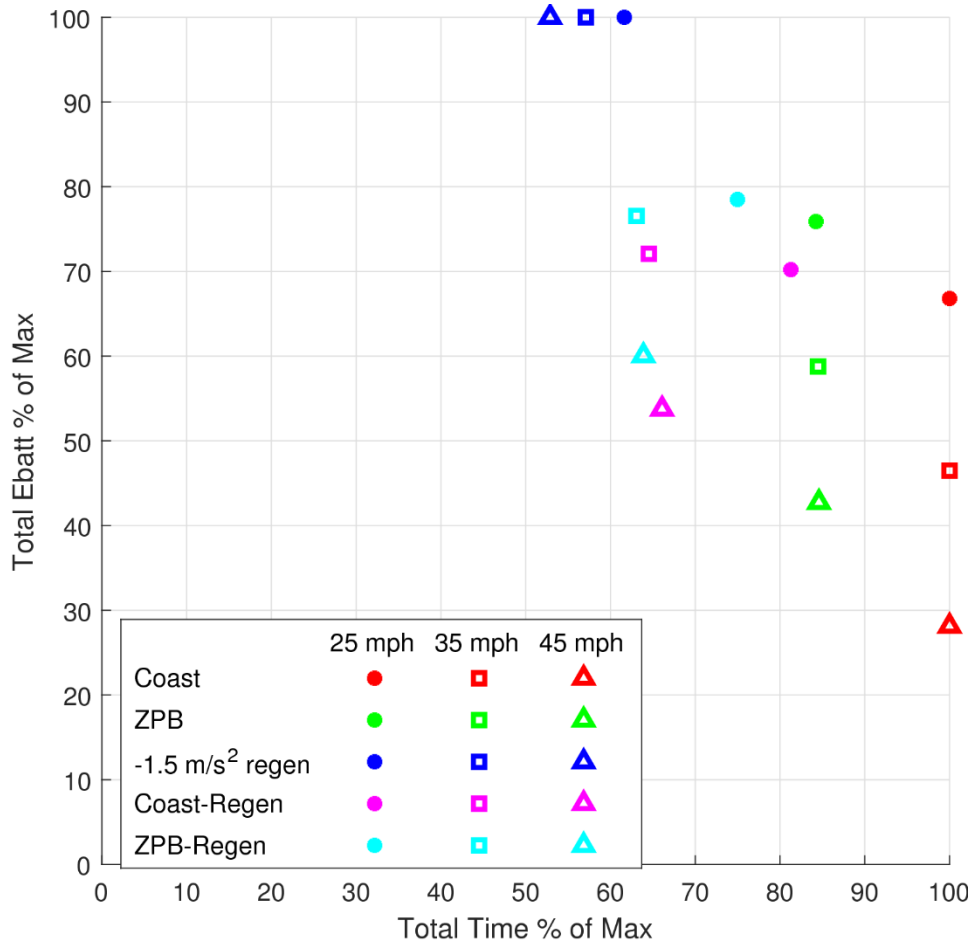


Figure 44: Energy Relative to Max vs. Time Relative to Max, Select Decel Strategies

In this study, the regen-only strategy has the greatest energy consumption, and coast-only the greatest travel time across all three solution sets. An ideal decel strategy would have the travel time of regen-only decel and the energy consumption of coast-only decel, but physics and vehicle dynamics make such a solution improbable. For each cruise



speed case, the set of decel strategies tends to fall along a curve of decreasing energy consumption and increasing travel time between the regen-only and coast-only strategies. The other strategies assessed in this work also fall along these curves.

The score assessing cost and bias towards a particular performance metric for each strategy uses polar coordinates. The radial coordinate is the overall cost of the strategy and is calculated by finding the magnitude of relative energy and time:

$$r_{strat}^* = \sqrt{t_{trip,\%MAX}^2 + E_{batt,\%MAX}^2}. \quad (58)$$

Since the two extreme cases do not take zero time or zero energy, the time-energy bias (the angular coordinate term) is calculated as

$$\theta_{strat}^* = 90 \left( \frac{\theta_{strat} - \theta_{coast}}{\theta_{regen} - \theta_{coast}} \right), \quad (59)$$

where  $\theta_{strat/coast/regen}$  is the angle between a data point and the x-axis in Figure 44:

$$\theta_{strat} = \tan^{-1} \left( \frac{E_{batt,\%}}{t_{trip,\%}} \right), \quad (60)$$

This bias score between 0 and 90 degrees measures how biased each strategy is with regards to minimizing only time or energy. Coasting scores 0 degrees of bias since it minimizes energy consumption the most at the expense of travel time. Regenerative braking scores 90 degrees of bias since it minimizes travel time while having the highest energy consumption. Figure 45 shows the cost-bias scores of the set of decel strategies.

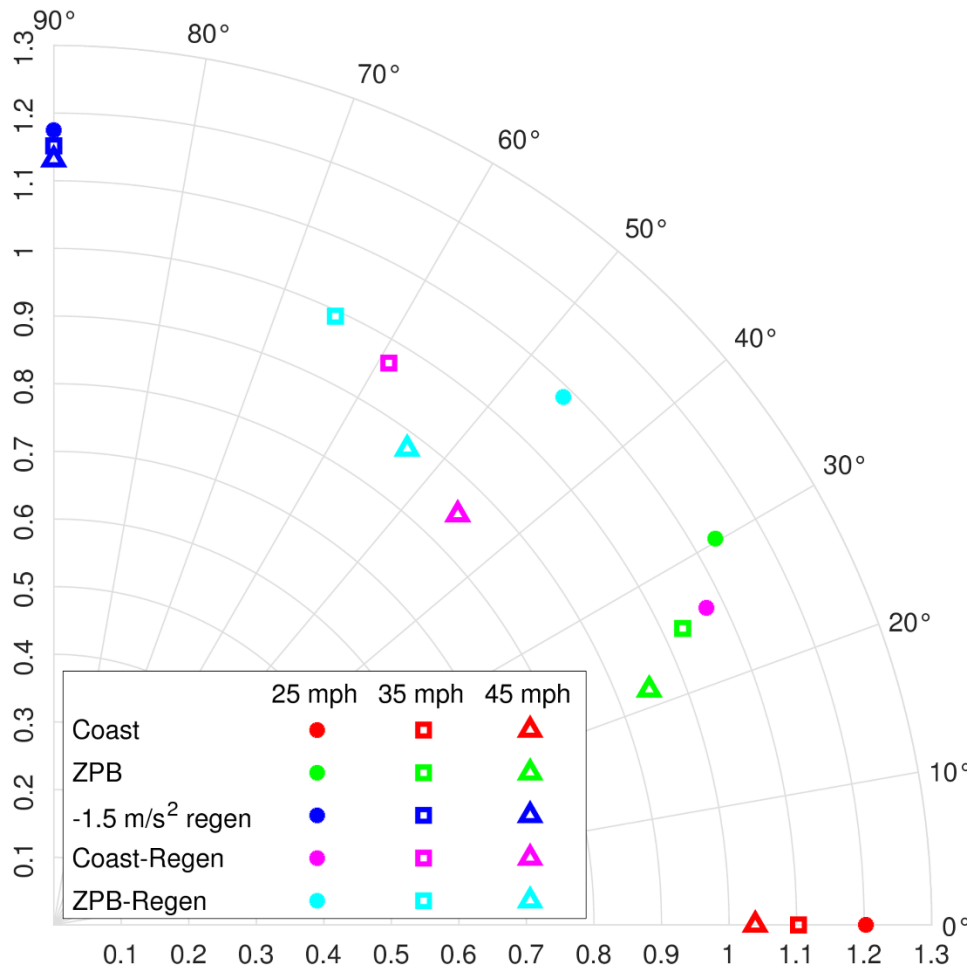


Figure 45: Cost-Bias Scores, Select Decel Strategies

For the 25 mph case, overall costs of 1.2 for coasting and regen confirms that, despite having the best time or energy, the other metric was significantly affected as a result. The multi-mode strategies exhibit 40-60 degrees of bias, and their overall cost is lower than both the regen- and coast-only strategies. Comparing coast to coast-regen and ZPB to ZPB-regen suggests that adding a regen phase reduces both bias towards minimization of a single parameter and overall cost. This trend is consistent across all three cruise speed cases. Furthermore, while the multi-mode strategies for the 35 mph case are more biased and have higher costs than those at 45 mph, the difference can be explained by the two cases sharing a common transition speed. Since the multi-mode strategies for 35

mph transition to regen braking after a smaller change in speed than those at 45 mph, the ones at 35 mph are more biased towards minimizing travel time. The biases could be made more similar by either lowering the transition speed for the 35 mph strategies or increasing the transition speed for the 45 mph strategies.

The cost-bias analysis demonstrates that, unless a driver wants to prioritize one performance metric over the other completely, using regen braking and coasting alone are not the ideal strategies for decelerating a BEV. While the driver saves the most travel time using only regen, energy consumption is at a maximum despite recovering energy while braking. These results for the regen-only strategies suggest that one pedal driving does not deliver the energy savings it is designed to. Similarly, a decel solution that uses only coasting minimizes energy consumption, but the increased time required for it makes its just as costly a decel strategy as regen braking. These issues are reflected in the fact that the coast-only and regen-only strategies have the highest overall cost at all cruise speeds that are tested. For drivers that value energy consumption and travel time more equally, multi-mode decel strategies offer a familiar and tunable way to slow down BEVs. The multi-mode approach is akin to lifting off the accelerator pedal and taking advantage of DFCO in an ICEV after cruising, gently slowing down to a certain speed, then service braking with regen until the vehicle comes to the stopping point. A coast-regen strategy provides the gentlest transition to deceleration compared to DFCO since some positive motor torque allows the vehicle to only being slowed down by road load.

Consider the ZPB-regen multi-mode strategy. Modifying the transition speed for a multi-mode decel like ZPB-regen affects both its bias and cost, making the strategy tunable based on driver requirements. Table 8 shows the effect of changing the decel mode

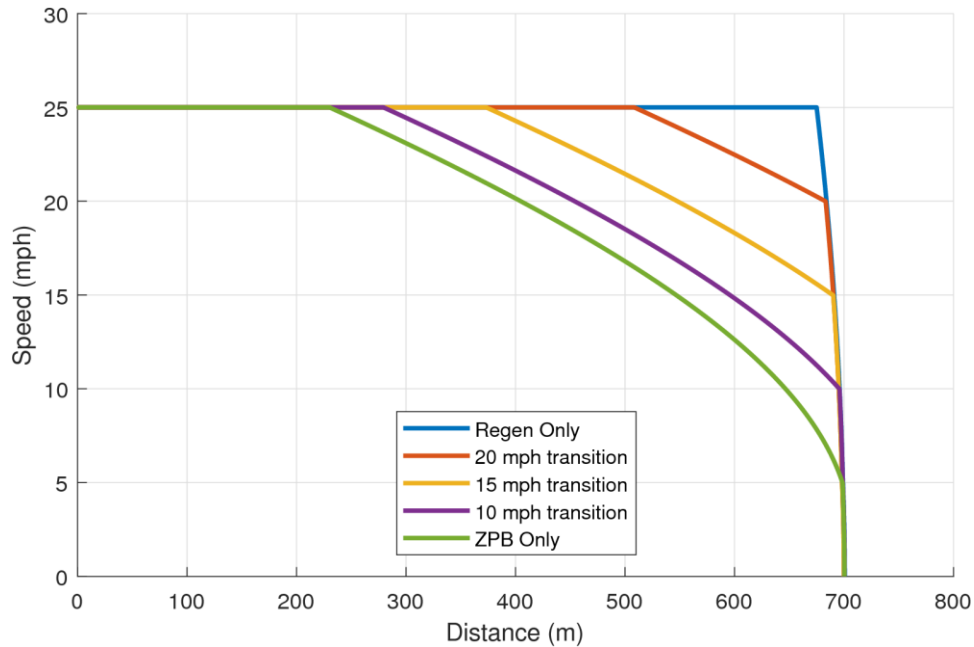
transition speed on the ZPB-regen cost-bias score. With a 10-mph transition speed, ZPB-regen is the most balanced strategy in the 25-mph dataset (42 degrees of bias). However, using a transition speed of 15 mph results in the lowest overall cost. The cost-bias scores of the 5 and 25 mph transition speeds represent the ZPB mode and -2.5 m/sec<sup>2</sup> regen solutions, respectively.

Table 8: Transition Speed vs. Cost-Bias Score, ZPB-Regen 25 mph case

$v_{transition}$ [mph]	$r_{strat}^*$	$\theta_{strat}^*$ [deg]
5	1.11	28.0
10	1.06	42.7
15	1.05	61.3
20	1.10	78.7
25	1.17	90

Figure 46 plots the effect of manipulating the transition speed of the ZPB-Regen strategy. As transition speed approaches cruise speed, and the speed delta induced by regen braking increases, the distance that the vehicle must cruise increases. Increasing the decel mode transition speed saves travel time, but battery energy consumption also increases due to the vehicle needing to travel at the cruise speed longer.

Assuming the powertrain control system is configured to default to a gentle decel mode like coast, ZPM, or ZPB mode when accelerator input is zero, it may be possible for a BEV driver to implement a crude multi-mode decel strategy by choosing the speed at which to begin regenerative braking. However, whether due to anxiety about stopping distance or sheer inexperience, actively calculating the best speed to start regen braking may be difficult for a human driver. It is also impossible for one to reprogram a powertrain control system coded by the vehicle manufacturer.



*Figure 46: Vehicle Trajectory with ZPB-Regen Strategy, Various Transition Speeds*

Alternatively, decel strategy selection can be integrated into a connected and automated vehicle (CAV) software suite, allowing the BEV to adapt a solution to conditions around it in real-time and with more precision than a human driver. While approaching an intersection (either controlled or uncontrolled), a connected vehicle can actively calculate the distance to a stop line or intersection using GPS and other vehicle-to-everything (V2X) signals. The costs of a set of decel solutions for the given distance and speed delta are calculated using the model and methodology outlined in this work, and then the vehicle controls the powertrain according to the chosen strategy. It is possible for the decision-making process to be influenced by the driver (or rider based on the level of autonomous capability the vehicle has) if he indicates a preferred bias towards minimizing energy or time. Applying the strategy scoring system in this work to a vehicle user interface, driver or rider input would be like selecting a specific powertrain mode (sport, all-terrain, eco-friendly, winter, etc.) or switching between one-pedal and normal driving modes. The driver can also indicate that solutions with the lowest overall cost are preferred, which

favors the multi-mode strategies discussed above. Such input from the driver narrows the set of possible solutions which the vehicle considers, which could reduce computation time and increase the likelihood of using a strategy that is appealing to the driver or rider. Furthermore, cost-bias scoring and solution determination could be in terms of any two metrics indicative of vehicle performance, granting some flexibility to those designing the vehicle control systems. Although *in situ* conditions that the vehicle faces, such as traffic or edge cases that require deviation from an ideal trajectory, must also be considered, they should not preclude the vehicle from developing a general decel solution.

### *Sensitivity Analysis*

Decel strategies are sensitive to changes in grade because it affects the magnitude of road load as well as the direction in which the road load force acts on the vehicle. For coasting, if road load is zero or acts in the positive-x direction (the direction of travel), then it is no longer a viable solution for slowing down the vehicle. This limitation is expressed in Equation 61 in terms of the components of road load,

$$F_{grade} \geq |F_{rr} + F_{aero}|, \quad (61)$$

where the quantity  $F_{rr} + F_{aero}$  is negative due to those forces acting opposite the direction of travel. If  $F_{grade}$  is greater or equal to than the magnitude of  $F_{rr} + F_{aero}$ , then coasting either results in constant speed or increasing speed. Table 9 documents the downhill grades at which grade force balances the other road load forces.

Table 9: Downhill Grade Limits, Coast Mode

Speed (mph)	Steady-State Grade (%)
0.1	-0.71%
10	-0.84%
15	-0.94%
20	-1.06%
25	-1.21%
30	-1.39%
35	-1.59%
40	-1.81%
50	-2.33%
60	-2.96%

For a given speed, if the hill down which the vehicle is travelling is steeper than the prescribed grade, then coasting only results in steady-state cruising at that speed. As speed approaches zero, where aerodynamic and velocity-dependent road load also approach zero, the maximum grade approaches the value of  $-C_{rr0}$ , -0.71%. Therefore, if road grade is less negative than -0.7%, then coasting is a viable decel solution regardless of speed. Similar restrictions apply for the ZPM and ZPB modes: if the grade force overcomes road load and powertrain drag, then those strategies also fail. However, for a multi-mode decel strategy, if the transition speed is above the speed at which coasting or pseudo-coasting fails for a given road grade, then a decel strategy that includes coasting is viable.

Table 10 shows the sensitivity of energy consumption to grade changes of up to +/- 2% for the selected 25 mph case decel strategies. The table shows the energy consumption in the base case for all strategies and the percent change that results from increasing or decreasing the grade.

Table 10: Energy Consumption Sensitivity to Grade

Grade	Coast Mode	ZPM Mode	ZPB Mode	-1.5 m/sec <sup>2</sup> Regen	Coast-Regen	ZPB-Regen	Units
-2%	N/A	N/A	N/A	-318%	N/A	N/A	
-1%	N/A	N/A	N/A	-159%	N/A	N/A	
-0.5%	N/A	N/A	N/A	-79%	N/A	N/A	
<b>0%</b>	<b>36.4</b>	<b>37.0</b>	<b>41.4</b>	<b>56.3</b>	<b>38.3</b>	<b>42.7</b>	<b>Wh/mi</b>
1%	256%	251%	220%	159%	245%	213%	
2%	507%	498%	439%	318%	484%	425%	

Due to the downhill grade, the solutions that incorporate coasting and pseudo-coasting could not be modeled at downhill grades due to the new decel phases being much longer than the base case. Since the -1.5 m/sec<sup>2</sup> decel is a backward model, any grade can be modeled without issue. As expected, battery energy consumption is reduced on steeper downhill grades by over 100%, meaning the trip turns into a net-regen event regardless of decel solution. To maintain the cruise speed, the powertrain is in braking mode, so regenerative braking is active. Even at a slight decline, energy consumption is reduced by 79% at a minimum. Additionally, when grade increases, energy consumption increases across the board by over 100%. The prescribed regen braking trajectory is most resilient to grade increases, and the most sensitive strategy is coasting (500% energy consumption increase). In the latter case, the increase is due to a longer cruise distance caused by additional road load from grade force shortening the coasting distance. Notably, the regen braking energy increase at one positive grade is equal to the negative of the corresponding energy decrease at the opposite, negative grade. These trends are consistent across other cruise speed cases.

Table 11 addresses total travel time sensitivity to changes in grade for the selected 25 mph case decel strategies. Energy consumption for the baseline case (zero grade) is



listed, and the percent change relative to the baseline is listed for all other grades. Excluding regen braking, all travel times decrease a moderate amount due to increased grade, most likely due to increased distance covered at the cruise speed due to road load shortening the coasting and pseudo-coasting decel distances. The change in time due to grade for the regen case is most likely an artifact of the 10 Hz simulation.

Table 11:  $t_{trip}$  Sensitivity to Grade

Grade	Coast Mode	ZPM Mode	ZPB Mode	-1.5 m/sec <sup>2</sup> Regen	Coast-Regen	ZPB-Regen	Units
-2%	N/A			-0.15%	N/A		
-1%							
-0.5%							
<b>0%</b>	<b>107.7</b>	<b>102.1</b>	<b>90.7</b>	<b>66.3</b>	<b>87.5</b>	<b>80.7</b>	<b>sec</b>
1%	-21.9%	-18.9%	-12.4%	-0.2%	-13.8%	-8.7%	
2%	-28.5%	-25.1%	-17.3%		-18.0%	-12.1%	

These tables demonstrate that the model is sensitive to changes in grade. It also provides insight into how different decel modes might be advantageous at different grades. The gap in energy consumption and travel time may be reduced as grade increased, and solutions that include regenerative braking may be advantageous in downhill situations. More data could be collected for the multi-mode strategies on downhill grades if the trip length is extended and the mode transition speed is raised. These trends are consistent across other cruise speed cases.

Sensitivity to changes in accessory load is assessed by studying changes in energy consumption for all cases. Since changing accessory load only changes how the powertrain model calculates necessary battery power, most velocity profiles are unchanged. The two exceptions are the ZPB mode and ZPB-Regen decel strategies. Those modes create different tractive forces, and thus different accelerations, based on how the accessory load changes. Table 12 shows the effect of increasing or decreasing

accessory load  $P_{accy}$  on energy consumption from 302 W for the selected 25 mph case decel strategies. Baseline energy consumption (the 302 W accessory load) is listed along with the percent change in energy consumption for the other loads.

Table 12: Energy Consumption Sensitivity to  $P_{accy}$

$P_{accy}$ (W)	Coast Mode	ZPM Mode	ZPB Mode	-1.5 m/sec <sup>2</sup> Regen	Coast- Regen	ZPB- Regen	Units
50	-47.6%	-44.4%	-45.7%	-19.0%	-36.9%	-37.9%	
150	-28.8%	-26.8%	-26.3%	-11.5%	-22.3%	-22.3%	
<b>302</b>	<b>36.44</b>	<b>37.03</b>	<b>41.36</b>	<b>56.30</b>	<b>38.26</b>	<b>42.75</b>	<b>Wh/mi</b>
750	84.4%	78.7%	65.6%	33.6%	65.3%	58.5%	
1500	225.9%	210.7%	158.4%	89.9%	174.7%	145.3%	

Strategies that Coast and ZPM modes are most sensitive to increases in  $P_{accy}$ . As shown in the energy vs. speed figures, those strategies operate at power levels much lower in magnitude than the regen braking strategy, meaning that energy consumption by accessory loads comprises most energy consumption in those cases. Coasting and strategies like it tend to result in longer total trip times than regenerative braking due to lower average decel rates during the decel mode. Since accessory loads act as a constant, time-invariant gain on power consumption in the HV bus, longer travel times result in larger overall energy consumption. Thus, the advantage of coasting, pseudo-coasting, and multi-mode strategies over regen with respect to energy consumption is slowly eliminated as accessory power rises.

Conversely, lowering accessory loads leads to the largest decreases in energy consumption among those same strategies. Using coast, ZPM, and ZPB modes only when accessory power is at 50 W results in nearly 50% less energy consumption; for comparison, regen braking at 50 W only results in 20% less energy consumption (which is still higher, in fact, than the base case of any other strategy). These results suggest

that coasting and pseudo-coasting may be better suited for cases with low accessory power than regen. These trends are consistent across other cruise speed cases.

Besides regen, the cases least sensitive to accessory load changes are the two strategies that use ZPB mode, during which accessory loads are neutralized by regenerated power during decel. Deceleration using the ZPB mode is determined by the amount of negative tractive power required to feed accessory loads, so higher  $P_{accy}$  results in more aggressive deceleration. A higher decel rate also increases the cruise distance required, and additional time at cruise speed means more energy consumption at high power levels. However, unlike with coast and ZPM modes, which require increased energy consumption from start to stop as accessory loads rise, strategies that use ZPB mode only require more energy while cruising as accessory loads rise. Model sensitivity to changes in accessory load across all solutions means it should be useful for assessing decel strategy performance with different expected accessory power levels irrespective of initial speed. The performance and model sensitivity results for this study of the Nissan LEAF® SV/SL confirms that not only can the model and methodology be applied to other configurations of this vehicle, but also to other BEV makes and models as well. Parameterization of a complete BEV model in terms of publicly available data allows this work to be replicated for any BEV whose manufacturer has supplied certification information to the EPA. No attempt to collect vehicle information for this model from other international regulatory agencies has been made, but such extension of this work would improve the universality of these methods.

## Chapter 6: Conclusions

This study proposes a process for developing and analyzing deceleration strategies for battery electric vehicles. The first contribution of this work is a two-part model based on publicly sourced vehicle data. A model of tractive effort is created based on road load parameters sourced from coastdown test data, and a model of mechanical and electrical power is formed based on bidirectional Willans lines of powertrain components that are calculated using regulatory certification information. The model also accounts for common electrified vehicle characteristics such as regenerative braking and powertrain behavior at low speeds. Applying model parameters for the 2019 Nissan LEAF® SV/SL trimlines and comparing modeled energy consumption to EPA-reported data confirms that BEV performance can be modeled backward from prescribed velocity profiles with an acceptable margin of error. The second contribution of the study is a method for calculating the vehicle speed trajectory and energy consumption for novel alternatives to regenerative braking. The model is enhanced to allow for forward modeling of vehicle velocity from a prescribed power input either in the tractive effort or powertrain model. Coasting (deceleration when the vehicle receives zero tractive effort from the powertrain at the wheel and acceleration is solely dependent on road load) is modeled using a 10 Hz discrete-time simulation. This speed trace is verified against an independently derived analytical solution. Additional methods of deceleration based on inputs such as zero mechanical power or zero battery power are also modeled. As a control, regenerative braking is simulated using several velocity profiles with linear deceleration. All strategies for decelerating a BEV are paired with an initial cruise phase to compare them over a 10 Hz fixed-route simulation. Decel strategies are assessed at three cruise speeds common

in urban driving. During the simulations beginning at 25 mph, coasting consumes 30% less battery energy than regen braking, but regen braking enables the vehicle to finish the trip in 40% less time than coasting. The solutions based on zero motor or battery power perform similarly as coasting except with slightly faster deceleration due to more negative tractive effort at the wheel. A multi-mode strategy, where coasting or a zero-power deceleration mode is used in series with regenerative braking, is implemented using a tunable parameter as an intermediate solution. It balances the weaknesses of each mode with the strengths of the other. The final contribution of this work is a method of scoring strategies using polar coordinates. Radius represents overall cost based on two performance metrics, and angle denotes bias towards minimizing a single metric. Scoring the solutions reveals that multi-mode solutions lower overall cost by balancing energy consumption with travel time better than either coasting or regenerative braking. Finally, the modeled solutions display sensitivity to both grade and accessory loads, which indicates that the model is robust enough to assess solution performance irrespective of the values of those parameters. Such versatility demonstrates the usefulness of the vehicle model presented and the viability of the novel deceleration strategies proposed. The model and methodology can be applied to other battery electric vehicles to assess their performance using these deceleration strategies. The model and strategies could enhance connected and automated vehicle (CAV) software solutions for electrified vehicle platforms. The ability to model and calculate an optimal deceleration strategy akin to the ones discussed in this work has the potential to enhance driver-assist systems and autonomous vehicle appeal as engineers strive to balance energy consumption with other performance metrics that are important to consumers.

## References

1. Chen, Yuche, Guoyuan Wu, Ruixiao Sun, Abhishek Dubey, Aron Laszka, and Philip Pugliese. 2021. "A Review and Outlook on Energy Consumption Estimation Models for Electric Vehicles." *SAE International Journal of Sustainable Transportation, Energy, Environment, & Policy* 2 (1): 79–96.  
<https://doi.org/10.4271/13-02-01-0005>.
2. Gohlke, David, and Yan Zhou. 2020. "Assessment of Light-Duty Plug-in Electric Vehicles in the United States, 2010 - 2019."  
<https://publications.anl.gov/anlpubs/2021/06/167626.pdf>.
3. Vahidi, Ardalan, and Antonio Sciarretta. 2018. "Energy Saving Potentials of Connected and Automated Vehicles." *Transportation Research Part C: Emerging Technologies* 95 (April 2018): 822–43.  
<https://doi.org/10.1016/j.trc.2018.09.001>.
4. Sakai, Akira, Tetsuya Miyazaki, Takahiro Okano, Kazunori Nimura, and Daisuke Nakata. 2014. "Regenerative Braking Systems." In *Encyclopedia of Automotive Engineering*, 1–15.  
<https://doi.org/10.1002/9781118354179.auto053>.
5. Koch-Groeber, Hermann, and Jue Wang. 2014. "Criteria for Coasting on Highways for Passenger Cars." SAE Technical Paper 2014-01-1157, 2014.  
<https://doi.org/10.4271/2014-01-1157>.
6. Bao, Ran, Philip Griggs, and James Baxter. 2018. "Simulation Based Control Strategy Design of All Wheel Drive Electric Vehicle Regenerative Braking System." SAE Technical Paper 2018-01-0411, 2018.  
<https://doi.org/10.4271/2018-01-0411>.
7. Björnsson, Lars Henrik, and Sten Karlsson. 2016. "The Potential for Brake Energy Regeneration under Swedish Conditions." *Applied Energy* 168: 75–84.  
<https://doi.org/10.1016/j.apenergy.2016.01.051>.
8. Yang, Zujie, Tan Gangfeng, Hongwei Ling, Puchun Zeng, Changxi Li, and Li Liu. 2021. "Research on Braking Energy Recovery Strategy of Pure Electric Vehicle." SAE Technical Paper 2021-01-1264, 2021.  
<https://doi.org/10.4271/2021-01-1264>.
9. Lv, Chen, Junzhi Zhang, Yutong Li, Bolin Zhao, and Ye Yuan. 2016. "Robust Control of Regenerative and Hydraulic Brakes for Enhancing Directional Stability of an Electric Vehicle during Straight-Line Braking." *SAE International Journal of Alternative Powertrains* 5 (2): 328–37.  
<https://doi.org/10.4271/2016-01-1669>.
10. Sovran, Gino, and Dwight Blaser. 2006. "Quantifying the Potential Impacts of Regenerative Braking on a Vehicle's Tractive-Fuel Consumption for the U.S., European, and Japanese Driving Schedules." SAE Technical Paper 2006-01-0664, 2006.  
<https://doi.org/10.4271/2006-01-0664>.

11. Sovran, Gino. 2011. "The Impact of Regenerative Braking on the Powertrain-Delivered Energy Required for Vehicle Propulsion." SAE Technical Paper 2011-01-0891, 2011.  
<https://doi.org/10.4271/2011-01-0891>.
12. Liu, Zheng, Walter J. Ortmann, Bernard Nefcy, Dan Colvin, and Francis Connolly. 2017. "Methods of Measuring Regenerative Braking Efficiency in a Test Cycle." *SAE International Journal of Alternative Powertrains* 6 (1): 103–12.  
<https://doi.org/10.4271/2017-01-1168>.
13. Rask, Eric, Danilo Santini, and Henning Lohse-Busch. 2013. "Analysis of Input Power, Energy Availability, and Efficiency during Deceleration for X-EV Vehicles." *SAE International Journal of Alternative Powertrains* 2 (2): 350–61.  
<https://doi.org/10.4271/2013-01-1473>.
14. Kulas, R.A., Rieland, H., and Pechauer, J., "A System Safety Perspective into Chevy Bolt's One Pedal Driving," SAE Technical Paper 2019-01-0133, 2019,  
<https://doi.org/10.4271/2019-01-0133>.
15. Won, M.W., "A Study on the Improvement of EV One-Pedal Driving System Interface and Cost Reduction," SAE Technical Paper 2022-01-0645, 2022,  
<https://doi.org/10.4271/2022-01-0645>.
16. Legg, T. and Nelson, D., "Development of a Willans Line Rule-Based Hybrid Energy Management Strategy," SAE Technical Paper 2022-01-0735, 2022,  
<https://doi.org/10.4271/2022-01-0735>.
17. Shakouri, Payman, Andrzej Ordys, Paul Darnell, and Peter Kavanagh. 2013. "Fuel Efficiency by Coasting in the Vehicle." *International Journal of Vehicular Technology* 2013 (August): 1–14.  
<https://doi.org/10.1155/2013/391650>.
18. Guo, Lulu, Hong Chen, Qifang Liu, and Bingzhao Gao. 2019. "A Computationally Efficient and Hierarchical Control Strategy for Velocity Optimization of On-Road Vehicles." *IEEE Transactions on Systems, Man, and Cybernetics: Systems* 49 (1): 31–41.  
<https://doi.org/10.1109/TSMC.2018.2826005>.
19. Sun, Daxu, Fengchong Lan, Yunjiao Zhou, and Jiqing Chen. 2015. "Control Algorithm of Electric Vehicle in Coasting Mode Based on Driving Feeling." *Chinese Journal of Mechanical Engineering (English Edition)* 28 (3): 479–86.  
<https://doi.org/10.3901/CJME.2015.0317.032>.
20. Lee, Heekwang, Muluneh Lemma Woldesemayat, and Kwanghee Nam. 2017. "Zero Torque Control for EV Coasting Considering Cross-Coupling Inductance." *IEEE Transactions on Industrial Electronics* 64 (8): 6096–6104.  
<https://doi.org/10.1109/TIE.2017.2681973>.
21. Harvey, Dan Raymond. "Willans Line Modeling for Powertrain Analysis and Energy Consumption of Electric Vehicles." MS Thesis, Virginia Tech, 2021.

22. Harvey, Dan, and Douglas Nelson. 2022. "Willans Line Bidirectional Power Flow Model for Energy Consumption of Electric Vehicles." SAE Technical Paper 2022-01-0531, 2022.  
<https://doi.org/10.4271/2022-01-0531>.
23. Philips, Patrick, Thomas Megli, and William Ruona. 2022. "Unified Power-Based Analysis of Combustion Engine and Battery Electric Vehicle Energy Consumption." SAE Technical Paper 2022-01-0532, 2022.  
<https://doi.org/10.4271/2022-01-0532>.
24. SAE International Surface Vehicle Recommended Practice, "Chassis Dynamometer Simulation of Road Load Using Coastdown Techniques," SAE Standard J2264, Rev. Jan. 2014.
25. SAE International Surface Vehicle Recommended Practice, "Road Load Measurement and Dynamometer Simulation Using Coastdown Techniques," SAE Standard J1263, Rev. Mar. 2010.
26. Nakamura, E., Soga, M., Sakai, A., Otomo, A., and Kobayashi, T., "Development of Electronically Controlled Brake System for Hybrid Vehicle," SAE Technical Paper 2002-01-0300, 2002,  
<https://doi.org/10.4271/2002-01-0300>.
27. U.S. Environmental Protection Agency. *Data on Cars used for Testing Fuel Economy*. Michigan, 2020.  
<https://www.epa.gov/sites/default/files/2020-10/19tstcar-2020-10-02.xlsx>
28. U.S. Environmental Protection Agency. *Certificate Summary Information for NISSAN MOTOR CO., LTD. 2019 model year test group KNSXV0000TS3 evaporative family not listed*. Michigan, 2018.  
[https://dis.epa.gov/otaqpub/display\\_file.jsp?docid=46941&flag=1](https://dis.epa.gov/otaqpub/display_file.jsp?docid=46941&flag=1)
29. Li, Candy. "Unified Willans Line Model for Estimating the Energy Consumption of Battery Electric Vehicles". MS Thesis, Virginia Tech, 2022
30. Dib, Wissam, Alexandre Chasse, Philippe Moulin, Antonio Sciarretta, and Gilles Corde. 2014. "Optimal Energy Management for an Electric Vehicle in Eco-Driving Applications." *Control Engineering Practice* 29: 299–307.  
<https://doi.org/10.1016/j.conengprac.2014.01.005>.
31. Moon, Seungwuk, and Kyongsu Yi. 2008. "Human Driving Data-Based Design of a Vehicle Adaptive Cruise Control Algorithm." *Vehicle System Dynamics* 46 (8): 661–90.  
<https://doi.org/10.1080/00423110701576130>.
32. Guzzella, Lino, and Antonio Sciarretta. 2013. *Vehicle Propulsion Systems: Introduction to Modeling and Optimization*. 3rd ed. Berlin, Heidelberg: Springer Berlin Heidelberg.  
<https://doi.org/10.1007/978-3-642-35913-2>.
33. Nelson, Douglas J. Virginia Tech College of Engineering, personal communication, Oct. 2021.



## Appendix A: Willans Line Overview

A Willans Line model describes power on one side of a components as a linear function of the power on the other side of the it. It can be applied to powertrain components in an electrified vehicle such as a gearbox and motor-inverter system. Inefficiency in these components is quantified using a marginal efficiency  $\eta$  and a constant power offset  $P_{loss}$ . Since electrified vehicles are capable of power flow in two directions, a bidirectional Willans Line is needed for both propel and regen modes. In propel mode, power is positive and flows from the high voltage bus to the wheel. The power required as an input to the component is a function of desired power output from the component such that

$$P_{in+} = \frac{1}{\eta} P_{out+} + P_{loss}. \quad (A.1)$$

As a result, the required input power upstream from the component larger in magnitude and more positive than the output power downstream. Figure A.1 shows the impact of the marginal efficiency and offset loss terms.  $P_{loss}$  is 1 kW and marginal efficiency  $\eta$  is 0.75. As output power increases, overall efficiency (the ratio of downstream power to upstream power) asymptotically approaches the marginal efficiency. Losses also increase linearly as downstream power increases. In regen mode, power is negative and flows from the wheel to the HV bus. The power that is output from the component towards the HV bus upstream is a function of power input to the component from the downstream direction such that

$$P_{out-} = \eta P_{in-} + P_{loss}. \quad (A.2)$$

Generally, the power output from the component is smaller in magnitude and less negative that what was input to the component during regen.

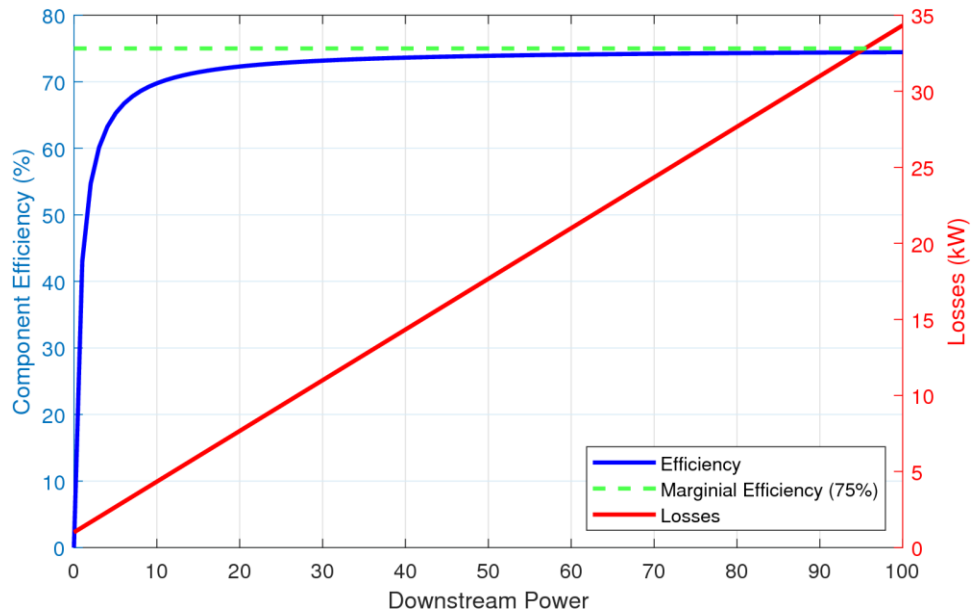


*Figure A.1: Component Efficiency vs. Output Power*

Figure A.2 plots a hypothetical bidirectional Willans Line. In this example,  $P_{loss}$  is 1 kW and marginal efficiency  $\eta$  is 0.75. The slope of the regen Willans Line (green) is 0.75, and the slope of the propel Willans Line (red) is 1.33. A slope less than unity for regen and one greater than unity for propel is consistent with power becoming smaller in magnitude as it travels through the powertrain from the HV bus to the wheel during propel and from the wheel to the HV bus during regen.

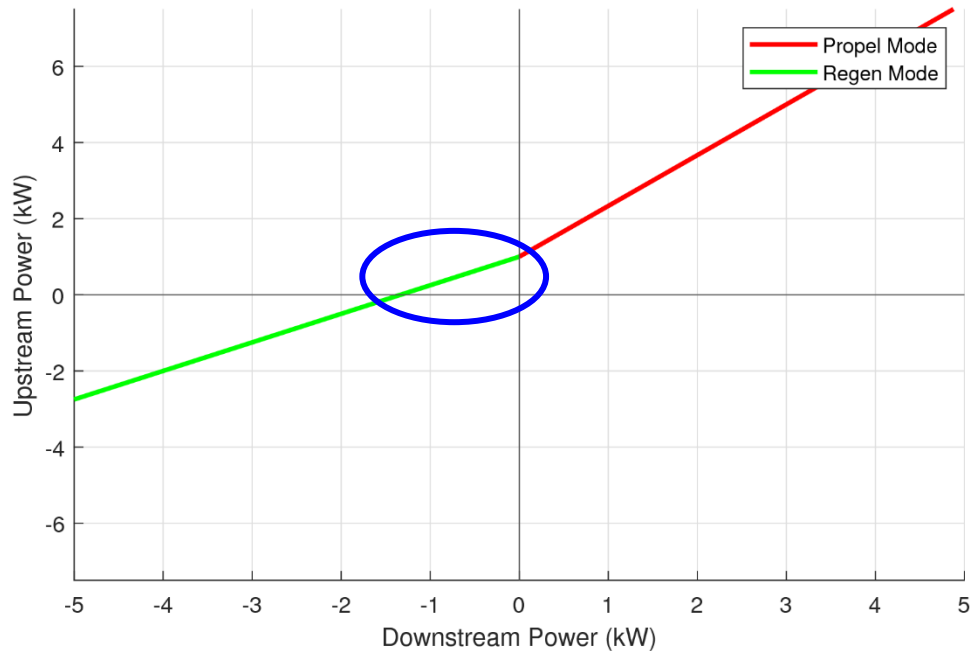


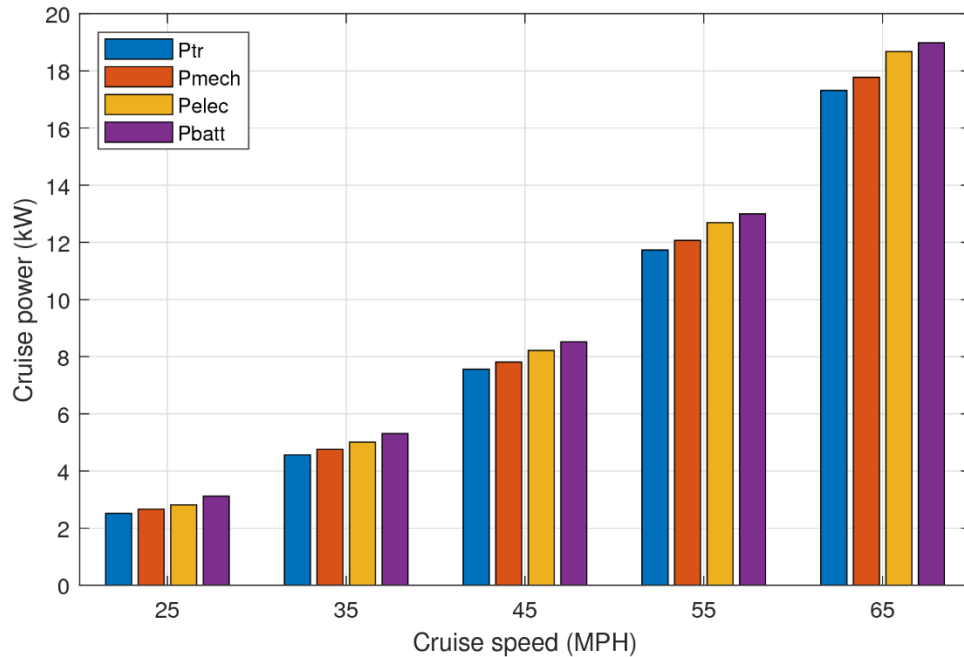
*Figure A.2: Bidirectional Willans Line Example*

An interesting artifact of the regen mode Willans Line is the range of values of downstream power that result in positive values of upstream power (circled in Figure A.2). Between the value of downstream power where upstream power equals zero and zero downstream power, downstream power is not negative enough to overcome losses and produce upstream power that is negative (i.e., power being transferred in the direction of the HV bus and battery pack). In this case, power flows from the HV bus downstream towards the wheel, meaning that regen braking is consuming battery energy rather than regenerating it.

These equations can be rearranged to solve for downstream power given a known upstream power value. Such forward modeling capability allows for study of pseudo-coasting scenarios whose solutions are based on zero power somewhere within the powertrain model.

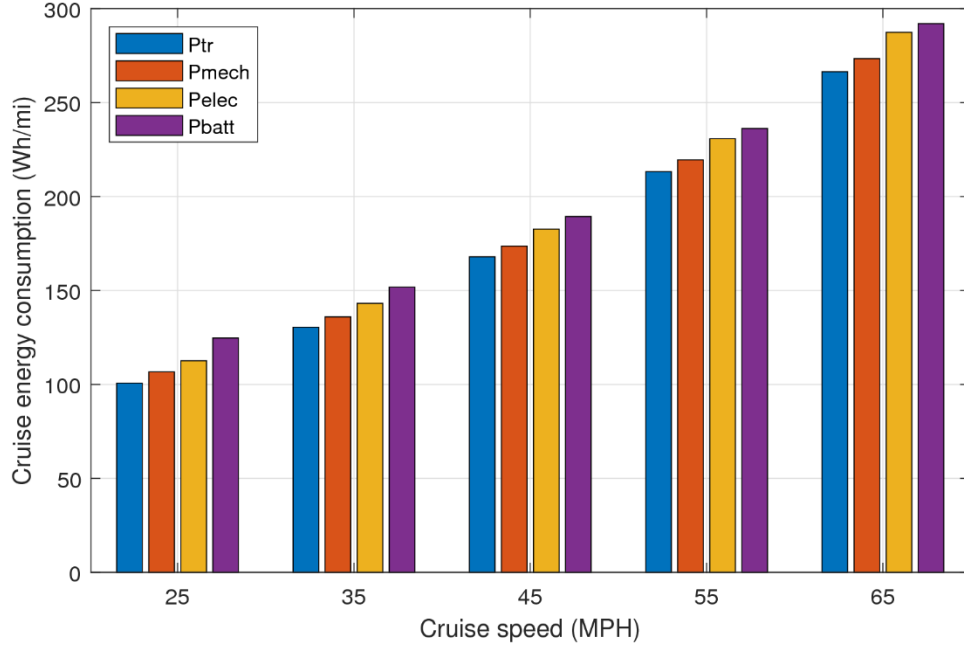
## Appendix B: Cruise Power and Energy Consumption

Figure B.1 illustrates the power needed at the wheels and throughout the powertrain for cruise speeds for situations ranging from urban to highway driving. As cruise speed increases, power levels increase in an approximately quadratic manner due to dominance of aerodynamic forces (which are correlated to speed-squared) at higher speeds.



*Figure B.1: Power Requirements vs. Cruise Speeds*

Energy consumption in terms of Wh/mi can be found by dividing the cruise power (converted to Watts) by speed (mph). The results are given for the same range of speeds in Figure B.2. Energy consumption is an approximately linear function due to an approximately quadratic power function being divided by a linear increase in speed.



*Figure B.2: Cruise energy consumption vs. Cruise speed*

These power requirements are used to determine the energy consumption of each decel strategy during the respective cruise portions of the simulation. Energy consumption, calculated via the model in Figure 11, is found to be

$$E_{cruise} = P_{cruise} t_{cruise}, \quad (55)$$

Where  $P_{cruise}$  is any of the power values given in Figures 26, and  $t_{cruise}$  is the time spent at cruise speed:

$$t_{cruise} = \frac{x_{cruise}}{v_{cruise}}. \quad (56)$$

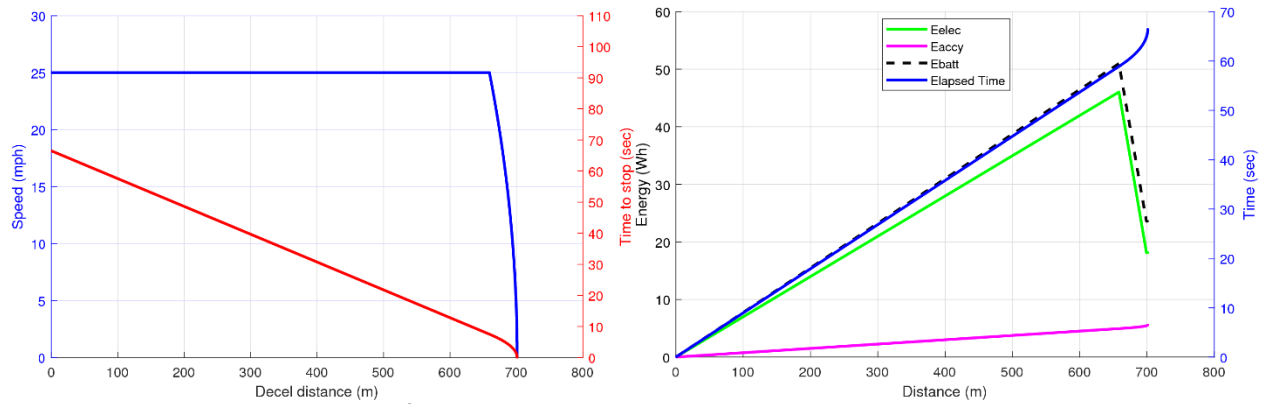
## Appendix C: 25 mph Simulation Results

Table 1C: Simulation Summary, 25 mph case

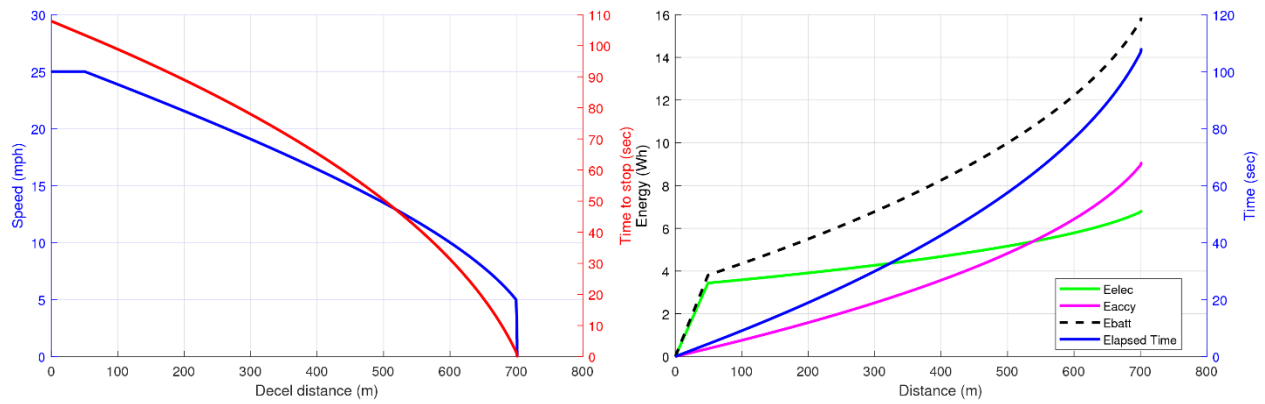
Parameter	Coast Mode	Zero Pmech (ZPM)	Zero Pbatt (ZPB)	-1 m/sec <sup>2</sup> Regen	-1.5 m/sec <sup>2</sup> Regen	Units
vi	11.18	11.18	11.18	11.18	11.18	m/sec
vf	2.24	2.24	2.24	2.24	2.24	m/sec
tf	101.80	91.40	68.60	8.90	5.90	sec
sf	648.96	595.58	468.26	59.86	39.83	m
accel_min	-0.11	-0.12	-0.18	-1.00	-1.50	m/sec <sup>2</sup>
accel_max	-0.07	-0.09	-0.12	-1.00	-1.50	m/sec <sup>2</sup>
accel_avg	-0.09	-0.10	-0.13	-1.00	-1.50	m/sec <sup>2</sup>
vel_min	2.24	2.24	2.24	2.28	2.33	m/sec
vel_max	11.18	11.18	11.18	11.18	11.18	m/sec
vel_avg	6.38	6.52	6.83	6.73	6.75	m/sec
Ebatt	42.68	28.72	0.00	-91.74	-96.06	kJ
E_pt	0.00	-9.33	-32.02	-108.76	-112.29	kJ
E_elec	11.91	1.10	-20.73	-94.43	-97.85	kJ
Tmot+, max	1.69	0.00	0.00	0.00	0.00	Nm
Tmot-, min	0.00	0.00	-5.56	-63.72	-98.76	Nm
Tmot,avg	0.72	0.00	-2.18	-63.13	-98.16	Nm
sCruise	49.3	102.7	230.0	638.4	658.5	m
tCruise	4.415	9.2	20.6	57.1	58.9	sec
sCycle	700.0	700.0	700.0	700.0	700.0	m
tCycle	107.7	102.1	90.7	67.5	66.3	sec
Ept, cruise	11.11	23.13	51.79	143.74	148.25	kJ
Ebatt, cruise	13.76	28.64	64.14	178.02	183.60	kJ
Ept, cycle	6.34	9.03	14.99	30.20	31.18	kJ
Ebatt, cycle	57.05	57.97	64.76	86.89	88.15	kJ
Energy consump., cycle	36.4	37.0	41.4	55.5	56.3	Wh/mi

Table 2C: Simulation Summary, 25 mph case, cont'd

Parameter	-2 m/sec <sup>2</sup> Regen	-2.5 m/sec <sup>2</sup> Regen	Hybrid Solution 1	Hybrid Solution 2	Hybrid Solution 3	Units
vi	11.18	11.18	11.18	11.18	11.18	m/sec
vf	2.24	2.24	2.24	2.24	2.24	m/sec
tf	4.40	3.50	73.00	67.70	54.20	sec
sf	29.81	23.80	553.03	516.04	419.26	m
accel_min	-2.00	-2.50	-2.50	-2.50	-2.50	m/sec <sup>2</sup>
accel_max	-2.00	-2.50	-0.08	-0.09	-0.12	m/sec <sup>2</sup>
accel_avg	-2.00	-2.50	-0.12	-0.13	-0.16	m/sec <sup>2</sup>
vel_min	2.38	2.43	2.46	2.47	2.46	m/sec
vel_max	11.18	11.18	11.18	11.18	11.18	m/sec
vel_avg	6.78	6.80	7.57	7.62	7.73	m/sec
E <sub>batt</sub>	-98.12	-99.27	18.79	9.53	-11.49	kJ
E <sub>pt</sub>	-113.94	-114.83	-13.47	-20.30	-38.40	kJ
E <sub>elec</sub>	-99.45	-100.33	-3.28	-10.93	-27.87	kJ
T <sub>mot+</sub> , max	0.00	0.00	0.85	0.00	0.00	Nm
T <sub>mot-</sub> , min	-133.81	-168.85	-168.85	-168.85	-168.85	Nm
T <sub>mot</sub> , avg	-133.19	-168.23	-1.32	-1.99	-4.18	Nm
sCruise	668.5	674.5	145.3	182.3	279.0	m
tCruise	59.8	60.4	13.0	16.3	25.0	sec
sCycle	700.0	700.0	700.0	700.0	700.0	m
tCycle	65.7	65.4	87.5	85.5	80.7	sec
E <sub>pt</sub> , cruise	150.51	151.86	32.71	41.03	62.82	kJ
E <sub>batt</sub> , cruise	186.40	188.07	40.51	50.82	77.81	kJ
E <sub>pt</sub> , cycle	31.79	32.26	14.47	15.96	19.65	kJ
E <sub>batt</sub> , cycle	88.89	89.42	59.91	60.96	66.93	kJ
Energy consump., cycle	56.8	57.1	38.3	38.9	42.7	Wh/mi



**Figure C.1:  $-1.5 \text{ m/sec}^2$  Regen Braking Fixed-Route Simulation, 25 mph Case**



**Figure C.2: Coast Mode Fixed-Route Simulation, 25 mph Case**

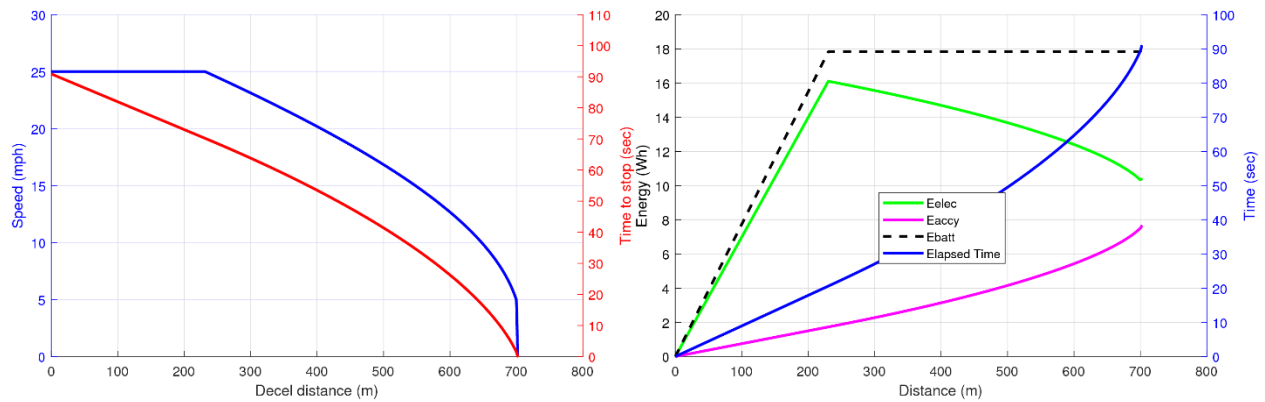


**Figure C.3: ZPB Mode Fixed-Route Simulation, 25 mph Case**



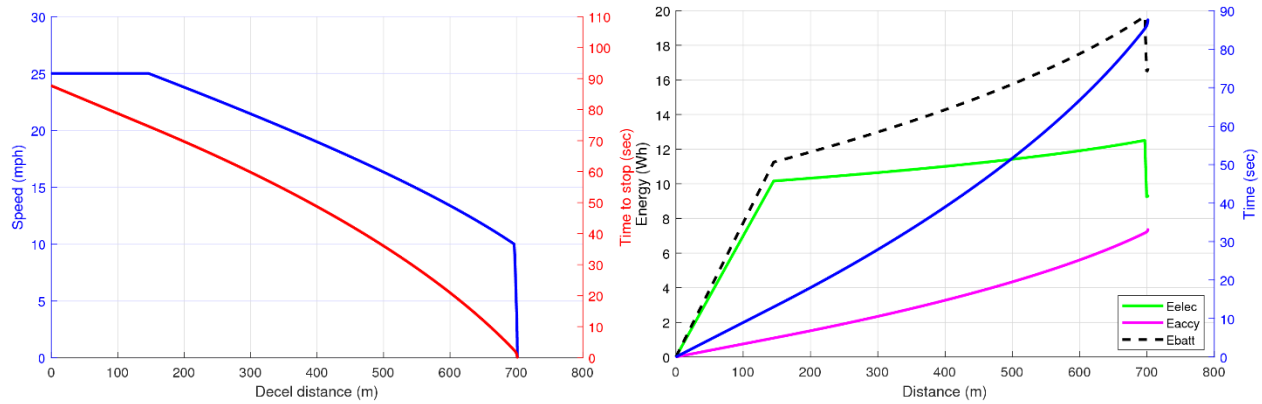


Figure C.4: Coast-Regen Fixed-Route Simulation, 25 mph Case

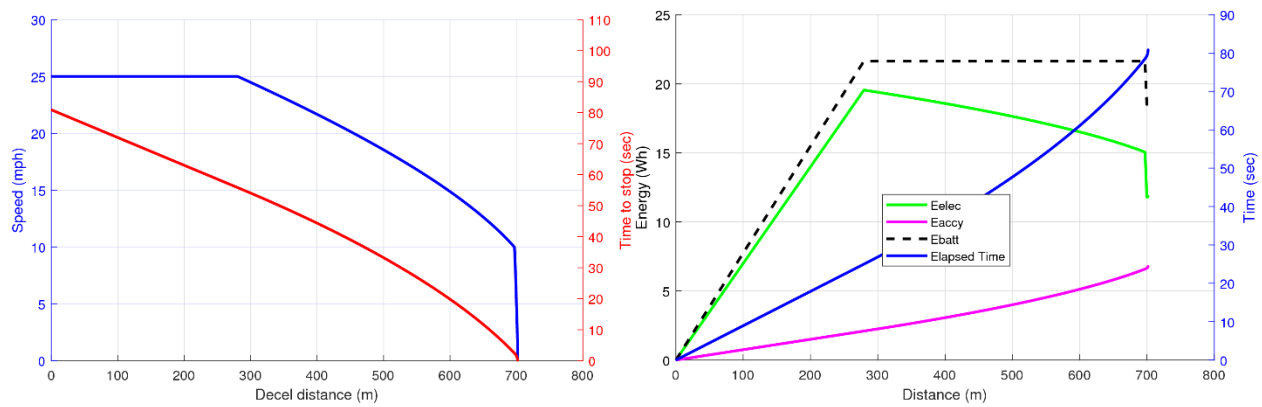


Figure C.5: ZPB-Regen Fixed-Route Simulation, 25 mph Case

## Appendix D: 35 mph Simulation Results

Table 1D: Simulation Summary, 35 mph case

Parameter	Coast Mode	Zero Pmech (ZPM)	Zero Pbatt (ZPB)	-1 m/sec <sup>2</sup> Regen	-1.5 m/sec <sup>2</sup> Regen	Units
vi	15.65	15.65	15.65	15.65	15.65	m/sec
vf	2.24	2.24	2.24	2.24	2.24	m/sec
tf	136.80	125.40	99.40	13.40	8.90	sec
sf	1115.50	1048.58	878.67	119.88	79.85	m
accel_min	-0.15	-0.15	-0.18	-1.00	-1.50	m/sec <sup>2</sup>
accel_max	-0.07	-0.09	-0.12	-1.00	-1.50	m/sec <sup>2</sup>
accel_avg	-0.10	-0.11	-0.13	-1.00	-1.50	m/sec <sup>2</sup>
vel_min	2.24	2.24	2.24	2.25	2.30	m/sec
vel_max	15.65	15.65	15.65	15.65	15.65	m/sec
vel_avg	8.15	8.36	8.84	8.95	8.97	m/sec
Ebatt	57.35	39.40	0.00	-181.81	-191.29	kJ
E_pt	0.00	-12.80	-46.40	-213.57	-222.28	kJ
E_elec	16.01	1.50	-30.04	-185.86	-193.98	kJ
Tmot+, max	1.69	0.00	0.00	0.00	0.00	Nm
Tmot-, min	0.00	0.00	-5.58	-63.72	-98.76	Nm
Tmot,avg	0.61	0.00	-1.80	-62.35	-97.37	Nm
sCruise	82.8	149.7	319.6	1078.4	1118.5	m
tCruise	5.3	9.6	20.4	68.9	71.5	sec
sCycle	1200.0	1200.0	1200.0	1200.0	1200.0	m
tCycle	143.6	136.5	121.3	83.8	81.9	sec
Ept, cruise	24.15	43.67	93.24	314.58	326.25	kJ
Ebatt, cruise	28.11	50.82	108.50	366.08	379.67	kJ
Ept, cycle	19.38	26.11	42.06	96.23	99.20	kJ
Ebatt, cycle	86.07	90.84	109.11	184.88	188.99	kJ
Energy consump., cycle	32.1	33.8	40.7	68.9	70.4	Wh/mi

Table 2D: Simulation Summary, 35 mph case, cont'd

Parameter	-2 m/sec^2 Regen	-2.5 m/sec^2 Regen	Hybrid Solution 1	Hybrid Solution 2	Hybrid Solution 3	Units
vi	15.65	15.65	15.65	15.65	15.65	m/sec
vf	2.24	2.24	2.24	2.24	2.24	m/sec
tf	6.70	5.30	58.90	56.90	50.80	sec
sf	59.94	47.81	694.66	671.42	600.26	m
accel_min	-2.00	-2.50	-2.50	-2.50	-2.50	m/sec^2
accel_max	-2.00	-2.50	-0.10	-0.10	-0.12	m/sec^2
accel_avg	-2.00	-2.50	-0.22	-0.23	-0.26	m/sec^2
vel_min	2.25	2.40	2.44	2.43	2.43	m/sec
vel_max	15.65	15.65	15.65	15.65	15.65	m/sec
vel_avg	8.95	9.02	11.79	11.80	11.81	m/sec
Ebatt	-196.30	-194.70	-38.07	-44.59	-61.61	kJ
E_pt	-226.96	-228.96	-71.54	-77.05	-93.97	kJ
E_elec	-198.32	-196.30	-55.87	-61.78	-76.96	kJ
Tmot+, max	0.00	0.00	0.42	0.00	0.00	Nm
Tmot-, min	-133.81	-168.85	-168.85	-168.85	-168.85	Nm
Tmot,avg	-132.41	-165.07	-7.12	-7.69	-9.61	Nm
sCruise	1138.4	1150.5	503.6	526.9	598.0	m
tCruise	72.8	73.5	32.2	33.7	38.2	sec
sCycle	1200.0	1200.0	1200.0	1200.0	1200.0	m
tCycle	81.0	80.3	92.6	92.1	90.5	sec
Ept, cruise	332.06	335.60	146.91	153.69	174.45	kJ
Ebatt, cruise	386.42	390.54	170.97	178.85	203.01	kJ
Ept, cycle	100.33	101.87	70.60	71.87	75.71	kJ
Ebatt, cycle	190.74	196.46	133.51	134.88	142.01	kJ
Energy consump., cycle	71.1	73.2	49.7	50.2	52.9	Wh/mi

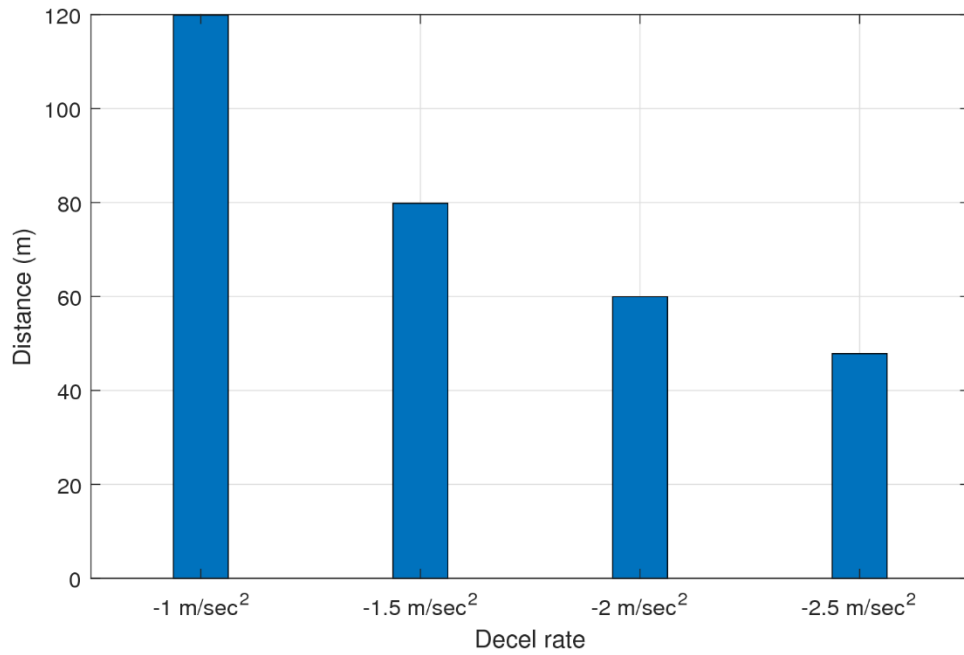


Figure D.1: Stopping Distance, Linear Decel, 35 mph Case

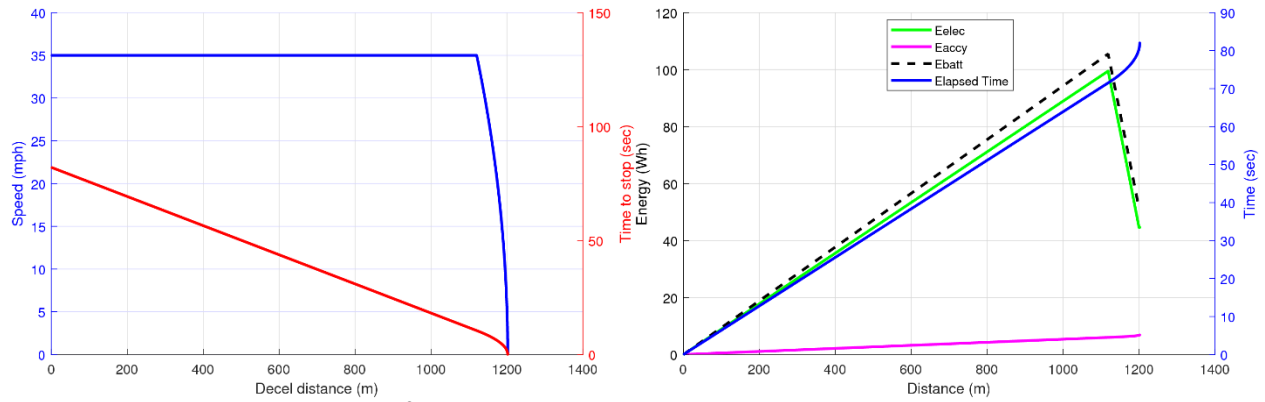


Figure D.2: -1.5  $\text{m/sec}^2$  Regen Braking Fixed-Route Simulation, 35 mph Case

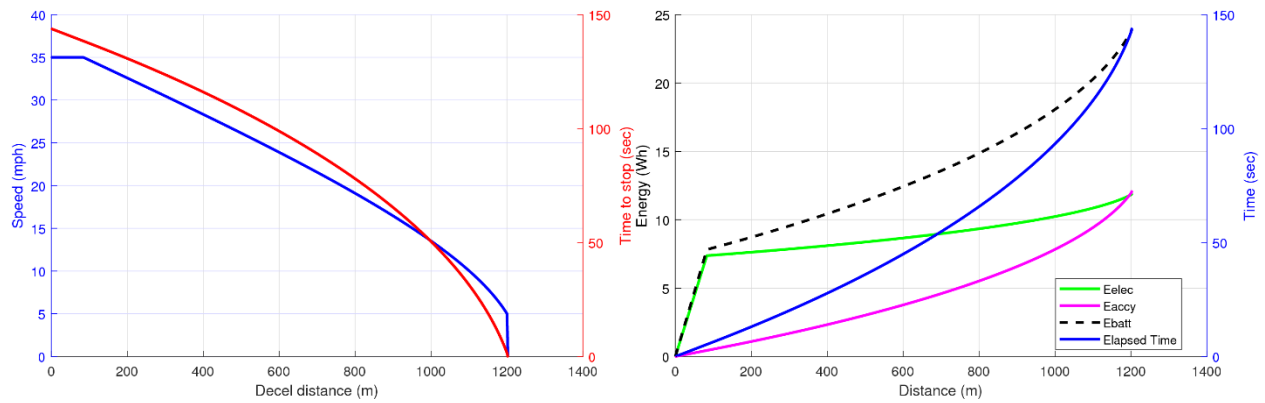


Figure D.3: Coast Mode Fixed-Route Simulation, 35 mph Case

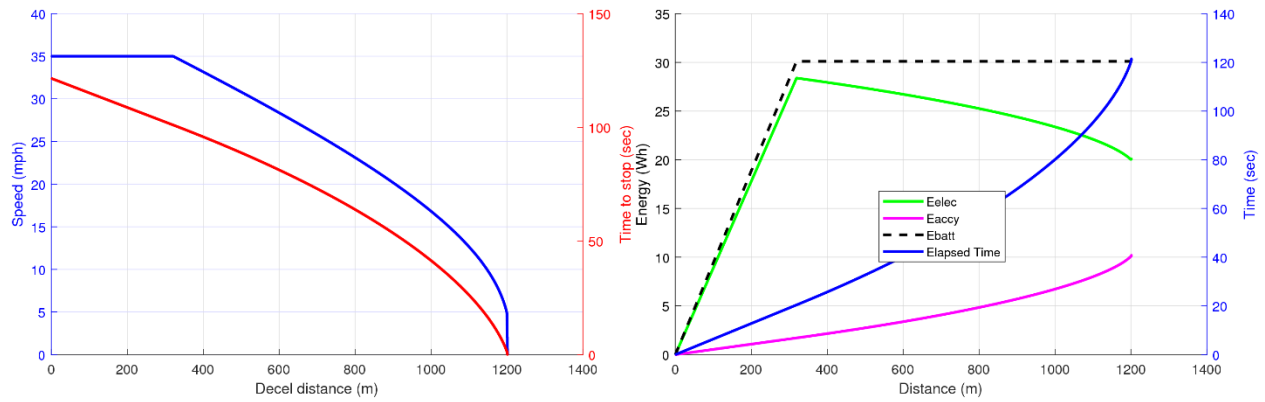


Figure D.4: ZPB Mode Fixed-Route Simulation, 35 mph Case

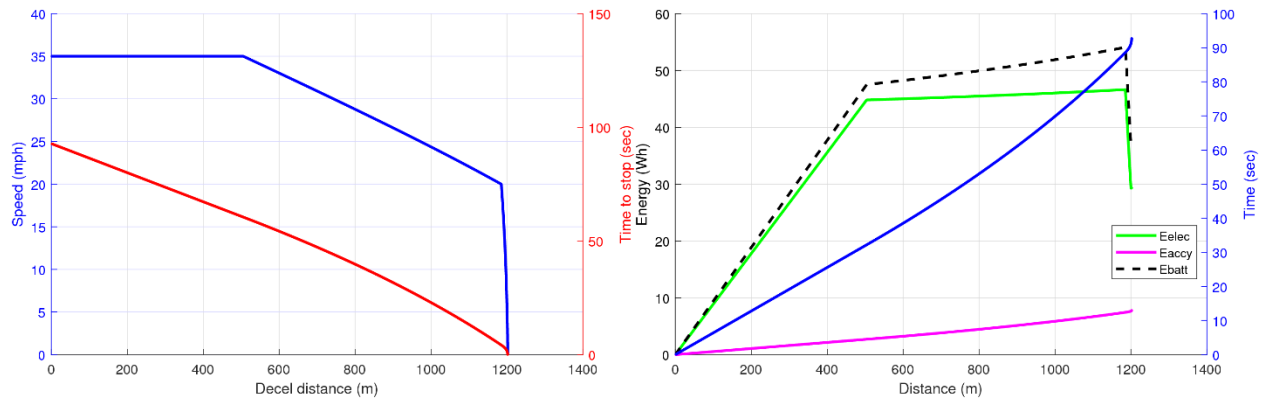


Figure D.5: Coast-Regen Fixed-Route Simulation, 35 mph Case

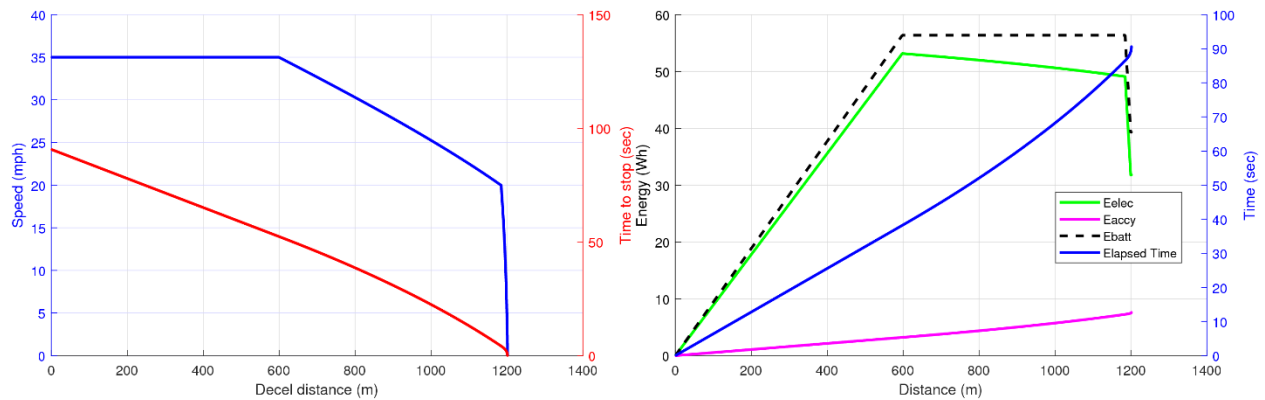


Figure D.6: ZPB-Regen Fixed-Route Simulation, 35 mph Case

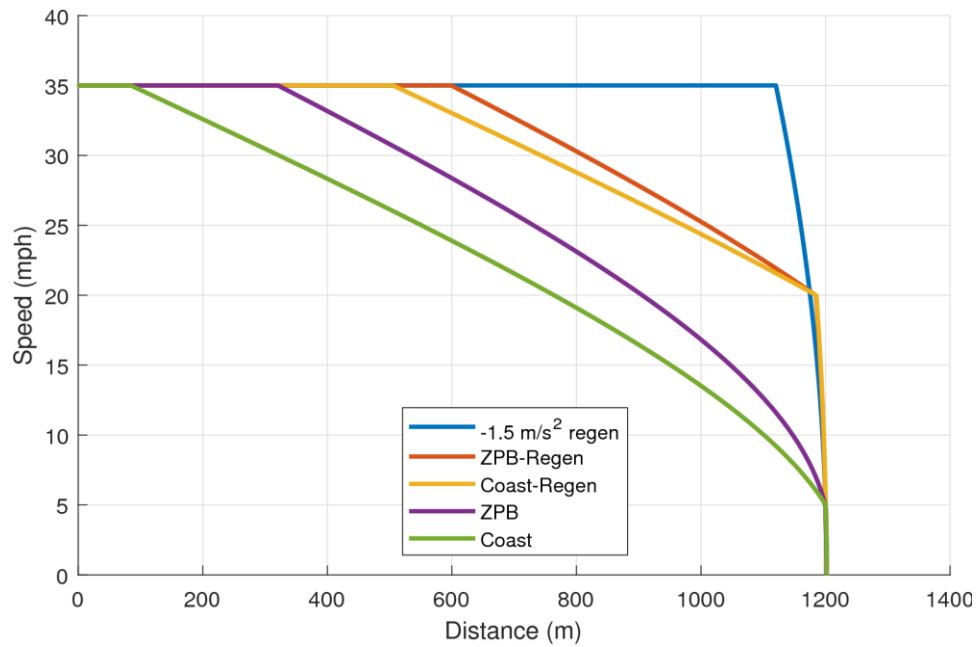


Figure D.7: Speed vs. Distance, Fixed-Route Simulations, 35 mph Case

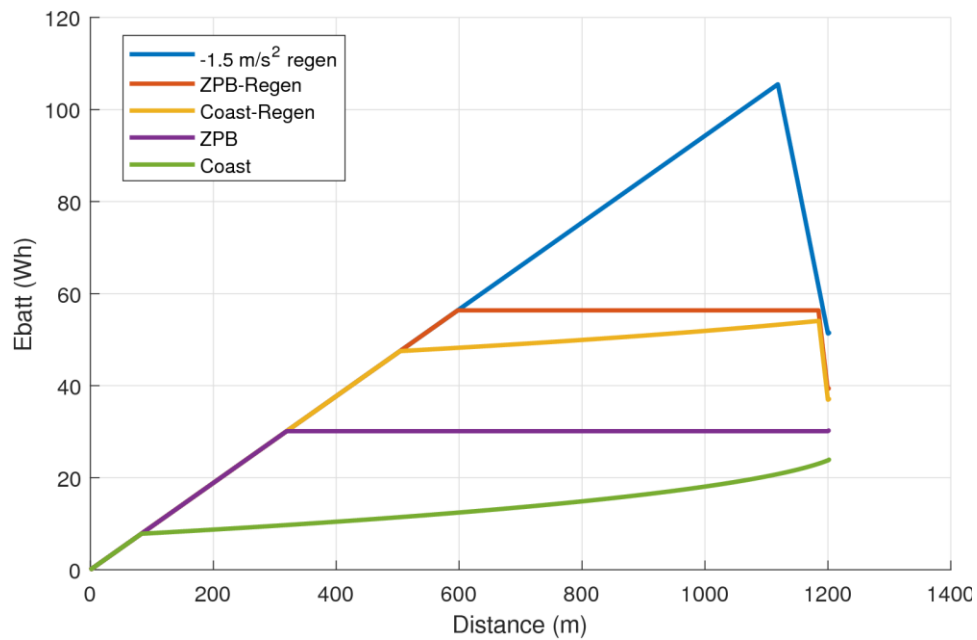
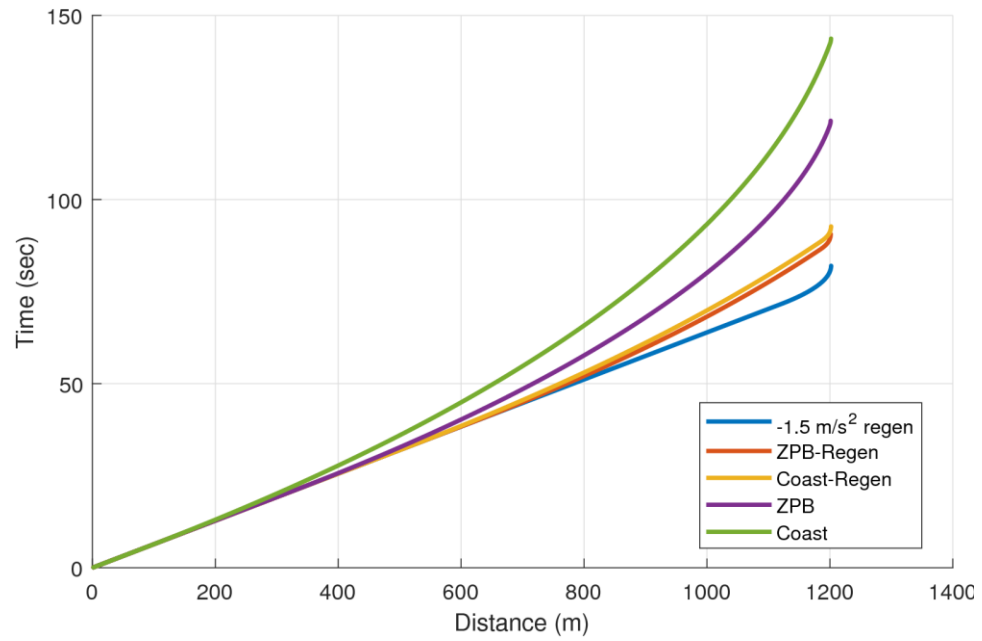


Figure D.8: Battery Energy vs. Distance, Fixed-Route Simulations, 35 mph Case



*Figure D.9: Time vs. Distance, Fixed-Route Simulations, 35 mph Case*

## Appendix E: 45 mph Simulation Results

Table 1E: Simulation Summary, 45 mph case

Parameter	Coast Mode	Zero Pmech (ZPM)	Zero Pbatt (ZPB)	-1 m/sec <sup>2</sup> Regen	-1.5 m/sec <sup>2</sup> Regen	Units
vi	20.12	20.12	20.12	20.12	20.12	m/sec
vf	2.24	2.24	2.24	2.24	2.24	m/sec
tf	163.90	152.00	124.40	17.80	11.90	sec
sf	1597.46	1522.21	1324.89	199.66	133.18	m
accel_min	-0.19	-0.19	-0.20	-1.00	-1.50	m/sec <sup>2</sup>
accel_max	-0.07	-0.09	-0.12	-1.00	-1.50	m/sec <sup>2</sup>
accel_avg	-0.11	-0.12	-0.14	-1.00	-1.50	m/sec <sup>2</sup>
vel_min	2.24	2.24	2.25	2.32	2.27	m/sec
vel_max	20.12	20.12	20.12	20.12	20.12	m/sec
vel_avg	9.75	10.02	10.65	11.22	11.19	m/sec
Ebatt	68.71	47.76	0.00	-296.88	-315.12	kJ
E_pt	0.00	-15.51	-58.07	-346.84	-364.87	kJ
E_elec	19.18	1.82	-37.59	-302.26	-318.71	kJ
Tmot+, max	1.69	0.00	0.00	0.00	0.00	Nm
Tmot-, min	0.00	0.00	-5.54	-63.72	-98.76	Nm
Tmot,avg	0.54	0.00	-1.58	-61.30	-96.34	Nm
sCruise	50.8	126.1	323.4	1448.6	1515.1	m
tCruise	2.5	6.3	16.1	72.0	75.3	sec
sCycle	1650.0	1650.0	1650.0	1650.0	1650.0	m
tCycle	167.9	159.8	142.0	91.3	88.7	sec
Ept, cruise	19.10	47.37	121.50	544.25	569.23	kJ
Ebatt, cruise	21.53	53.41	136.97	613.55	641.70	kJ
Ept, cycle	14.33	27.09	58.66	192.64	199.58	kJ
Ebatt, cycle	90.86	101.78	137.59	317.28	327.20	kJ
Energy consump., cycle	24.6	27.6	37.3	86.0	88.7	Wh/mi



Table 2E: Simulation Summary, 45 mph case, cont'd

Parameter	-2 m/sec^2 Regen	-2.5 m/sec^2 Regen	Hybrid Solution 1	Hybrid Solution 2	Hybrid Solution 3	Units
vi	20.12	20.12	20.12	20.12	20.12	m/sec
vf	2.24	2.24	2.24	2.24	2.24	m/sec
tf	8.90	7.10	86.00	83.50	75.80	sec
sf	99.83	79.82	1176.64	1144.89	1046.00	m
accel_min	-2.00	-2.50	-2.50	-2.50	-2.50	m/sec^2
accel_max	-2.00	-2.50	-0.10	-0.10	-0.13	m/sec^2
accel_avg	-2.00	-2.50	-0.21	-0.21	-0.23	m/sec^2
vel_min	2.32	2.37	2.44	2.44	2.44	m/sec
vel_max	20.12	20.12	20.12	20.12	20.12	m/sec
vel_avg	11.22	11.24	13.68	13.71	13.80	m/sec
Ebatt	-318.20	-294.18	-26.70	-36.26	-61.72	kJ
E_pt	-373.57	-378.68	-71.53	-79.80	-105.76	kJ
E_elec	-320.89	-296.32	-52.69	-61.49	-84.62	kJ
Tmot+, max	0.00	0.00	0.42	0.00	0.00	Nm
Tmot-, min	-133.81	-168.85	-168.85	-168.85	-168.85	Nm
Tmot,avg	-129.85	-154.74	-4.81	-5.24	-6.68	Nm
sCruise	1548.5	1568.5	471.7	503.4	602.3	m
tCruise	77.0	78.0	23.4	25.0	29.9	sec
sCycle	1650.0	1650.0	1650.0	1650.0	1650.0	m
tCycle	87.4	86.6	110.9	110.0	107.2	sec
Ept, cruise	581.76	589.28	177.20	189.13	226.28	kJ
Ebatt, cruise	655.83	664.31	199.76	213.21	255.10	kJ
Ept, cycle	203.42	205.82	100.89	104.56	115.75	kJ
Ebatt, cycle	338.25	370.74	173.67	177.57	194.00	kJ
Energy consump., cycle	91.6	100.4	47.1	48.1	52.6	Wh/mi

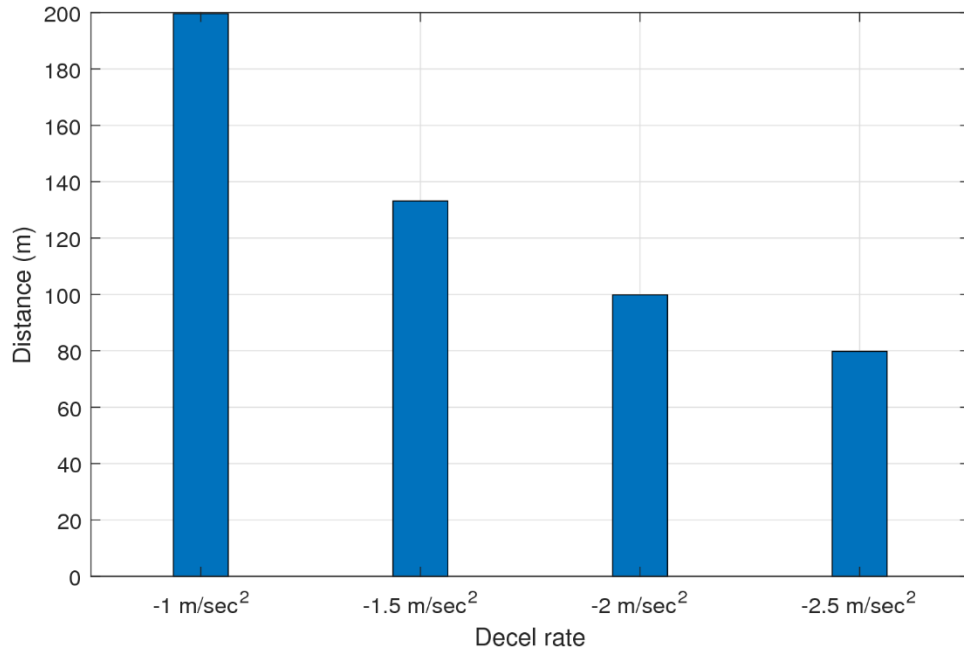


Figure E.1: Decel Distance, Linear Decel, 45 mph Case

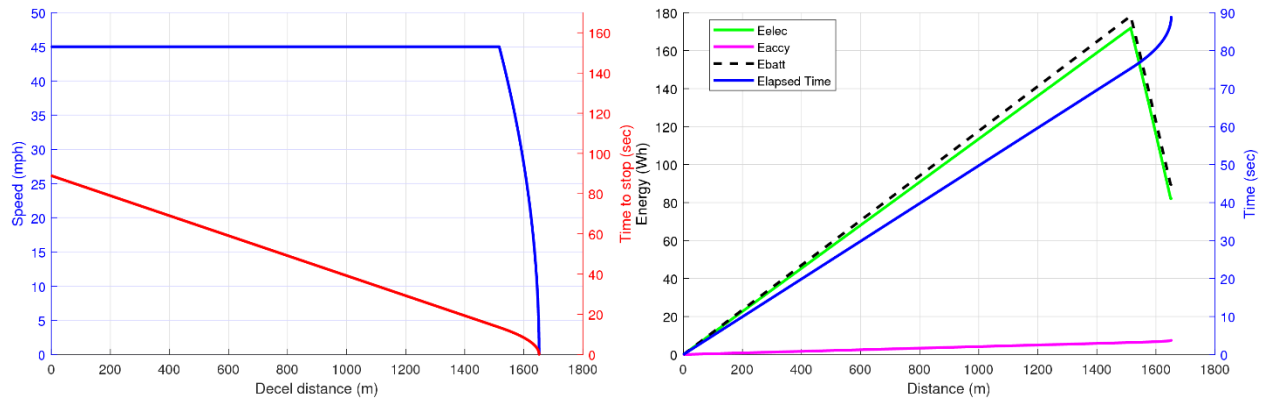


Figure E.2: -1.5  $\text{m/sec}^2$  Regen Braking Fixed-Route Simulation, 45 mph Case

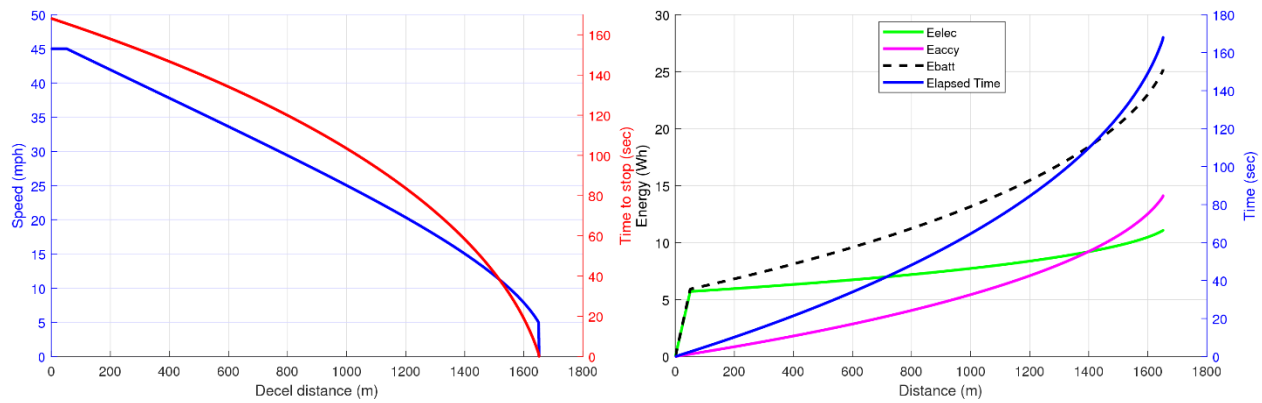


Figure E.3: Coast Mode Fixed-Route Simulation, 45 mph Case

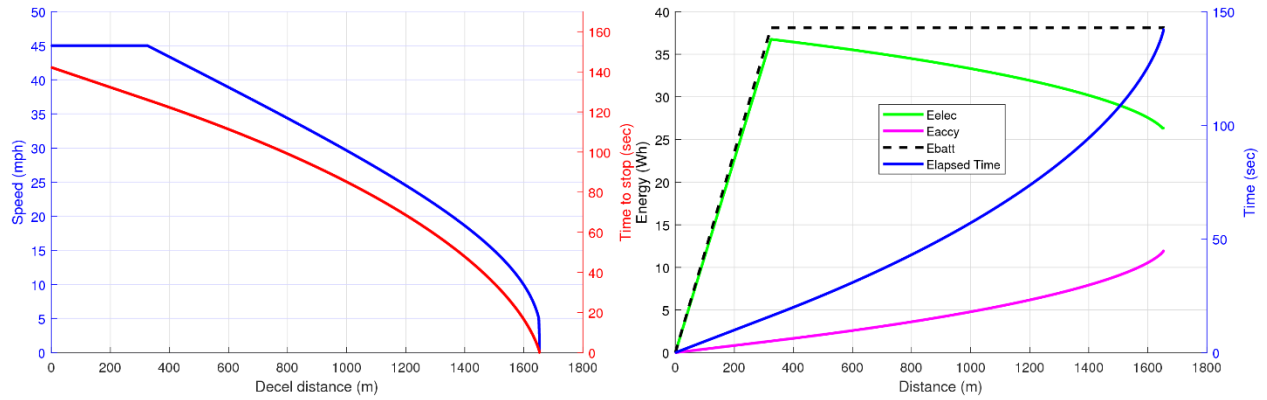


Figure E.4: ZPB Mode Fixed-Route Simulation, 45 mph Case

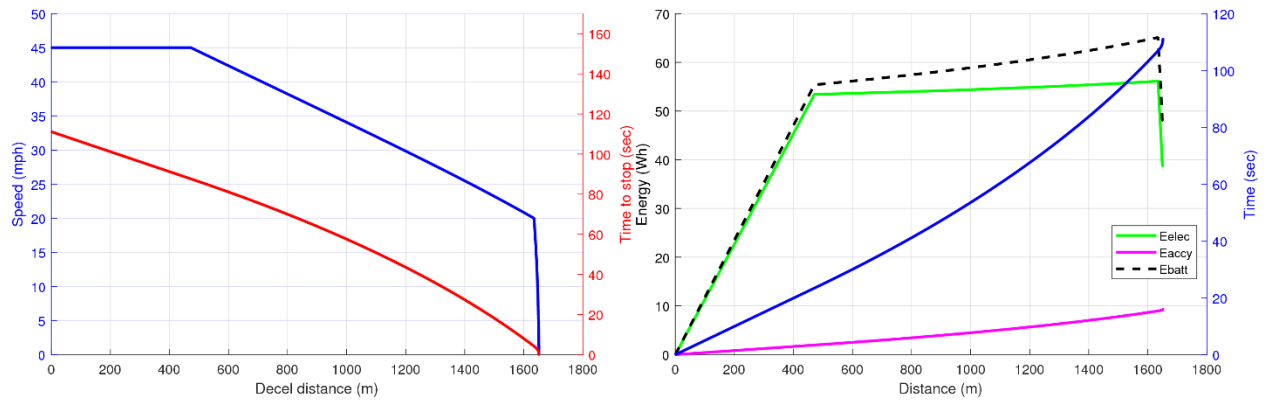


Figure E.5: Coast-Regen Fixed-Route Simulation, 45 mph Case

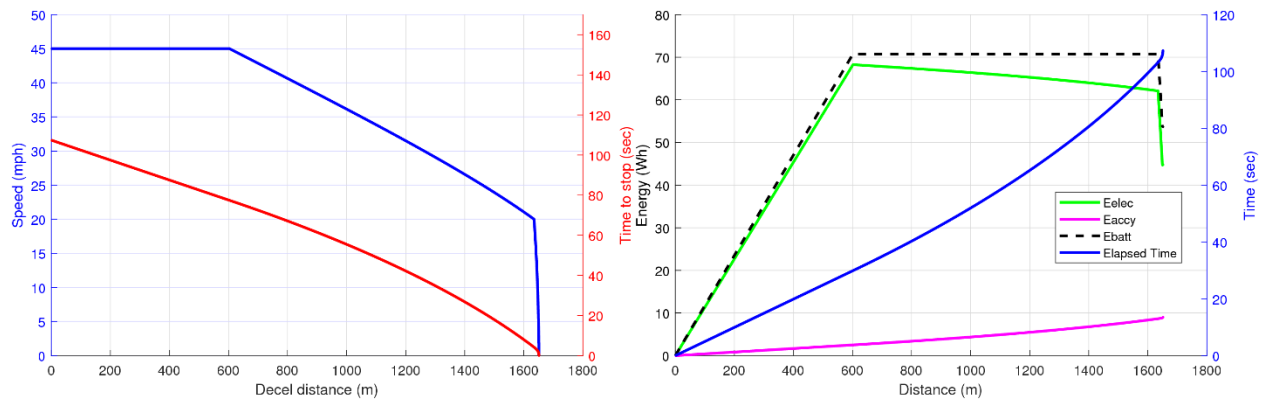


Figure E.6: ZPB-Regen Fixed-Route Simulation, 45 mph Case

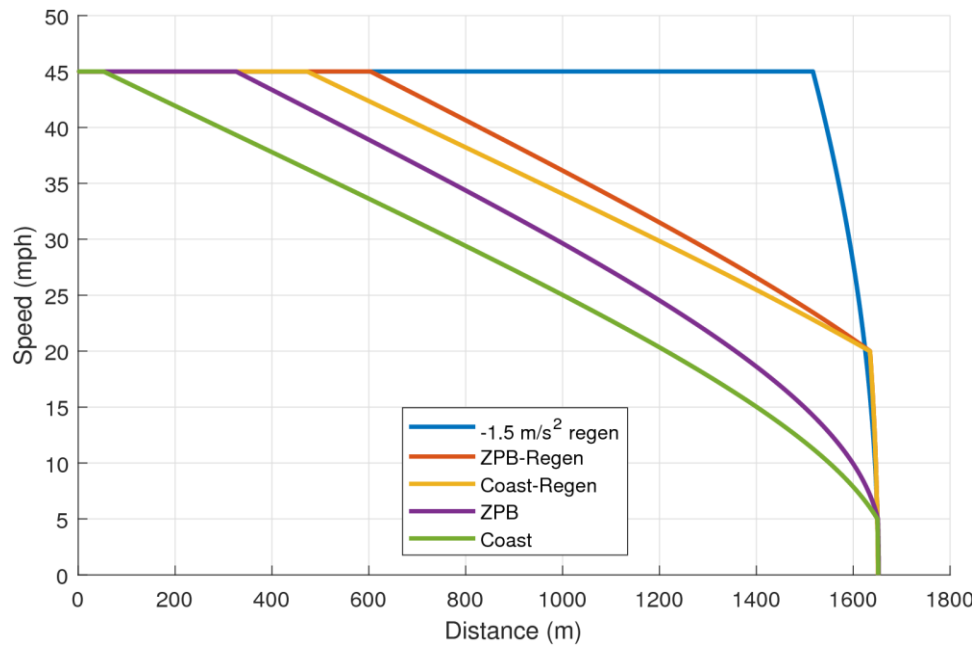


Figure E.7: Speed vs. Distance, Fixed-Route Simulations, 45 mph Case

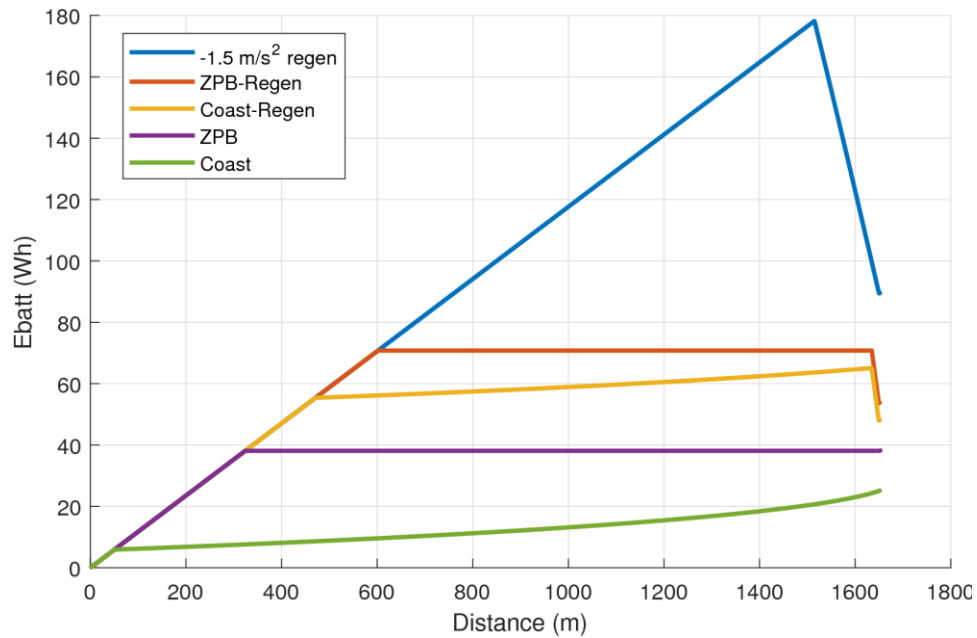
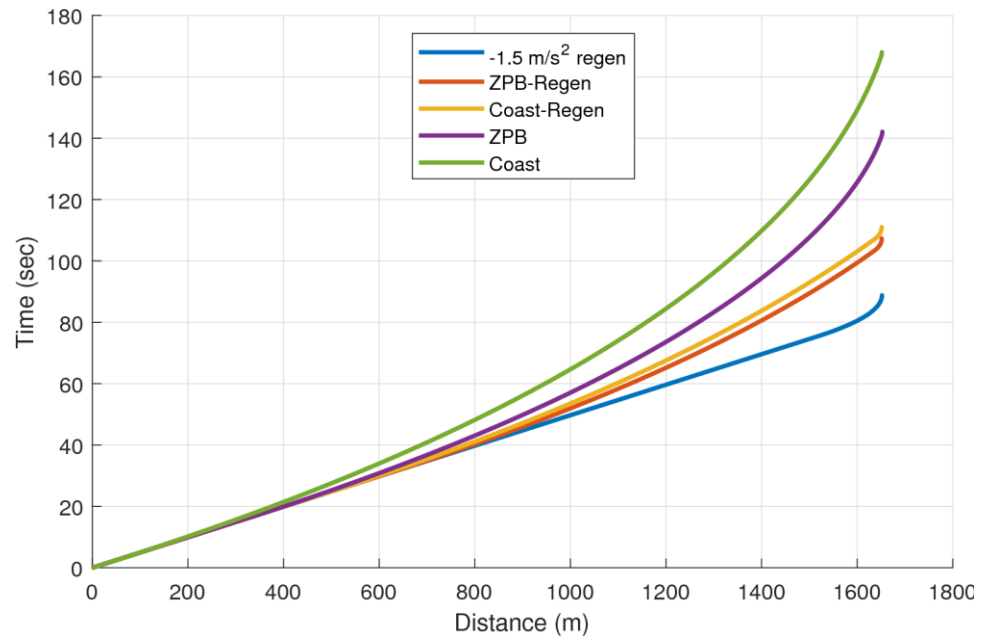


Figure E.8: Battery Energy vs. Distance, Fixed-Route Simulations, 45 mph Case



*Figure E.9: Time vs. Distance, Fixed-Route Simulations, 45 mph Case*